Title
Investigation of Adult Hippocampal Neural Stem Cell Behavior in Response to Complex Biomolecular Signaling Logic

Author
Bremer, Andrew William

Publication Date
2019

Peer reviewed|Thesis/dissertation

Investigation of Adult Hippocampal Neural Stem Cell Behavior in Response to Complex Biomolecular Signaling Logic

by

Andrew William Bremer

A dissertation submitted in partial satisfaction of the

requirements for the degree of

Joint Doctor of Philosophy
with the University of California, San Francisco

in

Bioengineering

in the

Graduate Division

of the

University of California, Berkeley

Committee in charge:

Professor David Schaffer, Co-chair
Professor Zev Gartner, Co-chair
Professor Daniela Kaufer

Summer 2019

Abstract

Investigation of Adult Hippocampal Neural Stem Cell Behavior in Response to Complex Biomolecular Signaling Logic

by

Andrew William Bremer

Joint Doctor of Philosophy in Bioengineering

with the University of California, San Francisco

University of California, Berkeley

Professor David V. Schaffer Co-chair
Professor Zev J. Gartner, Co-chair

Adult hippocampal neural stem cells (NSCs) retain the capacity to self-renew and differentiate down multiple cell lineages throughout adulthood. These and other cell fate decisions are regulated by the complex microenvironment that comprises the NSC niche. Understanding how biomolecular signals of the niche direct cell behavior is a necessary element in elucidating the biology of NSCs, and it also holds important implications for tissue engineering and regenerative medicine strategies. While previous work has revealed the influence of the presence or absence—that is, the simple binary logic—of several isolated factors in driving NSC fate, less is known about how more complex signaling typical of the niche is interpreted by cells to direct their behavior. In this dissertation I discuss our recent work, including the development of a novel culture platform, to expand the scope of our understanding of how biomolecular cues govern NSC fate beyond their simple binary logic, and instead through a more complex signaling logic.

First, I will present our work exploring competing cues that drive mutually exclusive behaviors. Our current understanding of the neural stem cell niche details a highly active signaling microenvironment in which neural stem cells send and receive a multitude of biomolecular cues simultaneously. For example, Eph/ephrin signaling via ephrin-B2/EphB4 instructs cells to neuronally differentiate. In contrast, Notch signaling directs stem cell self-renewal and maintenance. How might neural stem cells integrate these two mutually exclusive cues to decide which fate to choose? To address this question, we developed a novel single-cell patterning platform to recreate model niche microenvironments in which single neural stem cells are presented with these two opposing signals. By observing downstream fate decisions, our data reveal that neural stem cells display a preference for the self-renewal cue of Notch signaling over the Eph/ephrin signal to neuronally differentiate when presented with both cues simultaneously.

Second, I will present our results that reveal how the strength of biomolecular signaling pathway activation is a factor in the conditional logic that informs downstream cell behavior. Biomolecular signals fluctuate in strength in the niche, so understanding how cells might differentially respond

to weak, mid-level, or strong pathway activation is crucial to fully elucidating a signal's role in driving fate decisions. We focus on the canonical Wnt pathway and find that it operates through a strength-of-pathway-activation signaling logic to regulate NSC behavior. Using *in vitro* assays, we reveal proliferation and neuronal differentiation saturate at inequivalent activation strengths of the canonical Wnt/β-catenin pathway. While stronger pathway activation yields greater proportions of cells selecting a neuronal fate, mid-level activation strength drives greater cell proliferation over an extended time period. This proliferation largely occurs in neuronal-committed cells, thus mid-level Wnt activation strength yields greater total numbers of immature neurons than strong activation of the pathway. Further, single-cell tracking reveals this effect at the single-cell level, with mid-level Wnt enabling the greatest proliferative expansion and highest output of immature neurons from single NSCs.

Lastly, I will discuss evidence and propose further factors that may contribute to complex logic of adult hippocampal neural stem cell fate decisions in response to biomolecular signaling. I explore how varying cell density may differentially regulate stem cell behavior and discuss possible mechanisms through which cell density is communicated to and sensed by cells. Next, I discuss the possible influence that cell cycle phase during signaling has on determining cellular fate decisions. As signaling mechanisms broadly fluctuate throughout different phases of the cell cycle, this offers an attractive research direction.

In summary, we provide evidence to elucidate how several biomolecular signaling cues—Notch, Ephrin/Eph, and Wnt in particular—instruct NSC fate decisions through a complex logic. Beyond their simple presence, additional factors like the activation of other pathways and the strength to which a pathway is turned on contribute to how a cell responds to these biomolecular cues. Our results have implications for regenerative medicine, and further provides a deeper framework through which to explore the influence of biomolecular signaling on stem cell behavior.

Dedicated to my parents, Shirley and William Bremer,

for their unconditional love and constant support, and for instilling in my sisters and me a simple mission in life: to “Study hard, and do good things.”

Table of Contents

List of Figures

Acknowledgments

It is hard to remember a milestone in my life that has been as satisfying to the spirit than the completion of this document. Not only because of the enormity and difficulty of the task on a personal level, but because I feel it represents an accomplishment that my family, friends, and the metaphorical village have been helping me work toward my entire life. I am humbled by the number of people who have enabled me to reach this goal, both directly and indirectly. With enormous gratitude, I offer a sincere thank you to everyone who has played a role in leading me to this point, and give special thanks to:

My Ph.D. advisers Dave Schaffer and Zev Gartner, for their scientific guidance and willingness to try something new with me as a cross-campus co-advised student. My lab placement certainly presented unique challenges, but the opportunities it provided me to develop as a scientist have been more than I could have hoped for at the outset of grad school. In hindsight, each also taught me a unique vision to approaching research: Dave, his encouragement to let the science and data guide me on my path forward, and Zev, with reminders to always think about the big picture and the higher-level story. Each of these lessons have been vital to my progress, and they'll certainly stick with me.

Olivia Scheideler, who has been my unwavering research companion for all of grad school. You are an enormously talented scientist and artist, and an even kinder human being. Working with you has been an absolute joy. (And, you make the best cake balls!)

Alyssa Rosenbloom: In fraught situations, I was in dire need of assistance and believed my hypotheses helpless. Your friendship would have been enough, but you rose up to help me find my way out. The balance of my experimental outcomes shifted when our research rendezvoused, and I will always be satisfied with you in the narrative when I tell my grad school story.

Sisi Chen and Yun Suk Na, who agreed during an inopportune time to take me on as a rotation student. You brought me into a project that aligned so well with my research interests, and you were encouraging and patient. I am deeply grateful for all that I learned from you both.

Jessica Li, who worked with me as an undergraduate researcher from her sophomore through senior years. Thank you for all of your contributions to our work together in lab. Like my own undergraduate research, I hope you gained not only an appreciation for the day-to-day challenges of doing research, but also the immense joys that come with it. Lastly, I'm also grateful for our discussions of all things Taylor Swift, Hamilton, campus drama, and so, so much more.

Noem Ramey, who is a fearless lab director/admin for the Schaffer lab. You have made the process and logistics of working in a research lab so incredibly smooth. Even more, you recognize the importance that sharing experiences and time together outside of the lab is in building our lab culture and friendships. Thank you for everything, including the wonderful memories you've helped to facilitate.

My 2013 Schaffer labmates—Olivia Scheideler, Phil Kang, Nicole Repina, Sabrina Sun, Riya Muckom—I am so grateful to have had all of us going through the same stages of grad school around the same time. I'm so proud of the growth and progress we've made in our journeys together and will miss working with you all. The same goes for Christina Fuentes, who joined lab a year after and made my days all the more enjoyable, especially through sharing our mutual love (and pictures) of uncle/aunt-hood.

To all of my other Gartner & Schaffer lab members, past and present, who have contributed so meaningfully to my development as a scientist. I am deeply grateful for your helpful feedback, your words of support and encouragement, your constructive criticisms, your empathy, your guidance and training, the lab supplies you were willing to share with (and give to) me, your joint brainstorming sessions and suggestions for experiments, your input on data analysis and interpretation, and your humor, sarcasm and wit throughout the past 6 years. And, of course, your ability to put up with me singing in TC and talking about Wisconsin all the time.

Kristin Olson and the remarkable comfort provided by your office, your help in working through problems, but most importantly your friendship. Grad school simply wouldn't have been the same without you, and I know many others in my cohort would say the same.

My 2013 BioE Cohort. Bennett said it best: You can choose where you go to grad school, but you can't choose the people. I was so tremendously lucky to have our group, and to make and have such great friends almost immediately on Day 1. I'm excited for where post-BioE life takes us all, and I'm of course looking forward to a reunion.

My roommates for all (Daniel) or most (Phil) of grad school, who shared with me not only common grad school experiences but also a living space. I enjoyed living in Apt. 1A with you, decompressing with the likes of Smash Bros, GoT, and Last Week Tonight. And, I'm pleased to report that after 103 games of Catan, there appears to be no statistical advantage to placing first, and Phil appears to be the -slightly- worse player overall (data subject to scrutiny).

Other BEASTies of past and present. I chose Berkeley and UCSF BioE because of the strong sense of community and the tangible passion its students hold for making the world a better place, both of which I felt immediately during my visit weekend. Those first impressions certainly did not disappoint; it's been a privilege to be part of this community and to be surrounded by so many brilliant and committed individuals.

Amy Herr, John Deuber, Todd McDevitt, Tamara Allison, Steve Conolly, Ian Holmes, Tejal Desai, SarahJane Taylor, Terry Johnson, and so many other BioE faculty and administration, particularly those with whom I served on BioE's executive committee. Thank you for your mentorship, your willingness to listen to student input on how to make our program better, and most all—taking that student input seriously.

Kathy Shield, Stephanie Mack, and everyone else in our growing science policy group. I am so immensely proud of the group we've built, and for how true we've stayed to our original mission of helping scientists connect their research to our wider world in meaningful ways. I gained clarity and discovered expanded purpose through our group's work and our friendship, and for that I will

always be thankful for our first fateful meeting in Stanley Hall, and will always remember my oath to that most noble one-pager.

Billy Curtis, Harry Stark, Luis Tenorio, Aaron Smyth, Helen Kurkjian, Chris Hyun, Meckell Milburn, other members of CAC-LGBTQ and Queer Grads at Berkeley, and the many, many others past and present who have helped our communities at large, and me specifically, in big ways and small, on campus and off. Representation matters, visibility is important, and I've enjoyed working with you all to build a more inclusive campus. It really does get better.

The Graduate Assembly and all those involved these past few years during my time as a delegate. I thoroughly enjoyed working with such a diverse and passionate group of graduate students from across campus. Like many types of work that aren't high profile or often recognized, graduate student government isn't the most glamorous thing to do at Berkeley, but I'm thankful for and inspired by those who recognize its importance and show up to make efforts to ensure our campus is an accessible place for our graduate & professional student body.

Jill Dove, who believed in me as a 4th grader and gave me my first opportunity to go to "College". The late James Searls, who taught me scientific notation and the excitement of going on a scientific scavenger hunt for data and tree leaves. Jay Affeldt, who expanded my passion for the wondrous mysteries of life and (AP) biology in & around all of us. Joseph Frontier, who inspired me to always appreciate the moment that science becomes art, and who taught me about leadership on and off the court/track. Vic Levine, who was the first to completely blow my mind with the concept and calculus of an integral. Paul Ulrich, who taught me persistence and that even third trumpets have crucial role to play. Bill Bement & Kevin Sonnemann, who took a chance on me and taught me how to use a pipette. Beth Altschafl, who shared not only an infectious passion of human physiology with me but also the undeniable joys of teaching. And to all of the other teachers and educators throughout my life who have contributed to my academic journey. The high-quality education I have been privileged to attain is of the kind we should strive to provide every child.

Joseph Chavarria, Monica Kapil, Jorge Santiago, and AJ Habib. Words can't describe how thankful I am that our paths crossed during grad school; our friendship has meant so much to me these past several years. I'm going to cherish the memories of our Guerneville getaways, weekends in Tahoe, camping excursions, trips to Sac, watching music videos at MKs (that's with a "K", right?), and so much more from our adventures together for a very, very long time. A special shout-out and thank you to Joe, the nearly 3,000 miles (and 300k-ish feet climbing) that we've biked together these past 3+ years. Your companionship has meant the world to me during my difficult days of grad school, and I've been so lucky to find someone to share this new hobby of mine with. Thanks for helping me cross my finish lines these past few years. Our Sunday rides together are some of my favorite memories from these past few years, and I'm going to miss them and you dearly.

My extended family, especially my godmothers Aunt Sheila and Aunt Julie and so many other wonderful aunts, uncles, and cousins, who filled my early years with boundless love and who have continued to support me in all of my academic endeavors and other personal goals.

Ann, Kimberly, and Kristin. Many people don't even get to have one amazing sister; I don't know how I got so lucky to have three. Thank you for being such great big sisters to your little brother. From being such great role models for me (everything from watching you play sports growing up to overcoming tremendously difficult health challenges) to playing with me (ghost in the graveyard, mail, fantasy football, clean sweeps of those events during family Olympics…) to supporting me in all that I do (school, triathlons, and everything else!) you three really are the best sisters a brother could ask for. (Lastly, of course, thank you for growing our family with the wonderful guys I now get to call my brothers!)

My parents, Shirley and William Bremer, to whom this dissertation is dedicated. Not only did you give me your unconditional love, you instilled in me purpose, faith, morals, a love of science, a commitment to family and friends, and even further, you sacrificed to ensure I had the resources to pursue my dreams. I am beyond lucky to call you my mom and dad.

Finally, Elizabeth, Peyton, Addison, Emma, Nolan, Layne, Drew, and Grayson. Each of you arrived between the time I applied to grad school and the time I completed it, and you have kept me grounded in what's important in life. You have brought me so much joy. The completion of this dissertation affords me a new title, but the one you give me is far and away still my favorite.

President Barack Obama, in his first inaugural address, called for a "new era of responsibility–a recognition on the part of every American that we have duties to ourselves, our nation and the world." This moment came during a pivotal time in my life, and I wouldn't be where I am today without the inspiration he bestowed, his unyielding hope for and vision of a better future, and the unwavering belief that all of us have a role in getting us there. Now more than ever, scientists and researchers can and should play an active, visible part in working toward that better tomorrow: our science doesn't exist in a vacuum, so neither should we.

Long live the Wisconsin Idea.

Chapter 1: Introduction

1.1 Stem Cells and their characteristic fate decisions

1.1.1 Historical and Current Definitions

The term "stem cell" is first known to appear in the scientific lexicon in 1868[1]. In this first use, it described a postulated unicellular common ancestor of all multicellular organisms to provide support for Charles Darwin's theory of evolution. Over the next several decades, the term itself would evolve and be applied to the field of developmental biology. Here, "stem cell" was used to describe the single fertilized egg from which an entire organism develops[2]. In the 1960s, researchers studying hematopoiesis—the production of new blood cells—demonstrated the existence of "stem cells"[3] in bone marrow that could both proliferate to create an expanded clonal population, as well as differentiate into the multiple cell types found in blood[4].

These two qualifying properties give rise to the contemporary definition of "stem cell" that is widely recognized and used today. While there is still some nuanced debate on appropriate terminology[5], the term "stem cell" is generally applied to any cell that displays the two aforementioned hallmark properties: the ability to **self-renew** by undergoing cell division to create more cells of an identical nature, **and** the ability to **differentiate** into cells of a more specialized and mature identity (Figure 1.1).

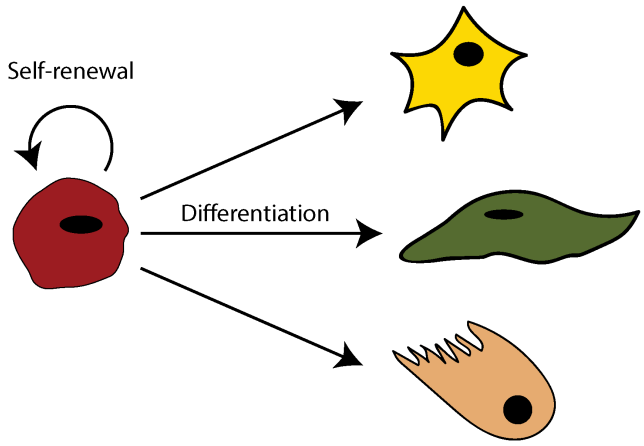

Figure 1.1 Stem cells and their characteristic behaviors. A stem cell (red) can self-renew through cell division to create two daughter stem cells, or differentiate down multiple lineages to create more-specialized cell types.

1.1.2 Stem Cell Potency

Stem cells can be described by their potency, referring to the extent of their differentiation potential. **Totipotent** stem cells have the greatest potency with the ability to differentiate into all cell types of an organism, including the embryonic and extraembryonic tissue. A fertilized egg, or zygote, is a prime example of a totipotent stem cell. **Pluripotent** stem cells have the ability to differentiate into any cell of the developing embryo (organized into so-called germ layers) that will comprise the eventual organism, but not the extraembryonic tissue. Embryonic stem cells, described in Section 1.1.3, are examples of pluripotent stem cells. **Multipotent** stem cells are found extensively throughout development and in adult organisms, and can differentiate down multiple (and typically tissue-related) cell lineages. The cells found in bone marrow that are

responsible for hematopoiesis—hematopoietic stem cells—are an example of multipotent stem cells. Adult neural stem cells, the primary subject of this dissertation and discussed in further detail in Section 1.2, are also an example of multipotent stem cells. While the totipotent, pluripotent, and multipotent terms are extensively used, some fields apply additional terminology. **Oligopotent** stem cells are similar to multipotent stem cells but can only produce cells of related identities: lymphoid stem cells, for example, are only capable of producing the various lymphocyte cell types. Finally, **unipotent** stem cells hold the most restricted potency, having the capacity to only produce one fully mature cell type[6].

1.1.3 Stem Cell Types

In addition to the spectrum of potency, there are several types of stem cells that are characterized by their origin. **Embryonic stem cells** (ESCs) are derived from the inner cell mass of a preimplantation embryo, and are pluripotent. The first successful isolation and propagation of ESCs occurred in 1981 using mouse embryos[7,8], and this technique was quickly merged with recently developed techniques in gene editing[9] to correct[10] or mutagenize[11] targeted genes. This research led to the landmark advancement that has opened new doors for scientists to study the function and phenotypic impact of specific genes: the knockout mouse[12,13]. Another landmark advancement occurred in the late 1990s with the first isolation of human ESCs from human blastocysts[14]. While controversial[15], this discovery has enabled research into human development and disease and offers promise for new therapeutic advances, including cell-based therapies[16].

The dogma of unidirectional permanent differentiation was challenged by pioneering work that displayed the ability of genetic material (i.e. DNA in the nucleus) from a mature, purportedly fully differentiated cell to retain the ability to generate a complete organism and all of its corresponding cell types[17]. This research paved the way for the eventual discovery of **induced pluripotent stem cells**, or iPSCs[18,19]. These cells are derived from fully differentiated somatic cells through the delivery of a set group of transcription factors, are pluripotent, and display the stem cell markers and properties of ESCs. Similarly, they have shown potential for new therapeutic strategies while largely avoiding the ethical debate surrounding ESCs, and also present some immune system-related advantages over ESCs when applied in cell-based therapies[20].

Lastly, **adult stem cells** are cells found in an organism after development and play important roles in many functions throughout life, including maintaining normal tissue homeostasis and responding to injury. Adult stem cells, including those blood cell-forming hematopoietic stem cells of the bone marrow, have been found in many tissues throughout the body, including the intestine, skin, the liver, adipose tissue, and the central nervous system (e.g. adult neural stem cells, Figure 1.2). As with ESCs and iPSCs, adult stem cells enable a multitude of research directions in tissue engineering and regenerative medicine[21].

1.1.4 Motivations for Studying Stem Cells

On account of their regenerative capacity, stem cells provide promise for a plethora of cell-based applications in medicine. To this point, they've already proven vastly impactful in addressing human health challenges and improving quality of life: since the first successful transplant of hematopoietic stem cells from a bone marrow donor in 1957, over one million transplants have

since been performed with increasing health outcomes over that time[22]. Beyond hematopoietic stem cells, clinical trials using a wide range of stem cell types—or cells derived from stem cells—are underway for a broad range of diseases and injuries[16,20,23]. Further, as other fields with therapeutic potential like gene therapy continue to mature, stem cells will continue to offer promise for next-generation therapies to address a host of human ailments. In addition to cell-based clinical applications, stem cells also offer an attractive model for *in vitro* drug discovery and disease progression, and downstream drug targeting *in vivo*[24].

Last but certainly not least, stem cells offer a unique avenue to gain insight into fundamental questions of life and biology. These questions alone are sufficient to spark the most basic aspects of human nature and curiosity, and the expedition to find their answers should need no warrant. The diversity, the nuances, and the underlying mysteries of stem cell behavior call to action the purest form of raw scientific exploration. As others have written, "the complexity and paradoxes of biology are also its beauty, which never ceases to beckon us to go deeply in search of answers[25]."

1.2 Adult Neural Stem Cells and Adult Neurogenesis

Neural stem cells (NSCs) are classic stem cells in that they display the two aforementioned hallmark properties that define all stem cells: the ability to self-renew and differentiate. NSCs have the capacity to differentiate into the main cell types of the central nervous system, including neurons, astrocytes, and oligodendrocytes[26]. Neural stem cells are present during, and necessary for, normal development of the nervous system[27]. Further, NSCs found in the adult brain—adult neural stem cells—retain the capacity to generate new cells throughout life (Figure 1.2)[28,29].

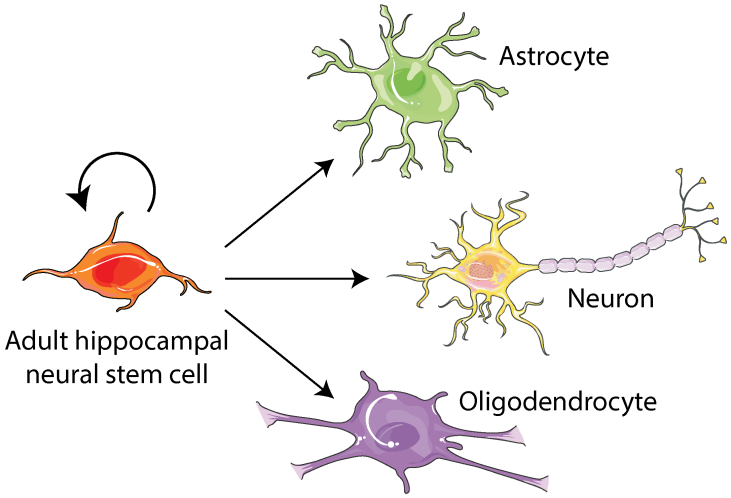

Figure 1.2 Self-renewal and differentiation of adult hippocampal neural stem cells. Adult hippocampal neural stem cells are classic stem cells in that they display the two hallmark properties of stem cells: self-renewal and differentiation into more specialized cell types.[157]

1.2.1 Historical context

A long-held dogma of the neuroscience field was the incapacity of the adult brain to regenerate and create new neural cells after development[30]. In the 1960s, the research of Dr. Joseph Altman challenged that belief by providing evidence in several mammalian species, including rats[31,32], cats[33], and guinea pigs[34], for the formation of new neurons in the post-natal and adult brain, a

process termed adult neurogenesis. While his research was initially dismissed by the field for several decades, evidence for cells with retained capacity to undergo self-renewal and differentiation in the adult brain continued to grow over time[35,36]. The field of adult neurogenesis exploded in 1998 with the landmark discovery of adult neurogenesis in humans[37], which rapidly accelerated the growth of this field. While the presence and significance of adult neurogenesis in humans has not gone unchallenged in recent years[38], further evidence and viable explanations for previous negative results[39] continue to establish the process as an important mechanism in humans[40–43].

1.2.2 Locations, Biomarkers, and Behavior of Adult Neural Stem Cells

Adult neural stem cells reside in at least two locations of the adult brain: the subventricular zone of the lateral ventricles (SVZ), and the subgranular zone (SGZ) of the dentate gyrus in the hippocampus[37]. While many questions still remain about their identity and function[44]—including the potential for multiple sub-populations of adult NSCs in the SVZ and SGZ that display variable behavior—much work has elucidated the characteristic biomarkers[45] of NSCs during the progression of their various behaviors[26].

Adult NSCs of the SVZ, termed "Type B" cells, reside in close proximity to the ependymal cell layer that separates the SVZ from the ventricular cavities[46]. These Type B cells are mostly quiescent or slowly-dividing, and express the glial marker GFAP and the intermediate filament protein nestin[46]. Evidence suggests Type B cells also maintain a unique morphology, with an apical cilium extending through the ependymal cell layer to reach the cerebrospinal fluid located within the ventricle[47], and a basal process that makes contact with blood vessels within this niche[48,49]. During neurogenesis, Type B cells give rise to more-rapidly dividing transient amplifying progenitors (Type C cells), which in turn further differentiate into neuroblasts (Type A cells)[29]. Type A cells migrate through the rostral migratory stream to the olfactory bulb, where they terminally differentiate into the various interneuron subtypes of that region[50]. Besides their neurogenic capacity, evidence also exists for the multipotent differentiation of Type B NSCs, including their differentiation into oligodendrocytes[51] and astrocytes[52].

Adult hippocampal NSCs found in the subgranular zone of the dentate gyrus, the main subject of the remainder of this dissertation, share many phenotypic, morphological, and other similarities with adult SVZ NSCs. Adult hippocampal NSCs (Type 1 cells) arise from a population of glial-like $GFAP^+$ cells[53] referred to as radial glia-like cells (RGLs)[54]. Similar to Type B cells in the SVZ, Type 1 cells of the hippocampus are mostly quiescent or slowly-dividing, directly engage with the vasculature of its surrounding niche, and extend a process through the granule cell layer to the molecular layer[55]. During adult neurogenesis, Type 1 cells differentiate into Type 2 cells, or intermediate progenitor cells (IPCs), which show increased mitogenic activity. Type 2 cells are further sub-divided into Type 2a cells, which no longer display the morphology of Type 1 cells but still maintain glial markers like GFAP, and Type 2b cells, which no longer express glial markers and instead show markers of a neuronal fate commitment, including the transcription factors NeuroD1 and Prox1 and the filament doublecortin (DCX). The loss of the marker nestin in Type 2b cells is used to demarcate the transition to a more slowly-dividing Type 3 (neuroblast) neuronal-committed cell. These cells exit the cell cycle, become post-mitotic, and migrate into the granule cell layer[56]. Even at this point, the differentiation cascade of newborn neurons is far from

over. During an early survival phase, most adult newborn neurons are eliminated through apoptosis[57] shortly after cell cycle exit, a still-unclear process that appears to be regulated by several factors[56]. Cells that survive this stage will extend their axon to the CA3 region of the hippocampus, begin dendritic arborization into the molecular layer, and eventually fully mature into glutamatergic granule cell neurons that receive synaptic input from the entorhinal cortex[56]. The complete picture of newborn neuron maturation is far from clear, and only just beginning to be visualized longitudinally *in vivo* (Figure 1.3)[58].

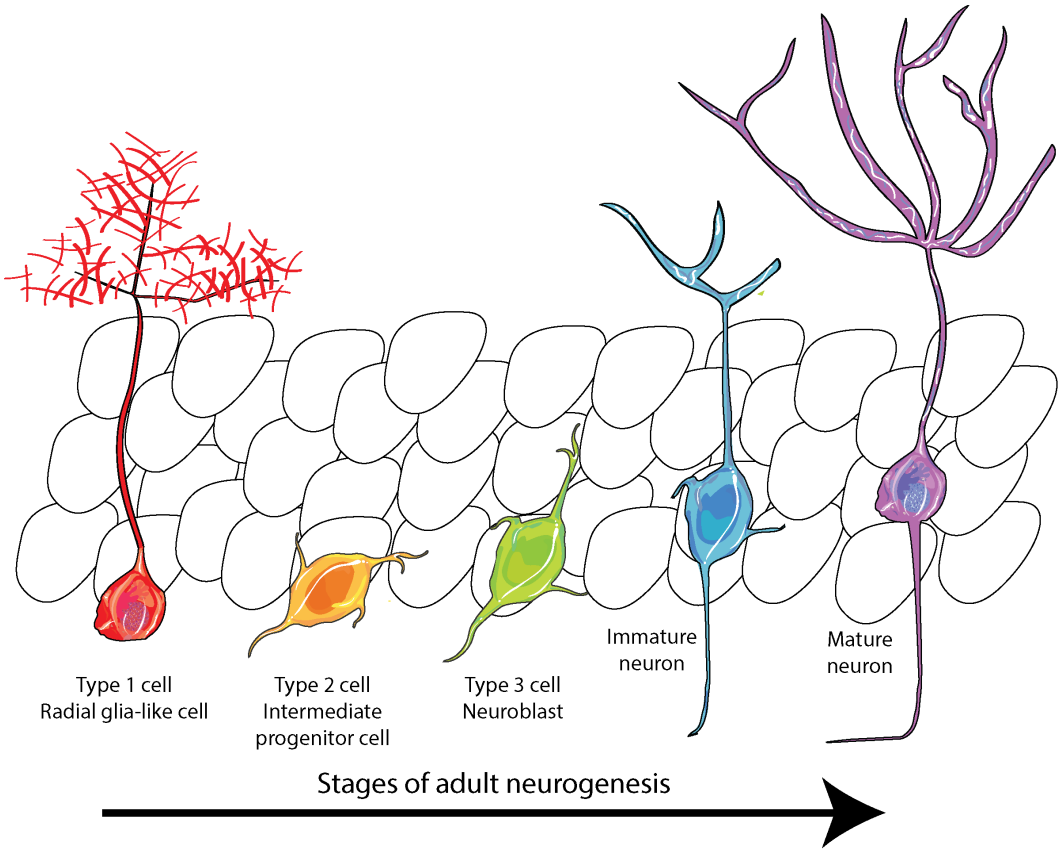

Figure 1.3 Stages of adult hippocampal neurogenesis. Adult hippocampal neural stem cells located in the subgranular zone of the hippocampal dentate gyrus undergo highly ordered and regulated stages during the process of neuronal differentiation to become fully mature neurons.

Expanding beyond adult neurogenesis, the full behavioral repertoire of Nestin$^+$ SGZ NSCs has recently been explored in *in vivo* clonal analysis using an inducible reporter mouse. In this study, researchers found individual Nestin$^+$ SGZ NSCs to be multipotent and capable of several distinct fate decisions including: remaining in quiescence; undergoing a single self-renewing symmetric cell division; undergoing asymmetric self-renewal that also produced neuronal and/or astrocytic daughter cells; and non-self-renewing differentiation. This study further displayed high variability in the total number of cells that a single SGZ NSC is capable of producing[54]. While this study did not find oligodendrocyte-lineage cells, others have shown the capacity for Nestin$^+$ hippocampal NSCs to differentiate into oligodendrocytes, and that the stress hormone corticosterone increases this process at the expense of neurogenesis[59]. These combined results of these two studies suggest the possibility of multiple sub-types of Nestin$^+$ NSCs in the adult hippocampus.

1.2.3 Adult Hippocampal Neural Stem Cells in Learning, Memory, Aging, and Disease

The ability of NSCs in the brain to create new cells throughout adulthood—particularly in the hippocampus—led to the exploration of how this process plays a role in normal brain function, and how it is impacted in the contexts of disease, aging, and injury[60,61]. While many studies rely on non-human models of adult neurogenesis and disease, similarities between humans and other species (mammals in particular, and especially rodents) gives promise to the usefulness of animal models in exploring its role, albeit with some limitations[62]. Adding further promise to the field, advanced techniques and the availability of tissue samples have recently enabled studies on adult human neurogenesis in normal, aged, and various diseased contexts to emerge[40–43,63].

The presence of NSCs and adult neurogenesis in the hippocampus has generated particular interest, as the hippocampus has long been established as a key brain region crucial for learning and the formation of new episodic memories[64]. Indeed, a number of studies have linked these processes with adult neurogenesis[65–68]. Further, adult neural stem cells have been explicitly investigated in—and linked to—the context of age- and disease-related declines in learning and memory[42,43,66,69,70], including Alzheimer's, Parkinson's, and Huntington's disease.

In addition to those human ailments, adult neural stem cells and/or adult neurogenesis have been explored in the context of numerous other neurological disorders and disease, and the underlying mechanisms that contribute to their progression and pathology. This includes schizophrenia[71], depression[72], post-traumatic stress disorder[73,74], sleep disorders and sleep loss[75], and epilepsy[76].

1.2.4 Motivations for Studying Adult Neural Stem Cells

The motivations for understanding adult neural stem cells and their behavior are vast. The contents of the previous subsection make one reason abundantly clear: increasing evidence suggests that NSCs offer deep insight into how and why human disease and aging impacts brain function. NSCs, therefore, could provide an attractive *in vivo* target to address the detrimental impacts found in those contexts, and could be applied in cell-based therapies or *in vitro* drug screening models. All of these avenues display their potential as cellular tools to yield new knowledge and therapeutics to address these human health challenges.

Finally, as previously alluded to, research for research's sake is a fundamental principle of human nature and intellectual curiosity. Our ability to expand our knowledge of the physical and biological world is alone sufficient to justify novel research directions. Further, history has proven that the outcome of research cannot be predicted—from the discovery of new organisms[77] and processes[78] that enable the advancement of next-generation scientific techniques, to visualizing what could not be previously be seen[160]. With this framework, not only do adult neural stem cells and adult neurogenesis offer a means to advance our understanding of human health and disease, they provide a window into one of the greatest scientific mysteries of our time: the human brain.

1.3 Biomolecular signaling factors that control adult neural stem cell behavior

1.3.1 Biomolecules and their role in controlling cell behavior

Organic chemistry provides the fundamental building blocks of life. Four major classes of organic compounds, termed **biomolecules**, form the foundation of the structure and function of all living things, from the cellular to the subcellular level. These biomolecules include carbohydrates, lipids, proteins, and nucleic acids. With only few common threads among all biomolecules—for example, the presence of carbon and hydrogen covalent bonds in their chemical structure—the large diversity of these compounds enables life as we know it[6,79].

Cells utilize biomolecules as chemical messengers to send and receive signals. Biomolecular signals, or cues, are produced and sent from signal-sending cells, then interact with signal receptors on the receiving cell. These cues are interpreted through often complex downstream mechanisms that ultimately drive cell behavior in the signal-receiving cells. These behaviors consist of the full repertoire of cellular function, including migration, programmed cell death, signal propagation, and the two hallmark properties of stem cells: self-renewal by means of entering the cell cycle and undergoing cell division, and differentiation into more specialized cell types[6,79].

Adult neural stem cells send and receive a multitude of biomolecular signals that ultimately determine their behavior. The *in vivo* microenvironment surrounding NSCs that harbors this signaling milieu capable of controlling NSC behavior—including self-renewal and differentiation—is termed the stem cell niche[26,55]. In this section, I provide a broad overview of biomolecular signaling cues that exist in the adult neural stem cell niche and the roles they play in controlling NSC fate.

1.3.2 Biomolecular Signals that Control Adult Neural Stem Cell Behavior

1.3.2.1 Receptor Tyrosine Kinases

Receptor tyrosine kinases (RTKs) are a large group of cell surface receptors that bind to their respective signaling biomolecules and propagate this extracellular signal through intracellular phosphorylation events. Here, I highlight the ephrin-Eph family of proteins, with brief commentary on RTK-binding growth factors including fibroblast growth factor (FGF), epidermal growth factor (EGF), and vascular endothelial growth factor (VEGF).

Eph/ephrins
Membrane-bound Eph receptor proteins belong to the complex superfamily of receptor tyrosine kinases (RTKs). Their ligands, termed ephrins (for Eph receptor interacting) also comprise a diverse group of proteins. Ephs and ephrins are both membrane-bound, demanding cell-cell contact for signal transduction to occur. The signaling direction and outcome in these interactions is extraordinarily diverse and context-specific, and depends on which specific Eph receptor (of the EphA and EphB subfamilies) is interacting with which specific ephrin ligand (of the ephrin-A and ephrin-B subfamilies). In general, however, as with other RTKs, ephrin-Eph interactions drive intracellular phosphorylation of tyrosine residues, which propagates the signal. Downstream impacts of this phosphorylation event can include restructuring of the cytoskeleton through Rho GTPases, leading to cellular repulsion, attraction, or migration, as well as transcriptional changes that can influence cell proliferation and fate determination[80].

Given the complexity and the magnitude of different ephrin-Eph interactions, it is unsurprising that they have been found to display large variances in their impact on adult neural stem cells and the process of neurogenesis. Eprhin-A2 and ephrin-A3, for example, constitute a negative regulatory role by inhibiting neural stem cell proliferation and neurogenesis through activation of EphA7[81]. On the contrary, EphB1 interacts with ephrin-B3 to increase NSC proliferation[82]. Even further, ephrin-B2-expressing astrocytes in the hippocampus have been shown to interact with EphB4-expressing SGZ NSCs to drive neuronal differentiation[83]. While the influential breadth of ephrin-Eph signals on adult neural stem cell behavior is already abundantly clear[84], there are undoubtedly many crucial, fundamental insights yet to be uncovered.

FGF, EGF, VEGF, and other RTK-binding growth factors

In addition to ephrin-Eph signaling, diverse roles for the expansive group of RTK-binding growth factors have been shown to be important in driving neural stem cell behavior. This includes FGF, EGF, VEGF, and others[85]. In general, binding of these ligands to their cognate receptor on the membranes of signal-receiving cells elicits intracellular signal transduction. Receptor dimerization or oligomerization—either before or after ligand-binding—typically plays a key role in initiating downstream kinase activation and subsequent phosphorylation of pathway players. The end result of these diverse, interconnected pathways includes cellular responses like cytoskeletal rearrangement and gene transcription[86].

Mediating divergent intracellular signaling pathways, these growth factors can display several roles in directing neural stem cell behavior. FGF-2, for example, has been shown to drive self-renewal and proliferation of NSCs[87], is required for long-term maintenance of adult neurogenesis *in vivo*[88], and is used to maintain stemness in *in vitro* NSC cultures[89]. Similarly, EGF has been shown to maintain stem cell cultures *in vitro*[90], but its effect appears to be species-specific with different effects between the two neurogenic niches of the adult brain[60,85]. VEGF has been shown to drive a hippocampal NSC cell-autonomous proliferative effect *in vivo*, mediating stem cell renewal while not biasing a neurogenic fate[91]. In contrast, insulin-like growth factor 1 (IGF-1) appears to drive a proliferative effect, but also induces adult hippocampal NSCs to differentiate into neurons[92] and, interestingly, oligodendrocytes[93]. In short, the effects of RTK-binding growth factors are diverse and highly context-specific.

1.3.2.2 The Canonical Wnt/β-catenin Signaling Pathway

The canonical Wnt/β-catenin signaling pathway is one of the most extensively studied signaling mechanisms, and for good reason. It plays a necessary role in development, is required for proper tissue homeostasis in adults, and dysregulation of key pathway components is a major driver of a multitude of human diseases[94]. Further, genomic evidence suggests it to be a primordial metazoan pathway[95], and some proteins necessary for signal transduction even have homologues in some plants[96]. While the secreted family of Wnt proteins can elicit so-called "non-canonical" pathways to regulate Rho family GTPases and $Ca2^{+}$ signaling[97], the focus of this section and Chapter 3 of this dissertation will focus on the canonical Wnt/β-catenin pathway, herein sometimes referred to simply as "Wnt" or "Wnt pathway".

The large family of Wnt proteins—19 in the human genome discovered to date—are lipid-modified proteins with limited capacity for diffusion after secretion by cells. As such, Wnts exert

their signaling effects through immediate cell-cell contact or over small cell-cell distances. During canonical Wnt signaling, Wnt proteins bind to their co-receptors LRP5/6 and Frizzled (FZD), which activates phosphorylation events on the intracellular domain of LRP5/6. This, in turn, drives membrane sequestration of the protein Dishevelled (Dvl) as well as key components of the so-called β-catenin "destruction complex", including the proteins Axin, GSK3, and Ck1. In the absence of signaling, this destruction complex phosphorylates constitutively active β-catenin, which leads to its degradation. However, when members of the destruction complex are sequestered to the membrane by active Wnt signaling, β-catenin proteins are released from this inhibition, accumulate in the cytoplasm, and eventually translocate to the nucleus where they bind to Tcf/Lef transcription factors and activate Wnt target genes. Wnt target genes include those for β-catenin inhibitory proteins, implying negative feedback regulation of the signaling pathway, as well as numerous cell- and tissue-specific targets[94,98].

Given its important role in morphogenesis and tissue homeostasis, the role of Wnt in driving neural stem cell behavior has been readily explored. And, perhaps unsurprisingly, it has been found to be a "master regulator" of adult neurogenesis. However, there are still many outstanding questions as to how this pathway precisely dictates cell behavior, especially as its effects are context specific.

Components of the Wnt signaling pathway are readily expressed within the NSC niche and in NSCs themselves. Wnt3 has been found to direct a neuronal fate specification, and leads to increased cell division within these neuronal-committed cells[99]. In spinal cord neural precursors, Wnt3 was also found to transiently increase proliferation before inducing increased neuronal differentiation, while Wnt3a showed a prolonged proliferative effect but no increased neurogenic effect[100]. Direct infusion of Wnt7a to the adult hippocampus leads to an increase in the number of newborn neurons[101], but has also been shown to be essential for NSC self-renewal and proliferation[102]. In a different study, autonomous Wnt signaling was found to be essential for the self-renewal and maintenance of a neural stem cell population, with loss of Wnt signaling driving a neurogenic response[103]. This finding was replicated in another study that found the orphan nuclear receptor TLX to mediate adult NSC self-renewal and proliferation by activating the Wnt pathway through Wnt7a and β-catenin[104]. Lastly, delivery of a constitutively active β-catenin to adult NSCs in the hippocampus replicated the finding that β-catenin drives self-renewal and proliferation of NSCs, but it was also found to drive increased neurogenic fate specification, suggesting that Wnt signaling is able to mediate each distinct NSC behavior[105]. This finding replicated previous studies that showed activation of β-catenin via inhibition of the destruction complex member GSK-3β using lithium induced both a self-renewal and pro-neurogenic fate decision[106,107].

Altogether, these results depict an intricate and context-specific landscape through which Wnt signaling drives self-renewal, neurogenic differentiation, or sometimes both. These results yield many questions on the exact nature of Wnt's role in driving neural stem cell behavior: most of all, what are the molecular and contextual factors that yield these opposing neural stem cell behavior in response to Wnt?

1.3.2.3 Notch Signaling Pathway

The importance of the Notch gene has been known for over a century[108]. This highly conserved signaling pathway consists of several signal transduction events, and is driven by cell-cell contact between cells that express respective signaling and receptor proteins. The single-pass transmembrane proteins Delta and Jagged serve as signal-sending ligands for Notch, a single-pass transmembrane receptor protein on the surface of signal-receiving cells. Interaction between Notch with Delta or Jagged engages the proteolytic function of gamma secretase, a membrane-bound enzyme, in the Notch-expressing cell. Gamma secretase cleaves the Notch intracellular domain (NICD), which frees it from the membrane to translocate to the nucleus where it engages and activates downstream transcription factors, including RBPj, that drive expression of Notch target genes[109,110].

Components of the Notch signaling pathway are present and active in the adult brain, including in the neural stem cells of the SVZ and SGZ[111]. To date, there is *in vivo* and *in vitro* evidence that Notch signaling—driven by Notch receptors on NSCs that engage with Jagged and Delta ligands on neighboring niche cells—is required for neural stem cell maintenance and promotes their proliferation. In an *in vivo* mouse model, Notch1 overexpression in NSCs was shown to increase hippocampal NSC proliferation, while ablation of key components of the Notch pathway drove cell cycle exit and led to differentiation into transit-amplifying cells[112]. In inducible knock-out mice that lack the downstream Notch effector RBPj in adult neural stem cells, Notch signaling was shown to be necessary for the maintenance of a stem cell pool. Under knock-out conditions, mice displayed a transient 3-week increase in neurogenesis (postulated to be due to the loss of the inhibition of Notch signaling), but this came at the expense of long-term stem cell maintenance, as the stem cell pool was depleted without Notch signaling[113]. Interestingly, the attenuation of Notch signaling in post-injury striatal astrocytes has also been shown to lead to new neurons, also suggesting that Notch signaling prevents the acquisition of a neuronal fate[114]. Other studies have also shown activated Notch signaling lead to increased neural stem cell proliferation[115,116]. Taken together with other evidence[117–119], Notch signaling promotes neural stem cell proliferation and maintenance, while preventing pro-neuronal fate specification.

1.3.2.4 Sonic hedgehog

Sonic hedgehog (Shh) is the most-studied ligand of the hedgehog signaling pathway. Shh has necessary functions as a morphogen during development[120], with continued signaling impacts during adulthood and in the context of disease[121]. In the context of hedgehog signaling pathway activation, Shh is transcribed, translating, and undergoes post-translational modification in a signal-sending cell before eventual secretion. After secretion, Shh binds to the membrane-bound receptor Patched on the signal-receiving cell (in autocrine signaling, the same cell that secreted it; in paracrine signaling, a different cell). In the absence of Shh, Patched inhibits the G-protein-coupled receptor Smoothened. However, Shh binding to Patched prevents this inhibition, and Smoothened in turn is then free to activate (through a still-incompletely understood pathway) the Gli family of transcription factors, ultimately leading to activation or repression of hedgehog target genes[122,120].

Shh has been found to be a key regulator of adult neural stem cell behavior, and in particular a regulator of adult NSC self-renewal and proliferation. The Shh receptor Patched is highly expressed in the adult hippocampus as well as specifically expressed in the SGZ Nestin^{+} neural

stem cells that reside there. *In vivo* and *in vitro,* Shh elicits a strong proliferative response from adult NSCs, but does not bias their differentiation[123]. Furthermore, Shh is a known downstream target of the transcription factor *Sox2*. The conditional deletion of *Sox2* in the nervous system of adult mice led to the loss of Shh-expressing NSCs in addition to adult neurogenesis, while a pharmacological agent of Shh signaling subsequently rescued neurogenesis[124]. Interestingly, adult NSCs are also depleted in mice with a conditional knockout of Smoothened[125], and in mice with genetic disruption of one copy of the gene that encodes Patched, a defect that drives deregulation of the Notch pathway[126]. Together, these studies suggest that Shh is required for the maintenance and self-renewal of adult neural stem cells, and interacts with additional NSC niche signals to regulate additional stages of neurogenesis.

1.3.2.5 Transforming growth factor-β, bone morphogenic protein, and the TGF-β family

Members of the transforming growth factor-β (TGF-β) family include TGF-β and bone morphogenic proteins (BMPs), all of whom interact with the serine/threonine kinase receptors. These ligands bind to heteromeric receptor complexes, a molecular interaction that causes a conformational change in the receptor complex that initiates downstream phosphorylation events on serine/threonine residues. This leads to the eventual phosphorylation and activation of SMAD proteins, which translocate to the nucleus and serve as transcription factors to mediate a cell's response to the TGF-β signal[127].

In general, signaling effects of the TGF-β family have been shown to negatively impact adult neurogenesis through several mechanisms. First, chronic overproduction of TGF-β1 led to inhibited proliferation of NSCs with an associated decline in newborn immature and mature neurons[128], an effect that has been seen by others[129]. BMPs have also been shown to inhibit NSC proliferation and maintenance, and decrease neurogenic fate specification in favor of an astrocyte identity[130,131]. Further, the BMP antagonist Noggin increases NSC proliferative and neuronal fate decisions[130,132], and has been functionally linked to learning and memory formation[133]. Inhibition of BMP has further been functionally linked to exercise-induced increases of adult hippocampal neurogenesis. Lastly, it has been shown that age-related BMP signaling increases correspond to reduced NSC proliferation, and that perturbation of BMP signaling rescued this effect[69]. Together, these results display TGF-β has a typically negatively impact on adult neurogenesis through the inhibition of NSC proliferation, maintenance, and neurogenic fate specification.

1.3.2.6 Neurotransmitters

Neurotransmitters are the signaling molecules that drive neuron-to-neuron chemical communication and electrical transduction in the nervous system. Several types exist, typically divided into two main classes: small-molecule substances (including acetylcholine, dopamine, serotonin, glutamate, γ-aminobutyric acid (GABA), nitric oxide, among others) and neuroactive peptides (including somatostatin, vasopressin, melatonin, neurotensin, neuropeptide Y, among others). These biomolecules are synthesized in neurons, released by the cell into a synapse (the specialized region where two neurons communicate), and elicit a cellular response in the signal-receiving cell through interaction with receptors on the cell membrane. Types of neurotransmitter receptors are just as diverse as the signaling molecules, and are divided into two classes: ionotropic receptors, which are ion channels directly modulated by neurotransmitters, and metabotropic

receptors, which indirectly activate ion channels through downstream second messengers that are activated upon neurotransmitter binding. In general, binding of neurotransmitters to their receptors changes the flux of ions across a cell's membrane through these ion channels, which alters the electrical potential of the cell, making it more or less likely to propagate the electrical signal through an action potential. This effect can be either excitatory or inhibitory[64].

Despite their fundamental nature to the nervous system, relatively little is known about how the broad range of neurotransmitters impact adult neural stem cell behavior compared to other signaling mechanisms. However, there is growing evidence that, beyond their role in potentiating chemical and electrical signals, neurotransmitters are key biomolecular modulators in determining adult neural stem cell behavior. The hippocampus is home to several key neuron subtypes, including interneurons, mossy cells, and the mature granule cells of the dentate gyrus that adult NSCs are known to differentiate into; several neurotransmitters released by these cells have been shown to impact adult NSC behavior[85,134].

For example, interneuron-derived GABA promotes SGZ NSC quiescence[135,136] or neuronal differentiation[134], depending on the signal receptor to which it binds and its downstream inhibitory or excitatory effect[137]. Excitatory glutamate receptors have been shown to be important for NSC proliferation and survival[138] or quiescence[139], depending on the subtype of receptor activated. Glutamate, more broadly, has been shown to be required for adult-born neuron survival and maturation[140]. Further, dopamine has been shown to be important for cell proliferation in the SGZ[141]. Altogether, these results display a growing body of evidence that neurotransmitters play key roles in directing adult NSC behavior, exciting results that indicate additional possible therapeutic interventions for neurological disorders[85,141–143].

1.3.2.7 The Extracellular Matrix and Integrins

The extracellular matrix (ECM) is an interconnected framework of molecules that provide structural support for cells and regulate their behavior through biophysical and mechanical cues, as well as sequestration of secreted signaling factors. ECM proteins include laminins, collagen, fibronectin, tenascin, and vitronectin, among others. Integrins on the surface of cell membranes recognize and bind to ECM proteins, fostering stable cell adhesion and initiating important signaling cascades. Integrins are intracellularly connected to cytoskeletal F-actin through a multiprotein complex that includes talin, vinculin, and focal adhesion kinase (FAK). This connection enables cell motility by allowing a cell to create propulsive forces, and also regulates an array of signal transduction events which facilitate various cellular behaviors.

ECM proteins and integrin functions have been shown to influence adult NSC behavior. Tenascin-R, for example, engages with β1-integrin to inhibit NSC proliferation and can induce multipotent differentiation, with lineage commitment determined by which region of the protein is engaged[144], a result that has been seen by others[145]. Different stiffnesses of ECM, sensed through RhoGTPases, mediates variable differentiation with "soft" ECM (as measured by elastic modulus) biasing neuronal differentiation and "stiff" ECM reducing neurogenic fate in favor of astrocytic differentiation[146]. In addition to fate specification, ECM proteins like laminin are important for neurite formation[147] and migration[148]. Together, these results suggest that ECM proteins that

comprise the biophysical of the adult NSC niche—and the integrins they engage—are important players in regulating NSC behavior and may provide useful tools for directing their fate[26,148,149].

1.3.2.8 Glucocorticoids and Steroid Hormone Receptors

Steroid hormones are chemically distinct biomolecules—specifically, lipids—that are produced within glands of multicellular organisms, transported through the circulatory system, and exert signaling effects by engaging with steroid hormone receptors on or in target cells. Glucocorticoids, one of two classes of the adrenal gland-produced corticosteroids, function by interacting with, and activating, the nuclear hormone receptor glucocorticoid receptor (GR). In the absence of the steroid hormone, GR is cytoplasmic and inactive. In the presence of its glucocorticoid ligand, GR undergoes a conformation change that leads to its activation and translocation to the nucleus. Once nuclear-localized, GR binds to glucocorticoid response element (GRE) DNA sequences, thereby regulating transcriptional activation or repression of target genes that drive a cell's response to signaling[150].

A growing body of research suggests that glucocorticoids, which are stress-response hormones, impart stress-induced negative impacts on adult hippocampal neurogenesis. Not only is proliferation of putative neural stem cells in the dentate gyrus reduced under stress[151], stress and the associated glucocorticoids negatively impacts NSCs survival[152] and inhibits NSC neuronal differentiation[153]. Further, stress has been shown to increase differentiation of $Nestin^+$ NSCs into oligodendrocytes *in vivo* with a corresponding decrease in neuronal fate specification; and, the glucocorticoid corticosterone (cort) was sufficient to replicate those cell fate observations. In concert with this result, cort was also shown to drive a pro-oligodendrocytic transcriptional program in *in vitro* hippocampal NSCs[59]. These results offer promise in shedding light on the role of adult neurogenesis in a multitude of neurological disorders that are stress- and stress hormone-related[60].

1.4 The case for investigating adult NSC behavior in response to complex biomolecular signaling logic

After the discovery of adult neural stem cells, much research (including the work in the previous section) has explored how and why they behave in particular ways. Much of this work has focused on a singular parameter space by isolating specific biomolecular targets, and shedding light on the behavior of NSCs in that specific context. Undoubtedly, this work has dramatically advanced the field and has offered crucial insight into how the presence or absence—that is, the simple binary conditional logic—of a single isolated factor influences NSC behavior. However, there are clear limitations to this framework.

Our understanding of the adult neural stem cell niche provides a much more complex picture than studying single cues through the framework of a simple binary conditional logic. *In vivo,* neural stem cells do not simply experience singular biomolecular cues in isolation that dictate one behavior or another; rather, NSCs are bombarded with a complex milieu of cues that include multiple biomolecular signals that, in isolation, drive mutually exclusive fate decisions[26,55]. In short, NSCs make decisions through a "complex logic". How does the neural stem cell integrate these multiple, often conflicting cues and decide which path to take? Should it self-renew?

Differentiate? Remain quiescent? Further, it is understood that various cues fluctuate in time, space, and intensity[154]. Beyond the simple presence or absence of a cue, how do these relative conditional factors influence the neural stem cell's ultimate decision? (Figure 1.4)

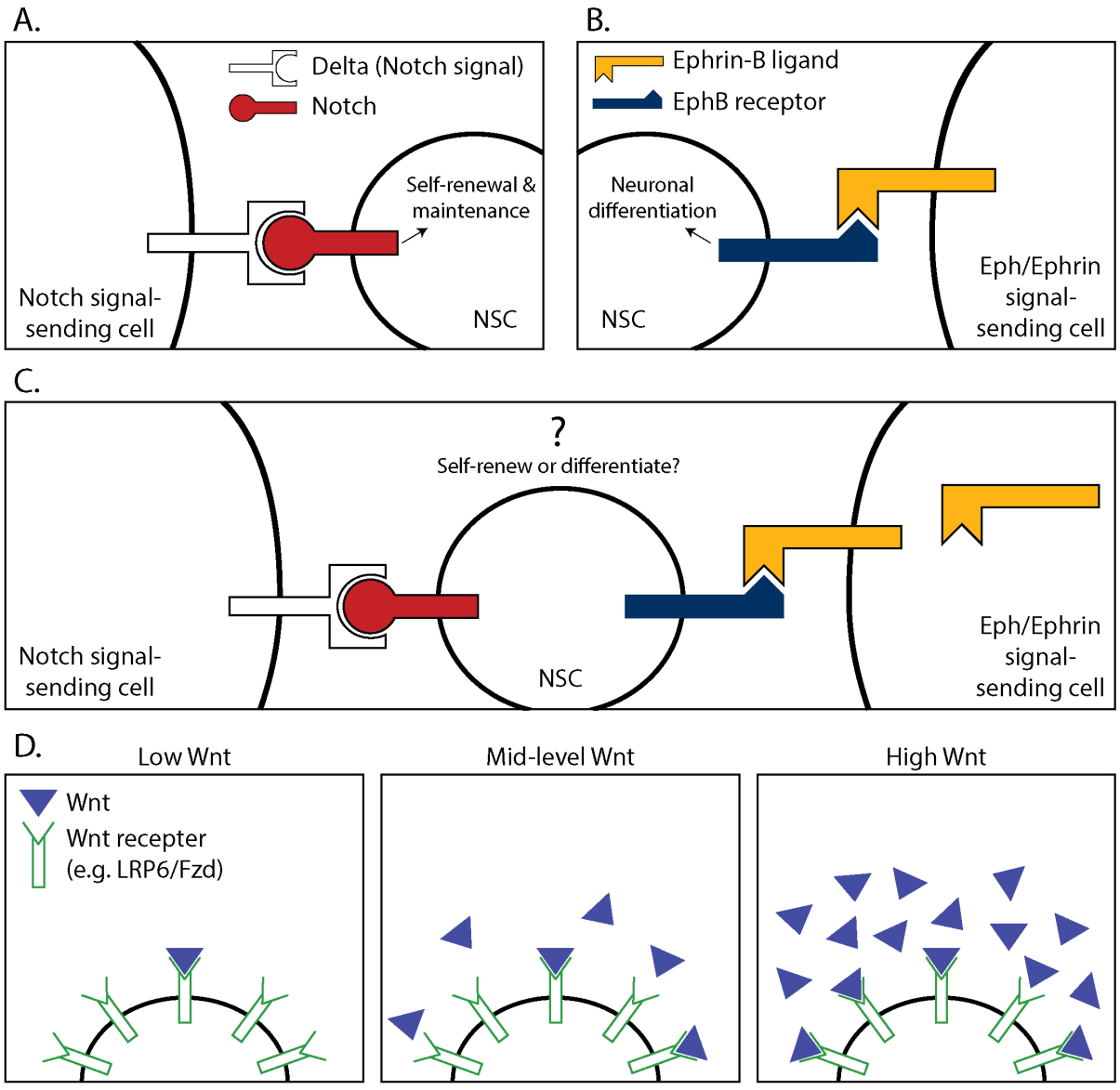

Figure 1.4 Adult neural stem cells experience complex biomolecular signaling logic. A. Notch signaling in isolation drives neural stem cell self-renewal and maintenance. B. Eph/ephrin signaling in isolation, in particular Ephrin B2/EphB4, drives neuronal differentiation in NSCs. C. Example of complex biomolecular signaling logic in which an NSC receives two mutually exclusive "competing" cues. D. Complex biomolecular signaling logic includes the relative strength of activation, for example the strength of Wnt signaling activation by varying concentrations of Wnt ligands.

The last several decades of research have offered much insight into the behavior of neural stem cells. To continue advancing the fields of neural stem cell biology and adult neurogenesis, our understanding of NSC fate decisions must continue to move toward an expanded framework of complex logic. Insight into how the full breadth of biomolecular signaling factors coordinate and integrate with one another to ultimately influence NSC behavior will continue to advance the field

and deepen our understanding of the *in vivo* relevance and function of neural stem cells. Further, while new tools have begun to emerge to explore questions of complex logic[155,156], continued development and application of novel techniques will certainly help advance this understanding. In particular, while the field of systems biology has contributed greatly to these efforts over the past decade-plus[158,159], platforms that further enable direct observation of final whole-cell fate outcome would enhance our overall view of how complex logic regulates stem cell behavior.

1.5 Scope of dissertation

This dissertation was motivated by the need to advance a deeper understanding of the signaling mechanisms that drive adult hippocampal neural stem cell fate behavior, and to elucidate the complex logic through which those decisions are made in response to complex biomolecular signaling. This insight not only advances our appreciation for the depth in which normal mammalian physiology functions, but also holds therapeutic potential for a host of neurological disorders, diseases, and age-related declines in cognitive function. In **Chapter 2**, we develop a single-cell patterning platform that enables long-term observation of our cells *in vitro* in precisely-defined cellular communities, which enables us to explore NSC fate behavior in response to conflicting cues. Specifically, we aim to address the question: if an NSC is presented with Notch signaling, which promotes maintenance and self-renewal, **and** Eph-ephrin signaling through ephrin-B2, which promotes neuronal differentiation, what fate does a cell choose? In **Chapter 3**, we expound on the canonical Wnt/β-catenin signaling pathway's role in driving NSC behavior, and link the pathway's influence on proliferation during differentiation to a strength-of-pathway-activation signaling logic. Finally, in **Chapter 4** we discuss early evidence of other factors in complex signaling logic that may play a role in driving NSC behavior, including cell density and cell cycle state.

1.6 References

1. Haeckel, E. *Natürliche schöpfungsgeschichte*. (Georg Reimer, 1868).
2. Ramalho-Santos, M. & Willenbring, H. On the Origin of the Term "Stem Cell". *Cell Stem Cell* **1**, 35–38 (2007).
3. Till, J. E., McCulloch, E. A. & Siminovitch, L. A stochastic model of stem cell proliferation, based on the growth of spleen colony-forming cells. *Proceedings of the National Academy of Sciences of the United States of America* **51**, 29 (1964).
4. Becker, A. J., McCulloch, E. A. & Till, J. E. Cytological Demonstration of the Clonal Nature of Spleen Colonies Derived from Transplanted Mouse marrow Cells. *Nature* (1963).
5. Tajbakhsh, S. Stem cell: what's in a name? *Nature Reports Stem Cells* (2009). doi:https://doi.org/10.1038/stemcells.2009.90
6. Raven, P., Johnson, G., Mason, K., Loso, J. & Singer, S. *Biology*. (McGraw-Hill, 2011).
7. Evans, M. J. & Kaufman, M. H. Establishment in culture of pluripotential cells from mouse embryos. *Nature* **292**, 154–156 (1981).
8. Martin, G. R. Isolation of a pluripotent cell line from early mouse embryos cultured in medium conditioned by teratocarcinoma stem cells. *Proceedings of the National Academy of Sciences* **78**, 7634–7638 (1981).
9. Gordon, J. W., Scangos, G. A., Plotkin, D. J., Barbosa, J. A. & Ruddle, F. H. Genetic transformation of mouse embryos by microinjection of purified DNA. *Proceedings of the National Academy of Sciences* **77**, 7380–7384 (1980).
10. Doetschman, T. *et al.* Targetted correction of a mutant HPRT gene in mouse embryonic stem cells. *Nature* **330**, 576–578 (1987).
11. Thomas, K. R. & Capecchi, M. R. Site-directed mutagenesis by gene targeting in mouse embryo-derived stem cells. *Cell* **51**, 503–512 (1987).
12. Zijlstra, M. *et al.* β2-Microglobulin deficient mice lack CD4-8+ cytolytic T cells. *Nature* **344**, 742–746 (1990).
13. Koller, B. H. & Smithies, O. Inactivating the beta 2-microglobulin locus in mouse embryonic stem cells by homologous recombination. *Proceedings of the National Academy of Sciences* **86**, 8932–8935 (1989).
14. Thomson, J. A. *et al.* Embryonic stem cell lines derived from human blastocysts. *science* **282**, 1145–1147 (1998).
15. Wertz, D. C. Embryo and stem cell research in the United States: history and politics. *Gene Therapy* **9**, 674–678 (2002).
16. Trounson, A., Thakar, R. G., Lomax, G. & Gibbons, D. Clinical trials for stem cell therapies. *BMC Medicine* **9**, (2011).
17. Gurdon, J. B. The Developmental Capacity of Nuclei taken from Intestinal Epithelium Cells of Feeding Tadpoles. *Development* **10**, 622–640 (1962).
18. Takahashi, K. & Yamanaka, S. Induction of Pluripotent Stem Cells from Mouse Embryonic and Adult Fibroblast Cultures by Defined Factors. *Cell* **126**, 663–676 (2006).
19. Yu, J. *et al.* Induced Pluripotent Stem Cell Lines Derived from Human Somatic Cells. **318**, 5 (2007).
20. Angelos, M. G. & Kaufman, D. S. Pluripotent stem cell applications for regenerative medicine: *Current Opinion in Organ Transplantation* 1 (2015). doi:10.1097/MOT.0000000000000244

21. Drost, J. & Clevers, H. Translational applications of adult stem cell-derived organoids. *Development* **144**, 968–975 (2017).
22. Henig, I. & Zuckerman, T. Hematopoietic Stem Cell Transplantation—50 Years of Evolution and Future Perspectives. *Rambam Maimonides Medical Journal* **5**, e0028 (2014).
23. CIRM-funded Clinical Trials. (2019).
24. Cohen, D. E. & Melton, D. Turning straw into gold: directing cell fate for regenerative medicine. *Nature Reviews Genetics* **12**, 243–252 (2011).
25. Simian, M. & Bissell, M. J. Organoids: A historical perspective of thinking in three dimensions. *The Journal of Cell Biology* **216**, 31–40 (2017).
26. Bond, A. M., Ming, G. & Song, H. Adult Mammalian Neural Stem Cells and Neurogenesis: Five Decades Later. *Cell Stem Cell* **17**, 385–395 (2015).
27. Paridaen, J. T. & Huttner, W. B. Neurogenesis during development of the vertebrate central nervous system. *EMBO reports* **15**, 351–364 (2014).
28. Gage, F. Adult neurogenesis in mammals. *Science* **364**, 827–828 (2019).
29. Lim, D. A. & Alvarez-Buylla, A. The Adult Ventricular–Subventricular Zone (V-SVZ) and Olfactory Bulb (OB) Neurogenesis. *Cold Spring Harbor Perspectives in Biology* **8**, a018820 (2016).
30. Gross, C. A. Neurogenesis in the adult brain: death of a dogma. *Nature Reviews Neuroscience* **1**, 67–73 (2000).
31. Altman, J. Are New Neurons Formed in the Brains of Adult Mammals? *Science* **135**, 1127–1128 (1962).
32. Altman, J. & Das, G. D. Autoradiographic and histological evidence of postnatal hippocampal neurogenesis in rats. *Journal of Comparative Neurology* **124**, 319–335 (1965).
33. Altman, J. Autoradiographic investigation of cell proliferation in the brains of rats and cats. *Anatomical Record* **145**, 573–592 (1963).
34. Altman, J. Postnatal neurogenesis in the guinea-pig. *Nature* **214**, 1098–1101 (1967).
35. Paton, J. A. & Nottebohm, F. N. Neurons generated in the adult brain are recruited into functional circuits. *Science* **225**, 1046–1048 (1984).
36. Reynolds, B. A. & Weiss, S. Generation of neurons and astrocytes from isolated cells of the adult mammalian central nervous system. *Science* **255**, 1707–1710 (1992).
37. Eriksson, P. S. *et al.* Neurogenesis in the adult human hippocampus. *Nature medicine* **4**, 1313 (1998).
38. Sorrells, S. F. *et al.* Human hippocampal neurogenesis drops sharply in children to undetectable levels in adults. *Nature* **555**, 377–381 (2018).
39. Kempermann, G. *et al.* Human Adult Neurogenesis: Evidence and Remaining Questions. *Cell Stem Cell* **23**, 25–30 (2018).
40. Spalding, K. L. *et al.* Dynamics of Hippocampal Neurogenesis in Adult Humans. *Cell* **153**, 1219–1227 (2013).
41. Boldrini, M. *et al.* Human Hippocampal Neurogenesis Persists throughout Aging. *Cell Stem Cell* **22**, 589-599.e5 (2018).
42. Tobin, M. K. *et al.* Human Hippocampal Neurogenesis Persists in Aged Adults and Alzheimer's Disease Patients. *Cell Stem Cell* **24**, 974-982.e3 (2019).
43. Moreno-Jiménez, E. P. *et al.* Adult hippocampal neurogenesis is abundant in neurologically healthy subjects and drops sharply in patients with Alzheimer's disease. *Nature Medicine* **25**, 554–560 (2019).

44. Ming, G. & Song, H. Adult Neurogenesis in the Mammalian Brain: Significant Answers and Significant Questions. *Neuron* **70**, 687–702 (2011).
45. Zhang, J. & Jiao, J. Molecular Biomarkers for Embryonic and Adult Neural Stem Cell and Neurogenesis. *BioMed Research International* **2015**, 1–14 (2015).
46. Doetsch, F., García-Verdugo, J. M. & Alvarez-Buylla, A. Cellular Composition and Three-Dimensional Organization of the Subventricular Germinal Zone in the Adult Mammalian Brain. *The Journal of Neuroscience* **17**, 5046–5061 (1997).
47. Mirzadeh, Z., Merkle, F. T., Soriano-Navarro, M., Garcia-Verdugo, J. M. & Alvarez-Buylla, A. Neural Stem Cells Confer Unique Pinwheel Architecture to the Ventricular Surface in Neurogenic Regions of the Adult Brain. *Cell Stem Cell* **3**, 265–278 (2008).
48. Shen, Q. *et al.* Adult SVZ Stem Cells Lie in a Vascular Niche: A Quantitative Analysis of Niche Cell-Cell Interactions. *Cell Stem Cell* **3**, 289–300 (2008).
49. Tavazoie, M. *et al.* A Specialized Vascular Niche for Adult Neural Stem Cells. *Cell Stem Cell* **3**, 279–288 (2008).
50. Batista-Brito, R., Close, J., Machold, R. & Fishell, G. The Distinct Temporal Origins of Olfactory Bulb Interneuron Subtypes. *Journal of Neuroscience* **28**, 3966–3975 (2008).
51. Menn, B. *et al.* Origin of Oligodendrocytes in the Subventricular Zone of the Adult Brain. *Journal of Neuroscience* **26**, 7907–7918 (2006).
52. Benner, E. J. *et al.* Protective astrogenesis from the SVZ niche after injury is controlled by Notch modulator Thbs4. *Nature* **497**, 369–373 (2013).
53. Filippov, V. *et al.* Subpopulation of nestin-expressing progenitor cells in the adult murine hippocampus shows electrophysiological and morphological characteristics of astrocytes. *Molecular and Cellular Neuroscience* **23**, 373–382 (2003).
54. Bonaguidi, M. A. *et al.* In Vivo Clonal Analysis Reveals Self-Renewing and Multipotent Adult Neural Stem Cell Characteristics. *Cell* **145**, 1142–1155 (2011).
55. Miller, F. D. & Gauthier-Fisher, A. Home at Last: Neural Stem Cell Niches Defined. *Cell Stem Cell* **4**, 507–510 (2009).
56. Kempermann, G., Song, H. & Gage, F. H. Neurogenesis in the Adult Hippocampus. *Cold Spring Harbor Perspectives in Biology* **7**, a018812 (2015).
57. Biebl, M., Cooper, C. M., Winkler, J. & Kuhn, H. G. Analysis of neurogenesis and programmed cell death reveals a self-renewing capacity in the adult rat brain. *Neuroscience Letters* **291**, 17–20 (2000).
58. Gonçalves, J. T. *et al.* In vivo imaging of dendritic pruning in dentate granule cells. *Nature Neuroscience* **19**, 788–791 (2016).
59. Chetty, S. *et al.* Stress and glucocorticoids promote oligodendrogenesis in the adult hippocampus. *Molecular psychiatry* **19**, 1275–1283 (2014).
60. Balu, D. T. & Lucki, I. Adult hippocampal neurogenesis: Regulation, functional implications, and contribution to disease pathology. *Neuroscience & Biobehavioral Reviews* **33**, 232–252 (2009).
61. Gonçalves, J. T., Schafer, S. T. & Gage, F. H. Adult Neurogenesis in the Hippocampus: From Stem Cells to Behavior. *Cell* **167**, 897–914 (2016).
62. Jessberger, S. & Gage, F. H. Adult neurogenesis: bridging the gap between mice and humans. *Trends in Cell Biology* **24**, 558–563 (2014).
63. Ernst, A. *et al.* Neurogenesis in the Striatum of the Adult Human Brain. *Cell* **156**, 1072–1083 (2014).

64. Kandel, E. R., Schwartz, J. H., Jessell, T. M., Siegelbaum, S. A. & Hudspeth, A. J. *Principles of Neural Science*. (McGraw-Hill, 2013).
65. Drapeau, E. *et al.* Spatial memory performances of aged rats in the water maze predict levels of hippocampal neurogenesis. *Proceedings of the National Academy of Sciences* **100**, 14385–14390 (2003).
66. van Praag, H. Exercise Enhances Learning and Hippocampal Neurogenesis in Aged Mice. *Journal of Neuroscience* **25**, 8680–8685 (2005).
67. Driscoll, I. *et al.* The aging hippocampus: A multi-level analysis in the rat. *Neuroscience* **139**, 1173–1185 (2006).
68. Lieberwirth, C., Pan, Y., Liu, Y., Zhang, Z. & Wang, Z. Hippocampal adult neurogenesis: Its regulation and potential role in spatial learning and memory. *Brain Research* **1644**, 127–140 (2016).
69. Yousef, H. *et al.* Age-Associated Increase in BMP Signaling Inhibits Hippocampal Neurogenesis: Increased BMP Signaling Inhibits Neurogenesis with Aging. *STEM CELLS* **33**, 1577–1588 (2015).
70. Curtis, M. A. *et al.* Increased cell proliferation and neurogenesis in the adult human Huntington's disease brain. *Proceedings of the National Academy of Sciences* **100**, 9023–9027 (2003).
71. Duan, X. *et al.* Disrupted-In-Schizophrenia 1 Regulates Integration of Newly Generated Neurons in the Adult Brain. *Cell* **130**, 1146–1158 (2007).
72. Miller, B. R. & Hen, R. The current state of the neurogenic theory of depression and anxiety. *Current Opinion in Neurobiology* **30**, 51–58 (2015).
73. Besnard, A. & Sahay, A. Adult Hippocampal Neurogenesis, Fear Generalization, and Stress. *Neuropsychopharmacology* **41**, 24–44 (2016).
74. Kheirbek, M. A., Klemenhagen, K. C., Sahay, A. & Hen, R. Neurogenesis and generalization: a new approach to stratify and treat anxiety disorders. *Nature Neuroscience* **15**, 1613–1620 (2012).
75. Meerlo, P., Mistlberger, R. E., Jacobs, B. L., Craig Heller, H. & McGinty, D. New neurons in the adult brain: The role of sleep and consequences of sleep loss. *Sleep Medicine Reviews* **13**, 187–194 (2009).
76. Jessberger, S. & Parent, J. M. Epilepsy and Adult Neurogenesis. *Cold Spring Harbor Perspectives in Biology* a020677 (2015). doi:10.1101/cshperspect.a020677
77. Brock, T. D. & Freeze, H. Thermus aquaticus gen. n. and sp. n., a Non- sporulating Extreme Thermophile. *J. BACTERIOL.* **98**, 9 (1969).
78. Barrangou, R. *et al.* CRISPR Provides Acquired Resistance Against Viruses in Prokaryotes. *Science* **315**, 1709–1712 (2007).
79. Mader, S. *et al. Biology*. (McGraw-Hill, 2013).
80. Kania, A. & Klein, R. Mechanisms of ephrin–Eph signalling in development, physiology and disease. *Nature Reviews Molecular Cell Biology* **17**, 240–256 (2016).
81. Jiao, J. -w., Feldheim, D. A. & Chen, D. F. Ephrins as negative regulators of adult neurogenesis in diverse regions of the central nervous system. *Proceedings of the National Academy of Sciences* **105**, 8778–8783 (2008).
82. Chumley, M. J., Catchpole, T., Silvany, R. E., Kernie, S. G. & Henkemeyer, M. EphB Receptors Regulate Stem/Progenitor Cell Proliferation, Migration, and Polarity during Hippocampal Neurogenesis. *Journal of Neuroscience* **27**, 13481–13490 (2007).

83. Ashton, R. S. *et al.* Astrocytes regulate adult hippocampal neurogenesis through ephrin-B signaling. *Nature Neuroscience* **15**, 1399–1406 (2012).
84. Laussu, J., Khuong, A., Gautrais, J. & Davy, A. Beyond boundaries—Eph:ephrin signaling in neurogenesis. *Cell Adhesion & Migration* **8**, 349–359 (2014).
85. Faigle, R. & Song, H. Signaling mechanisms regulating adult neural stem cells and neurogenesis. *Biochimica et Biophysica Acta (BBA) - General Subjects* **1830**, 2435–2448 (2013).
86. Lemmon, M. A. & Schlessinger, J. Cell Signaling by Receptor Tyrosine Kinases. *Cell* **141**, 1117–1134 (2010).
87. Gage, F. H. *et al.* Survival and differentiation of adult neuronal progenitor cells transplanted to the adult brain. *Proceedings of the National Academy of Sciences* **92**, 11879–11883 (1995).
88. Zhao, M. *et al.* Fibroblast Growth Factor Receptor-1 is Required for Long-Term Potentiation, Memory Consolidation, and Neurogenesis. *Biological Psychiatry* **62**, 381–390 (2007).
89. Peltier, J., Agrawal, S., Robertson, M. J. & Schaffer, D. V. In Vitro Culture and Analysis of Adult Hippocampal Neural Progenitors. in *Protocols for Adult Stem Cells* (eds. Conboy, I. M., Schaffer, D. V., Barcellos-Hoff, M. H. & Li, S.) **621**, 65–87 (Humana Press, 2010).
90. Walker, T. L. & Kempermann, G. One Mouse, Two Cultures: Isolation and Culture of Adult Neural Stem Cells from the Two Neurogenic Zones of Individual Mice. *Journal of Visualized Experiments* (2014). doi:10.3791/51225
91. Kirby, E. D., Kuwahara, A. A., Messer, R. L. & Wyss-Coray, T. Adult hippocampal neural stem and progenitor cells regulate the neurogenic niche by secreting VEGF. *Proceedings of the National Academy of Sciences* **112**, 4128–4133 (2015).
92. Åberg, M. A. I., Åberg, N. D., Hedbäcker, H., Oscarsson, J. & Eriksson, P. S. Peripheral Infusion of IGF-I Selectively Induces Neurogenesis in the Adult Rat Hippocampus. *The Journal of Neuroscience* **20**, 2896–2903 (2000).
93. Hsieh, J. *et al.* IGF-I instructs multipotent adult neural progenitor cells to become oligodendrocytes. *The Journal of Cell Biology* **164**, 111–122 (2004).
94. Wiese, K. E., Nusse, R. & van Amerongen, R. Wnt signalling: conquering complexity. *Development* **145**, dev165902 (2018).
95. Holstein, T. W. The Evolution of the Wnt Pathway. *Cold Spring Harbor Perspectives in Biology* **4**, a007922–a007922 (2012).
96. Sharma, M., Pandey, A. & Pandey, G. K. β-catenin in plants and animals: common players but different pathways. *Frontiers in Plant Science* **5**, (2014).
97. Steinhart, Z. & Angers, S. Wnt signaling in development and tissue homeostasis. *Development* **145**, dev146589 (2018).
98. MacDonald, B. T. & He, X. Frizzled and LRP5/6 Receptors for Wnt/β-Catenin Signaling. *Cold Spring Harbor Perspectives in Biology* **4**, a007880–a007880 (2012).
99. Lie, D.-C. *et al.* Wnt signalling regulates adult hippocampal neurogenesis. *Nature* **437**, 1370–1375 (2005).
100. David, M. D., Cantí, C. & Herreros, J. Wnt-3a and Wnt-3 differently stimulate proliferation and neurogenesis of spinal neural precursors and promote neurite outgrowth by canonical signaling. *Journal of Neuroscience Research* **88**, 3011–3023 (2010).
101. Ortiz-Matamoros, A. & Arias, C. Differential Changes in the Number and Morphology of the New Neurons after Chronic Infusion of Wnt7a, Wnt5a, and Dkk-1 in the Adult

Hippocampus *In Vivo*: Wnt signaling modulation and neurogenesis. *The Anatomical Record* (2019). doi:10.1002/ar.24069
102. Qu, Q. *et al.* Wnt7a Regulates Multiple Steps of Neurogenesis. *Molecular and Cellular Biology* **33**, 2551–2559 (2013).
103. Wexler, E. M., Paucer, A., Kornblum, H. I., Palmer, T. D. & Geschwind, D. H. Endogenous Wnt Signaling Maintains Neural Progenitor Cell Potency. *Stem Cells* **27**, 1130–1141 (2009).
104. Qu, Q. *et al.* Orphan nuclear receptor TLX activates Wnt/β-catenin signalling to stimulate neural stem cell proliferation and self-renewal. *Nature Cell Biology* **12**, 31–40 (2010).
105. Kotterman, M. A., Vazin, T. & Schaffer, D. V. Enhanced selective gene delivery to neural stem cells in vivo by an adeno-associated viral variant. *Development* **142**, 1885–1892 (2015).
106. Fiorentini, A., Rosi, M. C., Grossi, C., Luccarini, I. & Casamenti, F. Lithium Improves Hippocampal Neurogenesis, Neuropathology and Cognitive Functions in APP Mutant Mice. *PLoS ONE* **5**, e14382 (2010).
107. Wexler, E. M., Geschwind, D. H. & Palmer, T. D. Lithium regulates adult hippocampal progenitor development through canonical Wnt pathway activation. *Molecular Psychiatry* **13**, 285–292 (2008).
108. Mohr, O. L. Character changes caused by mutation of an entire region of a chromosome in drosophila. *Genetics* **4**, 275–282 (1919).
109. Artavanis-Tsakonas, S. Notch Signaling: Cell Fate Control and Signal Integration in Development. *Science* **284**, 770–776 (1999).
110. Kovall, R. A., Gebelein, B., Sprinzak, D. & Kopan, R. The Canonical Notch Signaling Pathway: Structural and Biochemical Insights into Shape, Sugar, and Force. *Developmental Cell* **41**, 228–241 (2017).
111. Stump, G. *et al.* Notch1 and its ligands Delta-like and Jagged are expressed and active in distinct cell populations in the postnatal mouse brain. *Mechanisms of Development* **114**, 153–159 (2002).
112. Breunig, J. J., Silbereis, J., Vaccarino, F. M., Sestan, N. & Rakic, P. Notch regulates cell fate and dendrite morphology of newborn neurons in the postnatal dentate gyrus. *Proceedings of the National Academy of Sciences* **104**, 20558–20563 (2007).
113. Imayoshi, I., Sakamoto, M., Yamaguchi, M., Mori, K. & Kageyama, R. Essential Roles of Notch Signaling in Maintenance of Neural Stem Cells in Developing and Adult Brains. *Journal of Neuroscience* **30**, 3489–3498 (2010).
114. Magnusson, J. P. *et al.* A latent neurogenic program in astrocytes regulated by Notch signaling in the mouse. *Science* **346**, 237–241 (2014).
115. Lin, R. *et al.* Systemic Factors Trigger Vasculature Cells to Drive Notch Signaling and Neurogenesis in Neural Stem Cells in the Adult Brain: Systemic VEGF Drives Brain Neurogenesis via DLL4. *Stem Cells* **37**, 395–406 (2019).
116. Wang, R. *et al.* Notch1 promotes mouse spinal neural stem and progenitor cells proliferation via p-p38-pax6 induced cyclin D1 activation. *Experimental Cell Research* **373**, 80–90 (2018).
117. Ottone, C. *et al.* Direct cell–cell contact with the vascular niche maintains quiescent neural stem cells. *Nature Cell Biology* **16**, 1045–1056 (2014).
118. Ables, J. L. *et al.* Notch1 Is Required for Maintenance of the Reservoir of Adult Hippocampal Stem Cells. *Journal of Neuroscience* **30**, 10484–10492 (2010).

119. Ehm, O. *et al.* RBPJ -Dependent Signaling Is Essential for Long-Term Maintenance of Neural Stem Cells in the Adult Hippocampus. *Journal of Neuroscience* **30**, 13794–13807 (2010).
120. Fuccillo, M., Joyner, A. L. & Fishell, G. Morphogen to mitogen: the multiple roles of hedgehog signalling in vertebrate neural development. *Nature Reviews Neuroscience* **7**, 772–783 (2006).
121. Yao, P. J., Petralia, R. S. & Mattson, M. P. Sonic Hedgehog Signaling and Hippocampal Neuroplasticity. *Trends in Neurosciences* **39**, 840–850 (2016).
122. Wilson, C. W. & Chuang, P.-T. Mechanism and evolution of cytosolic Hedgehog signal transduction. *Development* **137**, 2079–2094 (2010).
123. Lai, K., Kaspar, B. K., Gage, F. H. & Schaffer, D. V. Sonic hedgehog regulates adult neural progenitor proliferation in vitro and in vivo. *Nature Neuroscience* **6**, 21–27 (2003).
124. Favaro, R. *et al.* Hippocampal development and neural stem cell maintenance require Sox2-dependent regulation of Shh. *Nature Neuroscience* **12**, 1248–1256 (2009).
125. Balordi, F. & Fishell, G. Hedgehog Signaling in the Subventricular Zone Is Required for Both the Maintenance of Stem Cells and the Migration of Newborn Neurons. *Journal of Neuroscience* **27**, 5936–5947 (2007).
126. Antonelli, F., Casciati, A. & Pazzaglia, S. Sonic hedgehog signaling controls dentate gyrus patterning and adult neurogenesis in the hippocampus. *Neural Regeneration Research* **14**, 59 (2019).
127. Kandasamy, M., Reilmann, R., Winkler, J., Bogdahn, U. & Aigner, L. Transforming Growth Factor-Beta Signaling in the Neural Stem Cell Niche: A Therapeutic Target for Huntington's Disease. *Neurology Research International* **2011**, 1–13 (2011).
128. Wachs, F.-P. *et al.* Transforming Growth Factor-β1 Is a Negative Modulator of Adult Neurogenesis. *J Neuropathol Exp Neurol* **65**, 13 (2006).
129. Buckwalter, M. S. *et al.* Chronically Increased Transforming Growth Factor-β1 Strongly Inhibits Hippocampal Neurogenesis in Aged Mice. *The American Journal of Pathology* **169**, 154–164 (2006).
130. Lim, D. A. *et al.* Noggin Antagonizes BMP Signaling to Create a Niche for Adult Neurogenesis. *Neuron* **28**, 713–726 (2000).
131. Porlan, E. *et al.* Transcriptional repression of Bmp2 by p21Waf1/Cip1 links quiescence to neural stem cell maintenance. *Nature Neuroscience* **16**, 1567–1575 (2013).
132. Bonaguidi, M. A. *et al.* Noggin Expands Neural Stem Cells in the Adult Hippocampus. *Journal of Neuroscience* **28**, 9194–9204 (2008).
133. Xiao-Tang, F., Wen-Qin, C., Zhong, Y., Hai-Wei, X. & Jin-Hai, Z. Effect of antisense oligonucleotide of noggin on spatial learning and memory of rats. *Acta Pharmacol Sin* 4 (2003).
134. Tozuka, Y., Fukuda, S., Namba, T., Seki, T. & Hisatsune, T. GABAergic Excitation Promotes Neuronal Differentiation in Adult Hippocampal Progenitor Cells. *Neuron* **47**, 803–815 (2005).
135. Song, J. *et al.* Neuronal circuitry mechanism regulating adult quiescent neural stem-cell fate decision. *Nature* **489**, 150–154 (2012).
136. Felice, D., O'Leary, O. F., Pizzo, R. C. & Cryan, J. F. Blockade of the GABAB receptor increases neurogenesis in the ventral but not dorsal adult hippocampus: Relevance to antidepressant action. *Neuropharmacology* **63**, 1380–1388 (2012).

137. Catavero, C., Bao, H. & Song, J. Neural mechanisms underlying GABAergic regulation of adult hippocampal neurogenesis. *Cell and Tissue Research* **371**, 33–46 (2018).
138. Di Giorgi-Gerevini, V. *et al.* Endogenous activation of metabotropic glutamate receptors supports the proliferation and survival of neural progenitor cells. *Cell Death & Differentiation* **12**, 1124–1133 (2005).
139. Yoshimizu, T. & Chaki, S. Increased cell proliferation in the adult mouse hippocampus following chronic administration of group II metabotropic glutamate receptor antagonist, MGS0039. *Biochemical and Biophysical Research Communications* **315**, 493–496 (2004).
140. Tashiro, A., Sandler, V. M., Toni, N., Zhao, C. & Gage, F. H. NMDA-receptor-mediated, cell-specific integration of new neurons in adult dentate gyrus. *Nature* **442**, 929–933 (2006).
141. Höglinger, G. U. *et al.* Dopamine depletion impairs precursor cell proliferation in Parkinson disease. *Nature Neuroscience* **7**, 726–735 (2004).
142. Jansson, L. C. & Åkerman, K. E. The role of glutamate and its receptors in the proliferation, migration, differentiation and survival of neural progenitor cells. *Journal of Neural Transmission* **121**, 819–836 (2014).
143. Alenina, N. & Klempin, F. The role of serotonin in adult hippocampal neurogenesis. *Behavioural Brain Research* **277**, 49–57 (2015).
144. Liao, H. *et al.* β 1 Integrin-mediated Effects of Tenascin-R Domains EGFL and FN6-8 on Neural Stem/Progenitor Cell Proliferation and Differentiation in Vitro. *Journal of Biological Chemistry* **283**, 27927–27936 (2008).
145. Xu, J.-C. *et al.* The extracellular matrix glycoprotein tenascin-R regulates neurogenesis during development and in the adult dentate gyrus of mice. *Journal of Cell Science* **127**, 641–652 (2014).
146. Keung, A. J., de Juan-Pardo, E. M., Schaffer, D. V. & Kumar, S. Rho GTPases Mediate the Mechanosensitive Lineage Commitment of Neural Stem Cells. *Stem Cells* **29**, 1886–1897 (2011).
147. Mammadov, B., Mammadov, R., Guler, M. O. & Tekinay, A. B. Cooperative effect of heparan sulfate and laminin mimetic peptide nanofibers on the promotion of neurite outgrowth. *Acta Biomaterialia* **8**, 2077–2086 (2012).
148. Wilems, T., Vardhan, S., Wu, S. & Sakiyama-Elbert, S. The influence of microenvironment and extracellular matrix molecules in driving neural stem cell fate within biomaterials. *Brain Research Bulletin* **148**, 25–33 (2019).
149. Cope, E. C. & Gould, E. Adult Neurogenesis, Glia, and the Extracellular Matrix. *Cell Stem Cell* **24**, 690–705 (2019).
150. Ramamoorthy, S. & Cidlowski, J. A. Exploring the Molecular Mechanisms of Glucocorticoid Receptor Action from Sensitivity to Resistance. in *Endocrine Development* (eds. Maghnie, M., Loche, S., Cappa, M., Ghizzoni, L. & Lorini, R.) **24**, 41–56 (S. KARGER AG, 2013).
151. Gould, E., Tanapat, P., McEwen, B. S., Flugge, G. & Fuchs, E. Proliferation of granule cell precursors in the dentate gyrus of adult monkeys is diminished by stress. *Proceedings of the National Academy of Sciences* **95**, 3168–3171 (1998).
152. Wong, E. Y. H. & Herbert, J. The corticoid environment: a determining factor for neural progenitors' survival in the adult hippocampus. *European Journal of Neuroscience* **20**, 2491–2498 (2004).

153. Wong, E. Y. H. & Herbert, J. Raised circulating corticosterone inhibits neuronal differentiation of progenitor cells in the adult hippocampus. *Neuroscience* **137**, 83–92 (2006).
154. Purvis, J. E. & Lahav, G. Encoding and Decoding Cellular Information through Signaling Dynamics. *Cell* **152**, 945–956 (2013).
155. Bugaj, L. J., Choksi, A. T., Mesuda, C. K., Kane, R. S. & Schaffer, D. V. Optogenetic protein clustering and signaling activation in mammalian cells. *Nature Methods* **10**, 249–252 (2013).
156. Muckom, R. *et al.* High-throughput combinatorial screening reveals interactions between signaling molecules that regulate adult neural stem cell fate. *Biotechnology and Bioengineering* **116**, 193–205 (2019).
157. Images obtained or adapted from Servier Medical Art images, licensed under CC BY 3.0 for redistribution and adaptation. Original images obtained from https://smart.servier.com.
158. MacArthur, B.D., Ma'ayan, A., & Lemischka, I.R. Systems biology of stem cell fate and cellular reprogramming. *Nature Reviews Molecular Cell Biology **10**, 672-681 (2009)*.
159. Qin, B. & Cahan, P. Computation Tools for Stem Cell Biology. *Trends in Biotechnology* **34**, 993-1009 (2016).
160. The Event Horizon Telescope Collaboration. First M87 Event Horizon Telescope Results. I. The Shadow of the Supermassive Black Hole. *The Astrophysical Journal Letters* **875** (2019).

Chapter 2: Interrogating adult neural stem cell fate decisions in response to the complex logic of simultaneous, competing biomolecular cues.

This chapter is adapted from a manuscript published as

Chen, S., Bremer, A.W.*, Scheideler, O.J.*, Na, Y.S., Todhunter, M.E., Hsiao, S., Bomdica, P.R., Maharbiz, M.M., Gartner, Z.J., Schaffer, D.V. Interrogating cellular fate decisions with high-throughput arrays of multiplexed cellular communities. *Nature Communications* 7:10309 doi: 10.1038/ncomms10309 (2016).

2.1 Introduction

Networks of interacting cells regulate the biology and pathology of all mammalian tissues, including positive-negative selection in adaptive immune responses[1], tumor-stromal-vascular interactions during cancer progression[2], and stem cell-niche interactions during development and adulthood[3]. Within these intercellular signaling networks, the relative number and spatial organization of diverse cell types contributes to the behavior of the system as a whole[4]. The capacity to reconstitute *in vitro* these networks of interacting cells, or cell communities, would offer new insights into the logic and dynamics of collective cell-decision making.

The stem cell niche is an example of a cell community containing a diversity of interacting cells that orchestrate tissue development, maintenance, and repair[3]. Within this milieu, spatially-restricted extracellular signals guide stem cell self-renewal and differentiation[5]. These include juxtracrine signals that require cell-cell contact, lipoprotein ligands with limited diffusion, molecules that bind proteoglycans or matrix, and soluble close-range signals[6,7]. For example, adult neural stem cells (NSCs)[8-10] in the brain generate new neurons to modulate learning and memory, a process tightly regulated by a repertoire of neighboring cells (astrocytes, neurons, endothelial cells, etc.) that present a spectrum of signals (Eph-ephrin[11], Notch-Delta[12], Wnt[13], Shh[14], etc.). Elucidating the quantitative dynamics by which such disparate, local cues instruct sometimes mutually exclusive cell fate decisions would advance stem cell biology and regenerative medicine.

A number of methods have been developed to study networks of interacting cells. Trans-well and monolayer co-culture systems have yielded insights into intercellular signaling[13,15], but in general they cannot control the stoichiometries or contact times of close-range cell-cell interactions, do not extend beyond two cell types, and do not permit the longitudinal study of precisely defined groups of cells. Microfluidic and micropatterned platforms offer improved throughput and the capacity for single-cell analysis but are typically inefficient because they rely on Poisson statistics to generate arrays of interacting cells, are incapable of robust manipulation of more than two cell types at the single-cell level, and restrict cell motility and proliferation[16,17].

To study communication within cellular communities with improved efficiency and resolution, we engineered a high-throughput, patterned co-culture platform and investigated the effects of close-range signaling interactions on single NSC fate decisions. Our system integrates four key design criteria: 1) positional control over single cells to study their heterogeneous behaviors (**single-cell**

resolution); 2) the capacity to simultaneously pattern multiple cell types to examine the logic of cell-cell communication within a niche (**multiplexing)**; 3) longitudinal cell observation to reveal the dynamics of processes such as differentiation (**long-term lineage tracing)**; and 4) robust, scalable, reproducible system performance for statistical analysis (**large sample size)**.

With this DNA-based patterning platform, we demonstrate the unprecedented capability of reconstituting cellular communities comprised of up to four heterotypic cell types at high-throughput and with single-cell resolution. Moreover, we highlight the significantly improved efficiencies of this patterning technique over random Poisson loading as well as exhibit the strength of our system in manipulating cellular interactions by varying the initial position of patterned cell pairs, which translates to control over cell-cell contact. We then establish the promise of this platform by modeling and investigating complex cell signaling networks. Specifically, by patterning communities of NSCs with a niche cell that expresses the Notch ligand and another that expresses the Eph ligand, this platform enables us to dissect how NSCs resolve the simultaneous presentation of competing juxtacrine signals that promote different cell fates.

2.2 Results

2.2.1 DNA-Based Patterning Platform Overview

We fulfill the four design requirements mentioned above using a two-step patterning procedure. First, arrays of cell-adhesive "microislands" are generated on a non-adhesive background surface. Second, we prepare a programmably-adhesive substrate by printing short oligonucleotides within each microisland, which can capture multiple cell types that present complementary DNA strands temporarily tethered to their cell membranes. The result is a geometrically-organized, precisely-defined community of interacting cells for biological investigation (Figure 2.1).

2.2.2 Fabrication of Cell-Adhesive Microislands

In greater detail, to prepare cell-adhesive microislands, we harnessed ultraviolet-ozone (UVO) patterning to etch cell-adhesive microisland features into a non-adhesive polyhydroxyethylmethacrylate (polyHEMA) film coating an aldehyde-functionalized glass slide (Figure 2.1a). Unlike other non-fouling biomaterials, polyHEMA could be deposited as a thick film and was stable for at least 7 days (Figure 2.1b, Supplementary Figure 2.1). The resulting array of visible microislands (Figure 2.1d) obviated the need for alignment markers in subsequent printing steps, simplified image registration on consecutive days, and offered a means for lineage tracing. Importantly, these microislands restricted close-range cellular signals to confined communities, yet their size could be tuned to provide space for cell migration and division as needed.

2.2.3 DNA-Programmed Assembly for Heterotypic Cell Patterning

To generate a programmably-adhesive surface, we rely on DNA-programmed assembly,[18,19,20] a technique wherein DNA oligonucleotides are chemically incorporated into cell membranes to allow "velcro"-like attachment to substrates functionalized with the complementary sequences. We use direct microscale writing of DNA strands within the adhesive microislands for single-cell

capture (Figure 2.1c). We printed up to four orthogonal DNA sequences as cell-sized spots within each microisland (Fig. 1d), but additional sequences would enable the capture of even more cell types. After stabilization of DNA to the surface by reductive amination (Figure 2.1c box), each cell type is modified with unique lipid-conjugated complementary oligonucleotides, addressing the cell type to a specific DNA spot in the array. Cells are then serially flowed over the surface within the confines of a polydimethylsiloxane (PDMS) flow cell. Intervening washes remove unbound cells to reveal cellular communities with precisely-defined composition and relative spacing (Figure 2.1e).

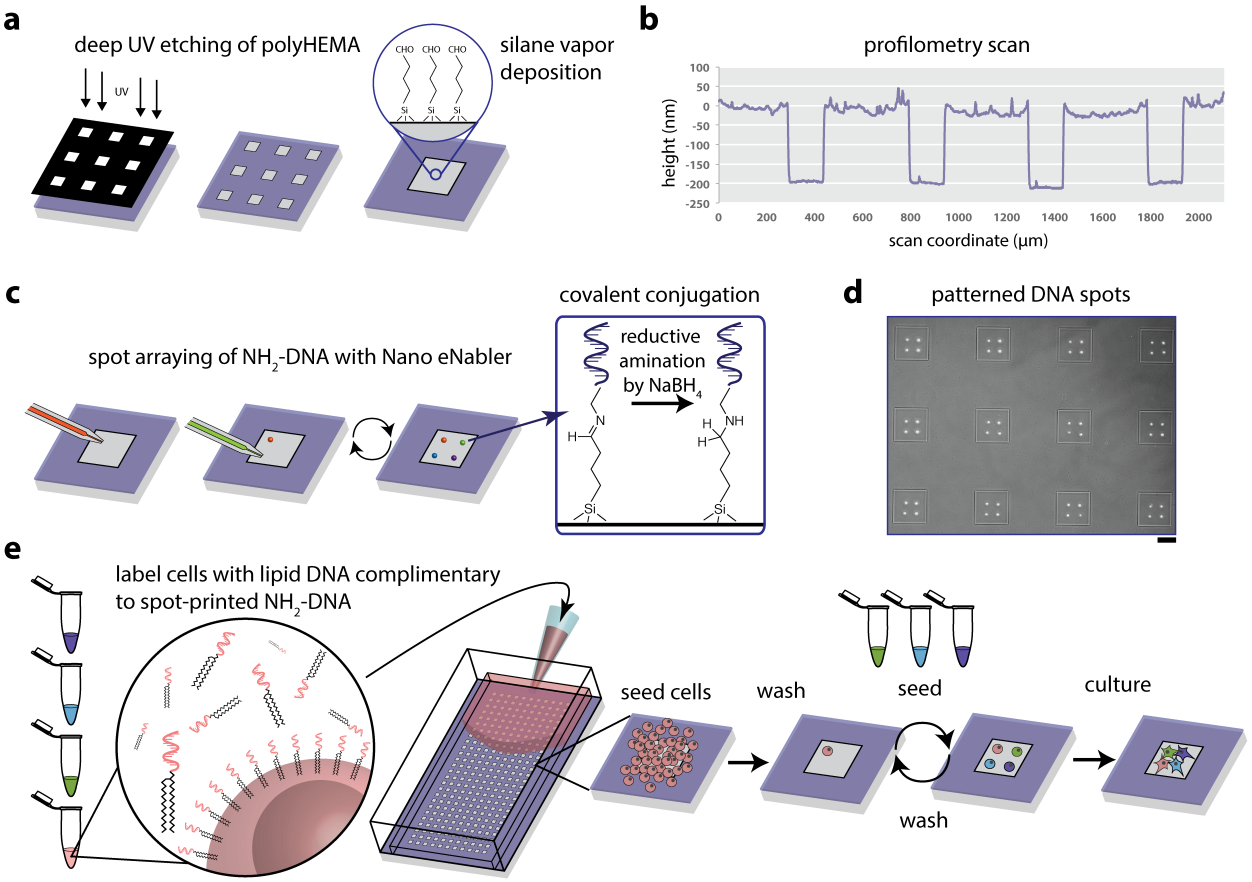

Figure 2.1 Two-step patterning process and single-cell tethering workflow. (a) Microisland patterns were produced by UVO (185 nm) patterning into thin polyHEMA coatings (<0.5 μm). An aldehyde-functionalized organic silane was then vapor deposited to prepare for DNA printing. (b) Profilometry measurements show representative microisland features of 200 nm. (c) Spot arraying of NH_2-terminated oligonucleotides within each microisland was performed using the Nano eNabler system. After arraying of single-cell sized spots, the entire slide underwent reductive amination using $NaBH_4$. (d) Representative image of four-component printed DNA patterns (scale bar: 100 μm). (e) Multiple cell populations are labeled with distinct DNA molecules presenting sequences complementary to the microisland DNA strands, washed, and passed through a PDMS flow cell affixed to the patterned slides either sequentially at a density of ~800,000 cells cm^{-2} or in mixed solutions at a density of ~400,000 cells cm^{-2}. Untethered cells are washed away, and the process is repeated for each cell type.

This method for building arrays of cellular communities provides tunable control over the number, identity, and initial placement of individual cells, along with the ability to define the size and shape of a community's spatial constraints (Figure 2.2). For example, altering the number of DNA spots printed within a microisland determines the number of cells within each community. Moreover,

printing either identical or orthogonal DNA sequences – which are highly multiplexable due to the large number of orthogonal, 20-mer oligonucleotides – dictates the capture of cells from the same or different populations (Figure 2.2a). To demonstrate control over cell number and composition, we printed between one to four DNA sequences within each adhesive microisland. In parallel, we labeled four separate populations of MCF10A human mammary epithelial cells (each colored with a different cell tracker dye) with four complementary DNA strands, which addressed each population to the corresponding DNA spot within the microisland arrays (Figure 2.2a, 2.2b). Capture efficiencies were high, though occasional DNA spots neglected to capture a cell or captured more than one of the same cell-type. To enable quantitative comparison to standard Poisson loading used in microfluidic and micropatterned platforms, a single population – or a mixture of two, three, or all four cell populations – was seeded onto microislands lacking printed DNA at a low cell/surface area ratio (Supplementary Figure 2.2). In every case, loading efficiency was higher using DNA-programmed assembly, with improvements over Poisson loading exceeding an order of magnitude for seeding with two or more cell types (Figure 2.2c, 2.2d). For communities of four cell types, we achieved a nearly 25% yield compared to zero microislands seeded with the desired four cells for Poisson loading – at least a 195-fold improvement (Figure 2.2d).

2.2.4 Tunable Control of Cell-Cell Contact During Differentiation

In addition to controlling cell identities and numbers, altering the photomask used to etch polyHEMA during UVO patterning offers control over the size and shape of a community's spatial constraints (Figure 2.2e). Moreover, the initial position of each cell within the community can be controlled by precise placement of each DNA spot within the microislands, allowing geometric arrangement of cells with programmed cell-to-cell distances (Figure 2.2f). Control over these variables is important as spatial constraints determine the frequency and duration of cell-cell interactions – key determinants of cell fate decisions in the stem cell niche[21]. To examine how patterning distances regulate cell-cell contact probability and duration (Figure 2.3a), we arrayed pairs of adult NSCs and primary astrocytes at intercellular distances ranging from 50 – 125 μm and conducted live imaging over 48 hours. Both the percentage of cell pairs that came into contact, as well as the total cell-cell contact time, increased the closer the NSC-astrocyte pairs were initially patterned (Figure 2.3b, 2.3c). In contrast, cells cultured without confinement in microislands – as would occur in standard co-cultures – experienced reduced interactions and often migrated away from one another (Supplementary Figures 2.3-2.5). These results demonstrate the advantage of this system to directly control cell-cell distances and confinement geometry, which lies in stark contrast to previously-reported high-throughput co-culture systems that cannot control these parameters simultaneously [16,17,21].

We next applied the platform to investigate NSC fate decisions in response to model niche cells. First, we compared NSC behavior when co-cultured with cortical astrocytes over 6 days under two conditions: in bulk co-culture or with single astrocytes in microisland arrays (Figure 2.3d, Supplementary Figure 2.6). Patterns of differentiation and proliferation were quantified by recording initial and final cell counts for each microisland (Figure 2.3d-2.3f). Overall, NSCs exhibited greater neuronal differentiation (i.e. expression of beta-tubulin III, or Tuj1) after 6-day culture in microislands when compared to bulk co-cultures ($p < 0.05$, Student's t-test) (Figure 2.3e). This observation applied to bulk co-cultures having low cell density equivalent to the overall

cell density across the entire patterned substrate surface area (500 cells cm^{-2}) and high cell density equivalent to cell density within each microisland (5000 cells cm^{-2}). Additionally, NSCs that underwent neuronal fate commitment proliferated to a greater extent than NSCs that developed into glial fibrillary acidic protein (GFAP)-positive astrocytes ($p = 8e^{-4}$, Student's t-test) (Figure 2.3f), an interesting phenomenon also observed *in vivo*[22].

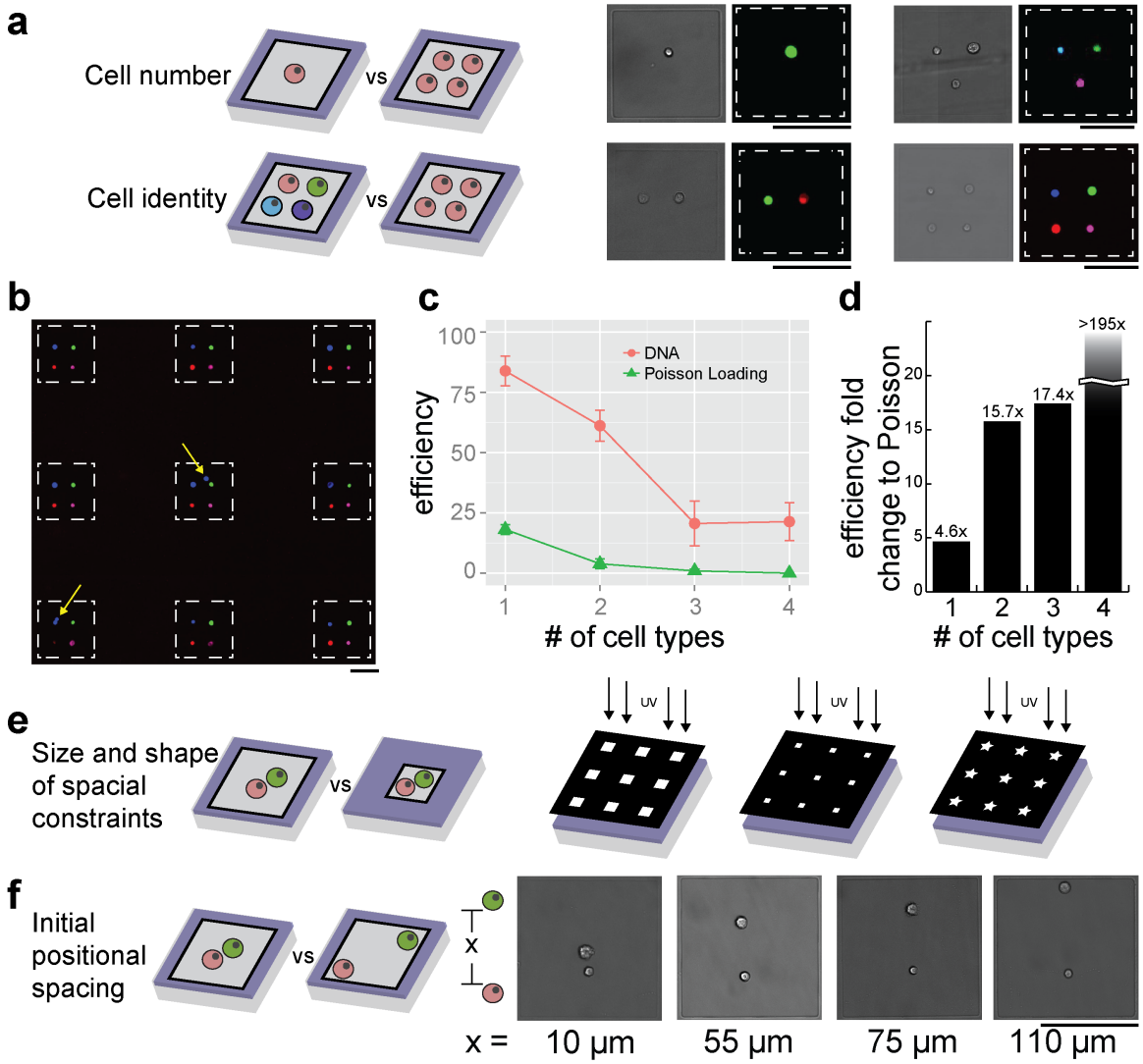

Figure 2.2 Customizable capabilities of two-step surface-patterning platform for modulating cellular interactions. (a) Both cell number and identity can be precisely controlled. (b) As an example of the latter, four MCF10A cell populations, each colored with a different dye, were labeled with distinct DNA strands and arrayed onto microislands printed with four of the complementary DNA oligonucleotides. Seven out of the 9 displayed microislands possessed the correct cellular community, with yellow arrows indicating microislands containing incorrect cellular components. (c) Using this DNA-based cell tethering, the efficiency of exact MCF10A cell patterning (red circles) was considerably higher than the same four cell populations plated at a low cell/surface ratio for random Poisson seeding (green triangles) of single-, double-, triple-, and quadruple-cell communities. (d) Efficiency, or fold improvement, of our DNA patterned compared to Poisson loaded arrays. (e) Variations to the microisland features for further modulation of cell-cell communication can be achieved by changing the size and shape of the photomask used during UV etching. (f) DNA printing enables precise control over the initial cell positions of NSC-astrocyte (bottom cell-top cell) pairs. All error bars are s.e.m. and n=4. All scale bars: 100 µm.

2.2.5 NSCs "listen" to Dll1 when Presented with Dll1 and EfnB2

In vivo, stem cells are exposed to conflicting signals that induce mutually-exclusive fate decisions. For example, Notch and Eph receptors play critical roles in mediating different cell fate decisions in the NSC niche. Notch signaling promotes the maintenance or self-renewal of early NSCs[12, 22], and we recently discovered that the cell surface ligand ephrin-B2 (EfnB2) presented from neighboring astrocytes induces neuronal differentiation of NSCs[11]. As both signals are presented to NSCs in the adult niche, they likely compete to regulate stem cell fate specification – a dynamic process that our system is ideally suited to investigate at the single-cell level. Therefore, we engineered primary cortical astrocytes as model niche cells to express either EfnB2 or Delta-like 1 (Dll1) translationally coupled to a nuclear-localized fluorescent protein (Supplementary Figures 2.7, 2.8).

We measured the distribution of cell fate decisions arising from NSCs patterned with EfnB2-astrocytes, Dll1-astrocytes, or both engineered cell types. Supplementary Table 1 provides a detailed overview of the density of events that we obtained for our different community compositions (n=44 for 1 NSC + 1 EfnB2, n=106 for 1 NSC + 1 Dll1, n=57 for 1 NSC + 1 EfnB2 + 1 Dll1). When NSCs were cultured alone with EfnB2-astrocytes, Tuj1 expression in NSCs increased, indicating a bias towards neuronal differentiation ($p < 0.001$, Student's t-test) (Figure 2.3g), and NSC proliferation rates decreased (Supplementary Figure 2.9), as anticipated based on our prior work[11]. In contrast, Dll1-astrocytes biased NSCs towards low Tuj1 expression (Figure 2.3h), consistent with its role in maintaining stem cell identity (Supplementary Figure 2.10). In the presence of both EfnB2- and Dll1-expressing astrocytes, NSCs adopted the Dll1-responding phenotype of low Tuj1 expression ($p < 0.05$, Student's t-test) (Figure 2.3i). Analogously, the distributions of percent $Tuj1^+$ cells island^{-1} and the total number of $Tuj1^+$ cells produced were similar when NSCs were cultured with an astrocyte expressing Dll1-alone or a Dll1 astrocyte plus an EfnB2 astrocyte (Supplementary Figure 2.11b). These results suggest that, in dynamic niche microenvironments, competing juxtacrine signals from Dll1 and EfnB2 may be interpreted by NSCs as a Dll1 signal.

2.3 Discussion

Here, we report an *in vitro* platform that tackles the shortcomings of current co-culture techniques and enables the investigation of more complex biological questions that address the role of cell-cell communication during NSC fate decisions. Using a combination of UV and DNA-based patterning, we establish a high-throughput system for generating multiplexed arrays of cellular communities having up to four cell types. These communities can be assembled with single-cell resolution and efficiencies at least 195-fold higher than practically achievable with Poisson loading. We demonstrate robust control over community composition with regards to cell number, identity, and positioning and apply the method to study NSC behavior and cell fate decisions in response to single and multiple signals presented from the surface of model niche cells. Our results reveal a potential signaling hierarchy between EfnB2 and Dll1 ligands during NSC differentiation.

In addition to exploring the effects of competing juxtacrine ligands, we anticipate that future applications of this technology include increasing the complexity of cellular communities by incorporating niche cell types that contribute other juxtacrine and/or paracrine signals, introducing

patterned protein cues, expanding the platform to generate three-dimensional niches, and quantitative real-time analysis of signaling. Together, these various approaches will yield a more complete understanding of how the logic and dynamics of intercellular signaling networks regulate the collective behaviors of cellular communities.

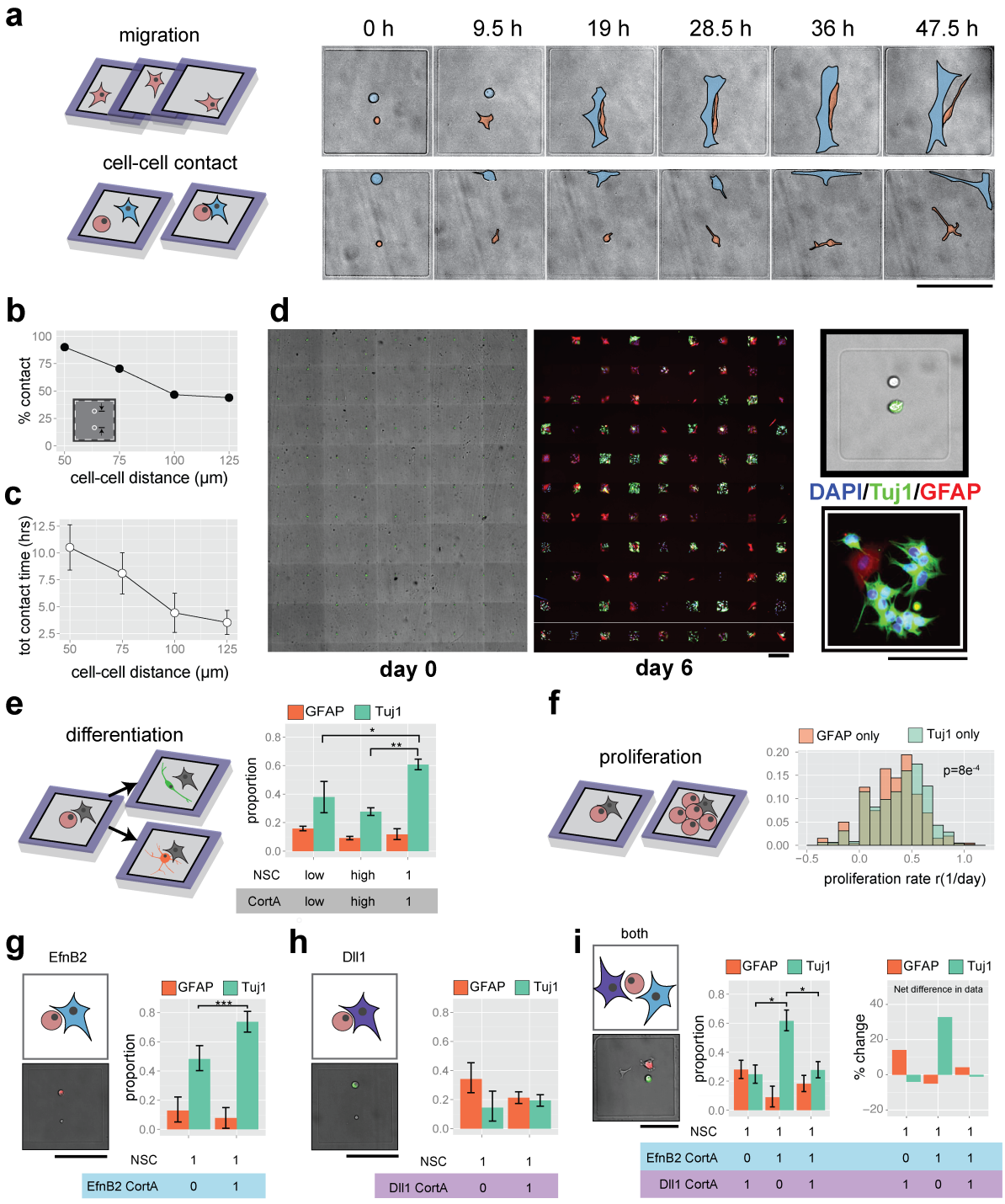

Figure 2.3 Arrays of cellular communities yield insights into cell dynamics and NSC differentiation, proliferation, and signal arbitration of opposing juxtacrine signals at the single-cell level. (a) Migration and cell-

cell contact for each microisland can be tracked with timelapse microscopy. Representative 48-hr timelapse images illustrating the dynamics of two NSC-astrocyte pairs initially patterned at different separations. NSC highlighted in red, and astrocyte highlighted in blue. (b) Percent of cellular communities that showed contact increased as the initial distance separating NSC and astrocyte decreased. (c) Total contact times also increased as initial cell-cell distance decreased. (d) Cell communities could be repeatedly imaged over long timescales with subsequent visualization of differentiation markers. Representative, stitched montages of NSCs (upper) and cortical astrocytes (lower, green) immediately after patterning (left), then upon immunostaining after 6 days for the neuronal marker Tuj1 and astrocyte marker GFAP (right). Higher magnification of a representative adhesive microisland shows that all progeny of this particular single NSC founder differentiated into $Tuj1^+$ neurons. (e) NSC differentiation can be tracked for each community. When patterned with single naïve astrocytes, NSCs exhibited enhanced Tuj1 differentiation and similar GFAP differentiation when compared to low-density and high-density bulk co-cultures. (f) Microisland confinement enabled analysis of proliferation rates. Proliferation rates (r) for Tuj1-biased lineages (lineages in which no GFAP cells were present) were higher than proliferation rates for GFAP-biased lineages ($p=8e^{-4}$). (g) NSCs patterned with a single hEfnB2-overexpressing astrocyte exhibited enhanced $Tuj1^+$ differentiation. (h) NSCs patterned with a single hDll1-overexpressing astrocyte displayed low Tuj1 expression. (i) When a single NSC was in the presence of both a Dll1-astrocyte and an EfnB2 astrocyte, the Dll1 phenotype (i.e. reduced Tuj1) dominated. The left graph represents immunostained proportions of NSCs in each condition, and the right graph depicts immunostaining changes compared to NSCs patterned 1:1 with a naïve cortical astrocyte. All error bars are 95% confidence intervals; all p values obtained from t-test. ***$p < 0.001$, **$p < 0.01$, *$p < 0.05$. All scale bars: 100 μm.

2.4 Methods

2.4.1 Substrate Preparation

Slides were initially coated with polyHEMA to generate a non-adhesive, background surface within which adhesive features could be patterned. First, polyHEMA (Sigma) was dissolved in a sonicator for 1 hour at 10 mg mL^{-1} in 100% ethanol. 150 μL of polyHEMA solution was then drop casted onto Nexterion AL (Schott) slides and allowed to dry under a clean polystyrene dish lid to block dust and slow the drying process. Slow drying over 1 hour at room temperature was helpful in reducing ridges on the surface, resulting in a glossy and flat polyHEMA film. To create cell-adhesive microislands within the polyHEMA film, UVO patterning was performed using a custom quartz mask (Photosciences Inc) and a UV-Ozone cleaner (Jelight). The quartz mask contains four 19 x 15 grids of clear square features (either 141 x 141 μm or 200 x 200 μm) arranged with a 500 μm pitch – all of which are aligned within the spatial dimensions of a Millipore 4-well EZ slide. Similar to water purification techniques that employ UV light to reduce organic contaminants, this deep UV patterning technique is thought to act through 185 nm light interacting with water and dissolved oxygen to create highly reactive hydroxyl radicals within the liquid layer, which then attack the organic polymer[23]. The very short half-life of these radicals ensures that only the clear square features are etched into the polyHEMA film. To achieve this patterning, the quartz mask was first cleaned using acetone and then irradiated in the UVO cleaner for 5 minutes at a distance of 5 cm to remove organic residues. A 160 uL drop of DI water was deposited across the chrome side of the mask, and the polyHEMA-coated side of the slide was lowered onto the wetted chrome surface slowly to avoid bubble formation. Water was necessary to provide an insulating layer from the ozone generated within the UVO machine. Excess water was pressed out gently and blotted off using a lint-free TexWipe. The mask-slide assembly was then inverted onto two small stands within the machine to prevent slipping of the slide relative to the mask. This results in the polyHEMA-coated slide facing upward with the chrome mask separating the slide from the UV source, controlling for the selective passing of the UV light. The slide was then illuminated for 5 minutes. Exposure times of less than 5 minutes resulted in an incomplete etch (Supplementary Fig. 1b). After illumination, the slide was detached gently from the mask by flooding the surrounding

area with DI water and using tweezers to slowly pull the slide up from the mask. The slide was then rinsed with DI water, dried under nitrogen gas, and immediately placed under vacuum. With the exception of the three- and four-component experiments, all experiments employed the smaller 141 μm square size.

Because the illumination may have scavenged the organic aldehyde groups originally present on the Schott Nexterion AL slide, we reconstituted the slide with trimethoxysilane aldehyde (UCT, PSX-1050) by chemical vapor deposition in a plastic vacuum chamber under house vacuum for 1 hour. Within this chamber, 100 μL of the silane was heated in a metal heat block at 110°C. After deposition, the slide was vacuum-sealed with a FoodSaver sealer and stored at room temperature until the DNA printing step.

DNA spots of controlled sizes were printed within the adhesive microislands using a Nano eNabler system (Bioforce Nano, Ames Iowa). First, 5'-NH_2-modified oligonucleotides were diluted to 1.5 mM in a 4X inking buffer (20% trehalose, 0.4 mg mL^{-1} N-octylglucoside pH 9.5, 900 mM NaCl, 90 μM Na Citrate). Surface patterning tools (SPTs; BioForce Nano) of different sizes (30S and 10S versions) were cleaned by a UVO cleaner and loaded with 0.4 μL of the DNA inking solution. 30S SPTs were used to print the 12-13 μm astrocyte-tethering spots. Spots for tethering NSCs were smaller (7-8 μm) and were printed using the 10S SPTs. These distinct, orthogonal DNA solutions were printed within close proximity of each other (10~20 μm gap). The SPTs and slides were loaded into the machine, and the humidity was allowed to equilibrate to 55-60% before printing. After DNA printing was complete, the slide was dried in a 120°C oven for 1 minute and vacuum sealed.

The printed DNA strands formed Schiff C=N bonds with the surface aldehyde. To convert the hydrolysable Schiff bases to single C-N bonds, reductive amination was performed by treatment with sodium borohydride (Sigma, 0.25% in PBS, supplemented with 0.25% LiCl) for 1 hour at room temperature. Li^+ ions were added to increase efficiency of BH_4^- as a reducing agent. This step also reduced unreacted aldehyde groups on the surface to non-reactive primary alcohols. Slides were stored under vacuum at room temperature until the cell-tethering step.

2.4.2 Lipid-DNA Conjugates

5'-OH oligonucleotides (sequences in Supplementary Table 2) were synthesized on controlled pore glass (CPG, Glen Research) on an Applied Biosystems Expedite 8909 DNA synthesizer, as developed elsewhere. A synthetic phosphoramidite (MMT-Amino Modifier C6, Glen Research) was then resuspended in anhydrous acetonitrile (Fisher Scientific) according to vendor instructions and added to the oligonucleotides using the synthesizer. Free amine groups were generated by removing the MMT group with Deblocking Mix (Glen Research), followed by an acetonitrile wash. The CPG with oligonucleotide-amine groups was then transferred from synthesis columns to Eppendorf tubes. A C16 fatty acid (Hexadecanoic acid, Sigma-Aldrich) was conjugated to oligonucleotides by adding 1mL of a dicholoromethane (DCM, Fisher Scientific) solution containing 200 mM fatty acid, 400 mM N,N-diisopropylethylamine (DIPEA, Sigma-Aldrich), and 200 mM diisopropylchlorophosphoramidite (DIPC, Sigma-Aldrich). Eppendorf tubes were wrapped in parafilm, secured with a cap locker, and placed on a shaker overnight. The next morning, CPG beads were rinsed with a series of DCM and N,N-dimethylformamide (DMF,

Sigma-Aldrich) washes and dried in a speedvac. Next, the lipid-conjugated DNA was cleaved from the CPG solid support by adding a small amount of a 1:1 mixture of ammonium hydroxide/40% methylamine (AMA, both from Sigma-Aldrich), sealing and cap-locking the tubes, and incubating at 70°C for 15-30 minutes. After cooling to RT, AMA was evaporated overnight using a speedvac. The resulting cleaved DNA/CPG was resuspended in 700μL of triethylamine acetic acid (TEAA, Fisher Scientific) and passed through a 0.2 μm Ultrafree centrifugal filter (Millipore) to remove the CPG solid support from the cleaved DNA solution. This DNA solution was next transferred to a polypropylene vial and carried through reversed-phase high-performance liquid chromatography (HPLC) to purify the desired lipid-modified DNA product. HPLC was performed with an Agilent 1200 Series HPLC system equipped with a diode array detector monitoring at 260 and 300 nm. A C8 column (Hypersil Gold, Thermo Scientific) was used with a gradient between 8 and 95% acetonitrile over 30 minutes with the pure fractions collected manually at the ~12 minute mark. Fractions were lyophilized, followed by three cycles of resuspension in distilled water and further lyophilization to remove residual TEAA salts. Fatty Acid-DNA concentrations were determined using a Thermo-Fisher NanoDrop 2000 series and measuring absorbance at 260 nm. Lipid-DNA stock solutions were resuspended at 250μM and stored at -20°C, with aliquots suspended in 1X PBS to make a 5μM working solution. CoAnchor strands were generated in similar fashion with exception to the lipid conjugation occurring on the 3' end.

2.4.3 Characterization of DNA-Strand Incorporation onto Cells

We quantified absolute numbers of DNA strands incorporated per cell using two types of DNA: NHS-conjugated[25] 20-bp oligonucleotides (purchased from Adheren, Inc.) and lipid-modified[19] 100-bp oligonucleotides.

First, the NHS-DNA was prepared by adding 1.2 μL of activator to 175 μL of DNA solution, and the mixture was allowed to react at room temperature for 20 minutes. During this reaction, we detached NSCs and astrocytes, counted cells, and added 2 x 10^6 NSCs or 1 x 10^6 astrocytes into each of three tubes. We resuspended each cell pellet with 100 μL of PBS (as a negative control), 176 μL NHS-DNA, or 60 μL of lipid DNA (5.5 mM). The NHS-DNA was reacted with cells for 20 minutes, and the lipid DNA was incubated with cells for 15 minutes. After the reactions, the cells were diluted with 1% BSA in PBS and washed three more times. We then hybridized Alexa 488 complementary strands to the DNA-labeled cells by resuspending in 50 μL of complementary Alexa 488-conjuated DNA at 1 ng μL^{-1} and incubating on ice in the dark for 30 minutes. Cells were washed 3x with 1% BSA in PBS and resuspended in a 1 mL volume before assessment on a Beckman Coulter FC 500 flow cytometer. Beads from an Alexa 488 Quantum MESF bead kit (Bang's Laboratories) were used to calibrate the total number of fluorophores conjugated to the cell surface.

Because our measurements showed that lipid DNA was superior in the extent of DNA incorporation onto both NSCs and astrocytes (Supplementary Table 3), we used lipid DNA for all subsequent experiments.

2.4.4 Cell Culture

Adult rat neural stem cells (NSCs) isolated from the hippocampi of 6-week-old female Fischer 344 rats (160-170 g)[26] were used for stem cell signaling experiments. To promote NSC adhesion, tissue culture polystyrene plates were coated with poly-L-ornithine (Sigma) overnight at room temperature and 5 μg mL^{-1} of laminin (Invitrogen) overnight at 37°C. Cells were cultured in monolayers in DMEM/F-12 high-glucose medium (Life Technologies) containing N-2 supplement (Life Technologies) and 20 ng mL^{-1} recombinant human FGF-2 (Peprotech), which supports self-renewal and proliferation. Medium was changed every other day, and cells were passaged using Accutase upon reaching ~80% confluency.

Rat primary cortical astrocytes from the cortices of embryonic day 19 Sprague-Dawley rats were purchased from Invitrogen (Cat. No. N7745-100). The cells were expanded on tissue culture plates in DMEM containing 4.5 g L^{-1} glucose and 15% fetal bovine serum (Invitrogen) and initially exhibited a doubling time of approximately 9 days. The cells were then adjusted to maintenance on poly-L-ornithine/laminin coated tissue culture plates in DMEM/F-12 high-glucose containing N-2 supplement, 10% fetal bovine serum and 1% penicillin/streptomycin (Gibco). Medium was changed every 2-3 days, and cells were passaged with 0.25% trypsin/EDTA as required upon reaching 100% confluency.

Human mammary epithelial (MCF10A) cells were cultured in DMEM/F12 (Invitrogen), supplemented with 5% horse serum (Invitrogen), 1% penicillin/streptomycin (Invitrogen), 0.5 μg mL^{-1} hydrocortisone (Sigma), 100 ng mL^{-1} cholera toxin (Sigma), 10 μg mL^{-1} insulin (Sigma), and 20 ng L^{-1} recombinant human EGF (Peprotech). Similarly, medium was changed every other day, and cells were passaged with 0.25% trypsin/EDTA upon reaching 80% confluency.

2.4.5 hDll1 and mEfnB2 Cell Lines

To create astrocyte cell lines overexpressing key signaling ligands, we infected astrocytes with lentiviral vectors carrying a multicistronic cassette containing either hDelta1[12] or hEphrinB2[11], an NLS tagged fluorophore (mCherry or Venus), and Puromycin resistance (Supplemental Fig. 7). Between each coding sequence is a viral 2A peptide that self-cleaves after translation, resulting in a 1:1 stoichiometry of expression.

Plasmid DNA is transfected into HEK 293T cells in the log phase of growth, along with third-generation lentiviral helper plasmids (RSV Rev, MDL gag/pol, and VSVG) using polyethylenimine (PEI) at 4:1 ratio (4 μg PEI:1 μg DNA). Media is collected at 44 hours and 68 hours after transfection, pooled, filtered with a 0.45 μm syringe filter, and centrifuged in a SW28 swinging bucket rotor in a Beckman Dickinson ultracentrifuge (2 hours, 24k rpm, 4°C). A 20% sucrose layer at the bottom of each tube provides effective separation of the viral pellet from the 293T media so that the final viral suspension is free of 293T contaminants. After centrifugation, the media and sucrose layer is aspirated, and the pellet is resuspended in sterile PBS, aliquoted, and frozen at -80°C. Infectious titers are determined by infecting astrocytes with serial dilutions of the virus, assessing infection rates by flow cytometry, and back-calculating the viral concentration using the Poisson distribution. The addition of polybrene (4 μg mL^{-1}) was essential for enabling lentiviral infection for cortical astrocytes.

To generate cell lines, cortical astrocytes were infected at MOI of 3 with 4 μg mL^{-1} polybrene. The

day after infection, the media was supplemented with 10 μg mL^{-1} puromycin for 7 days through feedings and passages. For further isolation of high expressing cells, we sorted the population by FACS using a MoFlo Cell Sorter, gating for positively fluorescent cells for both mCherry and Venus. After sorting, cells were replaced, expanded, and aliquots were frozen at passages 15-18. Before each experiment, astrocytes were thawed from the same stock.

Due to the 2A peptide linker, the NLS-XFP fluorescence could be used as a readout of ligand expression for each cell, which we confirmed by two-color immunoflow (Supplementary Fig. 8). To prepare cells for this analysis, astrocytes expressing NLS-mCherry hEfnB2 and NLS-mCherry hDll1 were detached from the plate using a brief Accutase treatment (instead of Trypsin to avoid excessive cleavage of membrane proteins). FBS-containing media was used to quench the enzymes, and 1 x 10^6 cells were fixed using 2% PFA and 1% BSA for 15 minutes. Cells were pelleted at 300 g for 5 minutes and washed 2x with PBS. Cells were blocked for 15 minutes in blocking buffer (5% donkey serum, 1% BSA, 0.1% triton-x-100 in PBS) and then stained with 100 μL of 1:50 rabbit polyclonal IgG for hDelta1 (sc-9102, Santa Cruz) or 1:100 rabbit polyclonal IgG for EfnB2 (HPA008999, Sigma) for 1 hour on a rocking shaker at room temperature. Cells were washed 3x with blocking buffer and then incubated in 100 μL of 1:250 Alexa 488 donkey anti-rabbit secondary antibody (Jackson Immunochemical) in the dark for 1 hour on a rocking shaker at room temperature. Cells were washed 2x in PBS and resuspended to < 500 cells μL^{-1} for assessment on the Guava easyCyte 6HT. Before collecting data, fluorescence compensation was performed using 488 labeled Quantum MESF beads (Bang's Laboratories) and unstained NLS-mCherry astrocytes.

2.4.6 Cell-Tethering Experiments

Slides were sterilized under a germicidal UV lamp in the laminar flow hood for 15 minutes. PDMS flow cells were plasma oxidized for 1 minute (to make the surface hydrophilic) and then sealed on top of the polyHEMA patterns for each well of a four-well chamber. A nontoxic grease marker was used to line off the inlet and outlet of each flow cell to ensure that flow travels through, and not around, the flow cells. 20 μL of 2% BSA (in PBS) was added to each flow cell for 1 hour to block nonspecific cell attachment.

NSCs and astrocytes were then detached and prepared at 4 x 10^6 and 2 x 10^6 cells, respectively, in PBS. Cells were labeled with 5 μM lipid DNA for 10 minutes at room temperature and, in some cases, 5 μM of a second, Co-Anchor lipid DNA strand was successively introduced to anchor the first strand into the cell membrane (also followed by a 10-minunte incubation step). Following incubation, cells were washed 4x with PBS with 3 minute spins at 300 g to pellet the cells in between washes. Cells were resuspended in 2% BSA (in PBS) to a final concentration of 4 x 10^7 NSCs mL^{-1} or 2 x 10^7 astrocytes mL^{-1} and stored on ice until ready for patterning. For some experiments, cell populations were combined before injecting the cell suspension (20 μL) into the flow cell. For all of the cell settling and washing steps, the slide was kept at 4°C to improve strand hybridization and slow down cellular metabolism during the lengthy experimental steps.

The cells were allowed to settle to the surface for 10 minutes and were then cycled through the well by adding 3 μL of cell suspension at the inlet, pipetting cells up at the outlet, and then adding the cell suspension back to the inlet. By cycling 15-20x, we enhanced the probability of

hybridization between matched pairs of surface-bound and cell-conjugated strands. Excess cells were washed away slowly, then vigorously, with progressively larger volumes of PBS. Gaskets from 4-well Millipore EZ slides were then fastened onto the slide without removing flow cells. DMEM/F-12 with 10 μg mL^{-1} laminin was flowed through the flow cells, and the slide was incubated at 37°C and 5% CO_2 for 10-30 minutes before high-throughput imaging on the ImageXpress Micro (IXM) high-throughput automated imager. Each well was imaged in its entirety using a 10X objective with transmitted light illumination and/or fluorescent illumination. After imaging, mixed differentiation media (50% conditioned media from NSCs in the log-phase of growth, 1% FBS, 1 μM retinoic acid (Enzo Life Sciences), 1% pen/strep in DMEM/F-12 media) was added through the flow cells and used to fill the rest of the wells. Cells could then be carried through culture and, due to the transient nature of the DNA tethering (DNA linkages generally break down within hours), free to migrate and interact within their confined community over time.

2.4.7 Fluorescent Labeling of MCF10As for Efficiency Experiments

Up to four distinct MCF10A cell populations were labeled with CellTracker fluorescent dyes (Life Technologies) prior to cell tethering and patterning. CellTracker Green CMFDA, CellTracker Deep Red, CellTracker Violet BMQC, and CellTracker Red CMPTX were prepared to a 10 mM concentration in DMSO. 4 x 10^6 MCF10As were resuspended in each CellTracker dye (0.1 μM for Green, 5 μM for Deep Red, 10 μM Violet, 5 μM Red) in 1X PBS for 10 minutes and subsequently washed 2x with PBS. Subsequent cell tethering steps were conducted as normal.

2.4.8 Poisson-Loading of MCF10A Populations into Microislands

Up to four populations of MCF10As were labeled with distinct CellTracker fluorescent dyes for 10 minutes (as described in detail in the above section). Cells were then washed 2x with 1X PBS and prepared as a mixed population. Cells from each population were prepared at a concentration of 5 x 10^5 cells mL^{-1} – a concentration that was previously determined by investigating a range of cell concentrations (1.25 x 10^6 cells mL^{-1} to 5 x 10^5 cells mL^{-1}) and analyzing which concentration supplied an optimal singe cell per microisland coverage. 20 μL of the mixed cell population was then injected into the PDMS flow cell and allowed to settle. Slides were imaged with the IXM and quantified for efficiencies. Microislands that contained exactly one cell type from each population was considered to be efficient.

2.4.9 Data Analysis

Acquired images for each well (a 7 x 14 grid) were tiled to form a whole-well montage in MetaXpress. These montages were rotated with bilinear interpolation in ImageJ, scaled with consistent scalings for each set of experiments, and then converted to 8-bit. Centroid coordinates for the upper left adhesive microisland were manually determined and recorded in a spreadsheet. These values were then inputted into a custom Matlab script, which cropped the images around each microisland and stored these images in an aligned array. A custom Matlab GUI, which displays the images from the array in succession, was used to record cell counts for day 0 images and immunostained images (Supplementary Fig. 12). Mean and integrated intensity values for nuclear NLS-Venus fluorescence were determined by automated segmentation using Otsu and Minimum Error thresholding, followed by end-user error correction for low-intensity cases.

Cell counts were compiled in a Matlab data structure, which was then filtered to remove sites that were uncountable (due to poor image quality, overlapping cells that make quantification impossible, or imperfections in polyHEMA) and sites in which all NSCs died by day 6. The proliferation rate for each site was calculated according to the following equation:

$$C_f = C_i * 2^{rt}$$

where C_i is the initial NSC count at day 0, C_f is the final count of NSC-derived progeny, and t is the time elapsed in days. We note that this definition of proliferation includes the effects of apoptosis on cell counts. These data were then ported into R for statistical analyses and plotting using the ggplot2 package. Error bars for proportion data were generated using the MultinomialCI package on raw cell counts. A complete description of calculation metrics can be found in Supplementary Note 1.

2.4.10 Immunostaining

On day 5-6 of differentiation, flow cells were removed, and the cells were fixed with 4% PFA for 10 minutes at room temperature. The cells were washed 3x with PBS and then blocked in blocking buffer (PBS with 5% donkey serum and 0.3% Triton-X-100) for 1 hour. The cells were stained overnight at 4°C on a rocking shaker with 1:1000 mouse monoclonal IgG for beta-tubulin III (Tuj1) (T8578, Sigma) and 1:1000 rabbit polyclonal IgG for glial fibrillary acidic protein (GFAP) (ab7260, Abcam), diluted in blocking buffer. The next day, the antibody solution was removed, cells were washed 3x with PBS and then incubated in the dark for 1-2 hours at room temperature on a rocking shaker with secondary antibodies, 1:250 Alexa Fluor 488 donkey anti-mouse IgG (H+L) and 1:250 Cy3 donkey anti-rabbit (H+L) (all Jackson Immunochemical) in blocking buffer. After secondary incubation, cells were washed 3x with PBS (with 1:1000 DAPI in the second wash) and kept in PBS until imaging.

2.4.11 Timelapse Experiments

NSCs and astrocytes were tethered onto DNA spots in polyHEMA-patterned and non-polyHEMA-patterned substrates, as described above. After cell tethering and washes, mixed differentiation media supplemented with 10 μg mL^{-1} laminin was flowed through the flow cells, and excess media was added to the wells. The slide was then imaged with transmitted light on the IXM using a 10X objective at 30-minute intervals for 44 hours. During imaging, an environmental control chamber maintained the slide at 37°C with a continuous supply of 5% CO_2. Movies from 50-60 sites were collected for each of 2-3 wells in each type of substrate.

Timelapse movies were analyzed manually. For each pair of patterned cells, we recorded moments of contact and disengagement, division and death events, and the final and maximum distances between cell nuclei and membranes. The total contact time and number of contact events are calculated from these data.

2.4.12 Flow Cell Production

Simple PDMS flow cells were produced using a 200 µm-thick mold created by stacking two white tough-tags and a piece of clear tape. Using a razorblade, the sticker stack is cut to 31 mm x 6 mm and affixed to the bottom of a 10 cm petri dish. Sylgard 184 (Ellsworth Adhesive) prepolymer is mixed with its curing agent at a 10:1 ratio, and 12 g of the mixture is poured onto the mold. PDMS is cured at 80°C for 1 hour, and flow cells are cut to 1 x 0.8 cm.

2.5 Acknowledgements

We thank Dr. Mary West, Wanichaya Ramey, Dr. Lukasz Bugaj, Dr. Dawn Spelke, Dr. Randolph Ashton, Jorge Santiago, David Ojala, Dr. Alyssa Rosenbloom, Robert Weber, and Max Coyle. This work was funded by NIH grants R21 EB014610, R01 ES020903, DP2 HD080351-01, and DOD grant W81XWH-13-1-0221. Y.S.N was supported by the Samsung Scholarship. O.J.S. was supported by the National Science Foundation Graduate Research Fellowship.

2.6 Appendices

2.6.1 Supplementary Figures

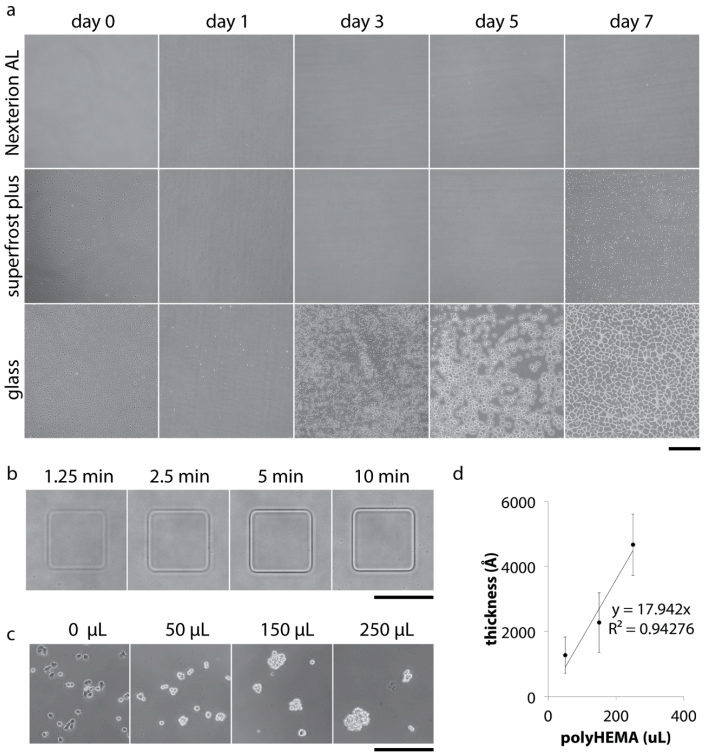

Supplementary Figure 2.1. PolyHEMA patterning characterization. (a) Optimizing substrate chemistry strongly enhanced polyHEMA stability in aqueous solutions. Schott Nexterion AL slides performed well relative to other options with little to no degradation over 7 days. PolyHEMA coated on plain glass slides began to detach after one day, while SuperFrost+ slides displayed slight improvement with little observable detachment until day 5. (b) Phase contrast microscopy showed that 5 minutes of deep UV illumination was sufficient to etch through our standard thickness of polyHEMA coatings (150 µL of 10 mg mL^{-1} polyHEMA). (c) PolyHEMA was effective at blocking cell adhesion down to 50 µL $slide^{-1}$. (d) The thickness of polyHEMA coating was modulated by depositing different volumes of polyHEMA solution (10 mg mL^{-1}). Profilometer measurements were performed at 9 different locations sampled over the entirety of two coated slides for each deposition. All scale bars: 200 µm.

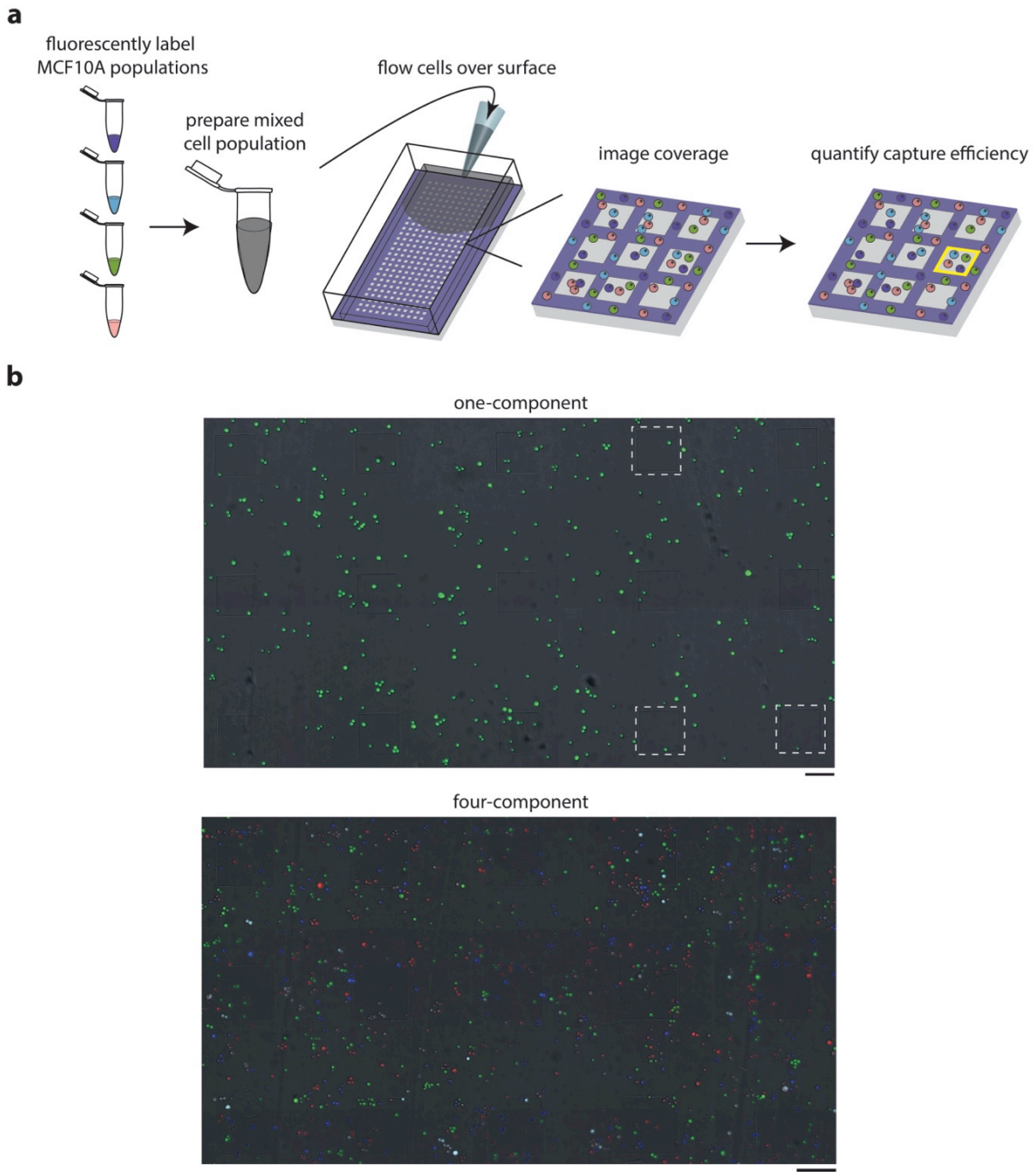

Supplementary Figure 2.2: Overview of experimental Poisson loading of MCF10As into microislands. (a) Schematic for conducting Poisson-loading experiment with 4 distinct, fluorescently-labeled MCF10A populations. (b) Representative one-component (top) and four-component (bottom) images of microislands that contain cells seeded using random Poisson loading. White, dashed boxes indicate microislands that possess the correct cellular components. All scale bars: 100 μm.

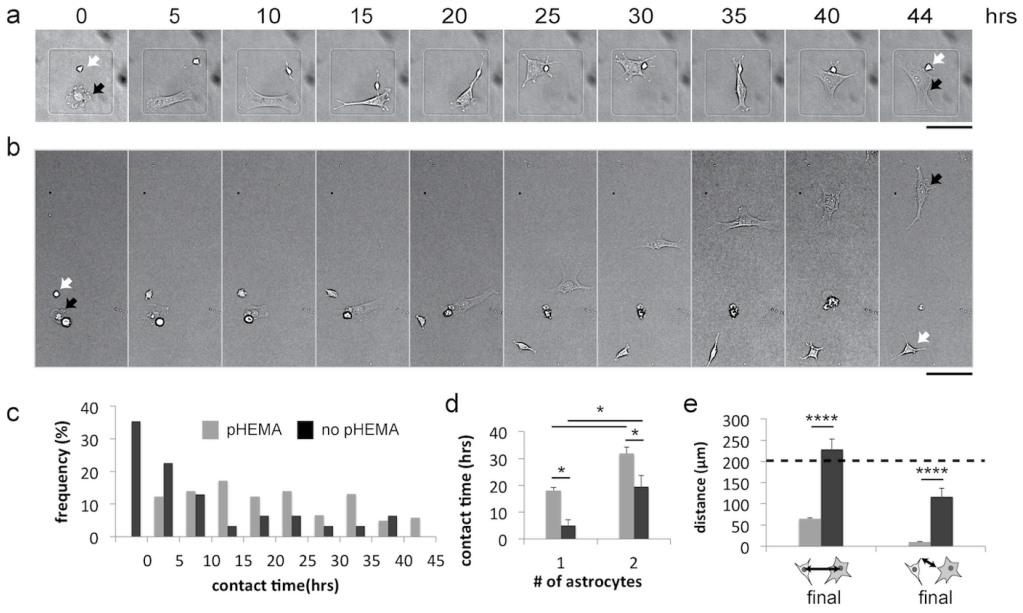

Supplementary Figure 2.3: Confinement to a small adhesive microisland sustains intercellular contact for extended times. (a) 141 x 141 µm adhesive microislands enabled extensive membrane contact between patterned NSCs (white arrow) and patterned astrocytes (black arrow). (b) On standard aldehyde slides lacking adhesive microislands, patterned NSCs and astrocytes migrated up to hundreds of microns away from each other over the course of 2 days. (c) Histograms of total contact times between patterned single NSCs and astrocytes showed that, without polyHEMA confinement, almost 35% of pairs made no contact at all. (d) The total amount of time that a NSC made contact with a single astrocyte was substantially increased with polyHEMA microisland confinement, and the addition of a second astrocyte further increased contact time (*: $p<0.05$, ANOVA with Tukey HSD, error bars: s.e.m). (e) The final inter-nuclear distance (left) and membrane distance (right) between patterned pairs were significantly less compared to pairs that were not confined (****: $p<1e-4$, t-test, error bars: s.e.m). The dotted line indicates the maximum corner-to-corner distance within the adhesive microislands. All scale bars: 100 µm.

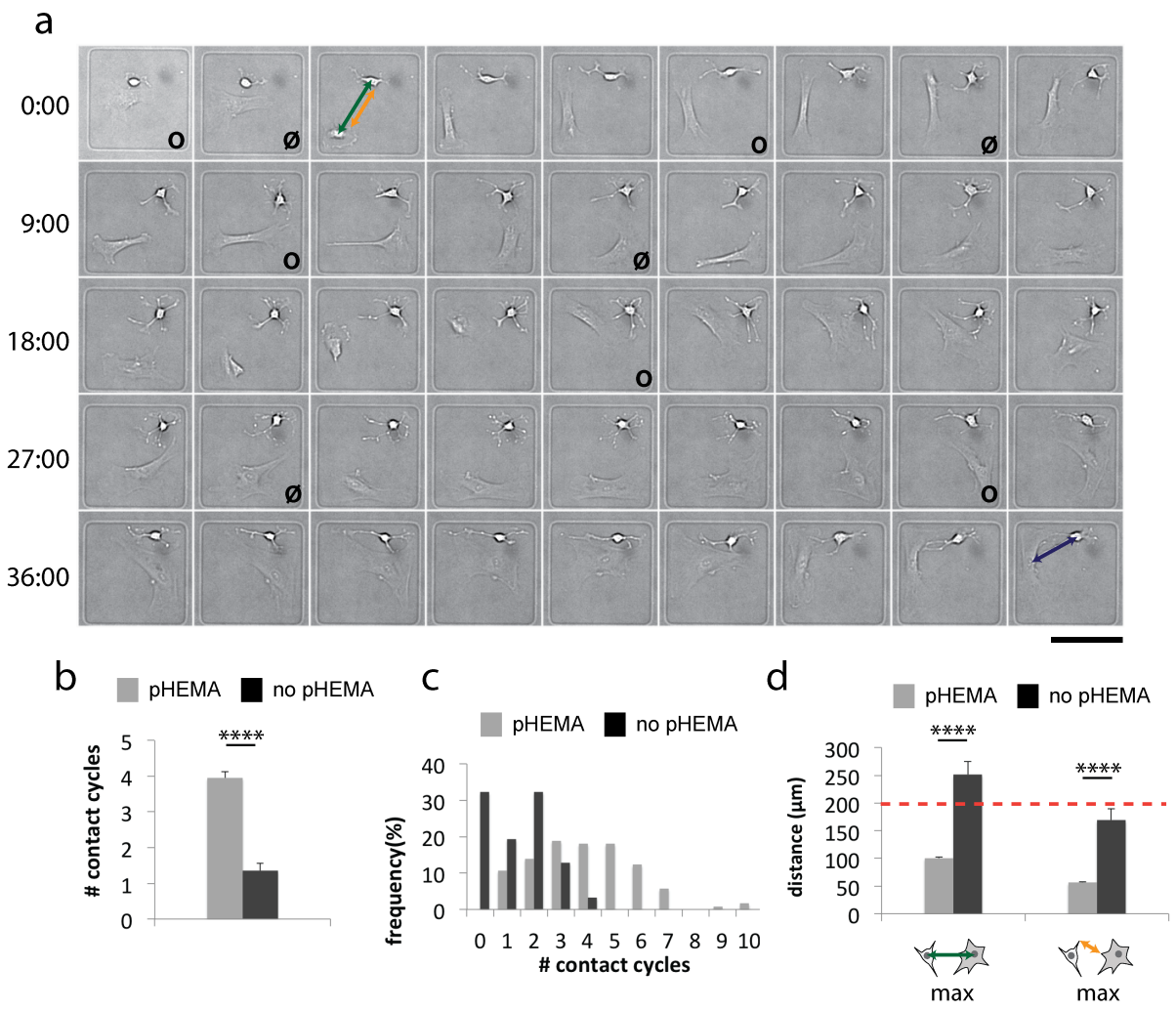

Supplementary Figure 2.4. Additional timelapse montages to show analysis framework. (a) DNA-tethered NSC and astrocyte pairs in polyHEMA patterns make several apparent cycles of contact (O) and disengagement (Ø). The green arrow shows the maximum distance between nuclei, and the yellow arrow shows the maximum cell membrane distance over the course of the experiment. The blue arrow shows the final distance between nuclei at 44 hours and, in this case, the final cell distance was 0 since the membranes were in contact at 44 hours. Hours are denoted on the left. (b) PolyHEMA-bounded pairs experienced significantly more contact cycles over 44 hours compared to pairs without polyHEMA (where representative images for no polyHEMA are shown in Supplementary Figure 5) ($p<1e-13$, error bars: s.e.m.). (c) The histogram of contact cycles shows a wider spread for polyHEMA-bounded pairs. (d) The maximum nuclear and membrane distances (green and yellow) between pairs were also significantly lower for polyHEMA-bounded pairs ($p<1e-5$, error bars: s.e.m.). All scale bars: 100 µm.

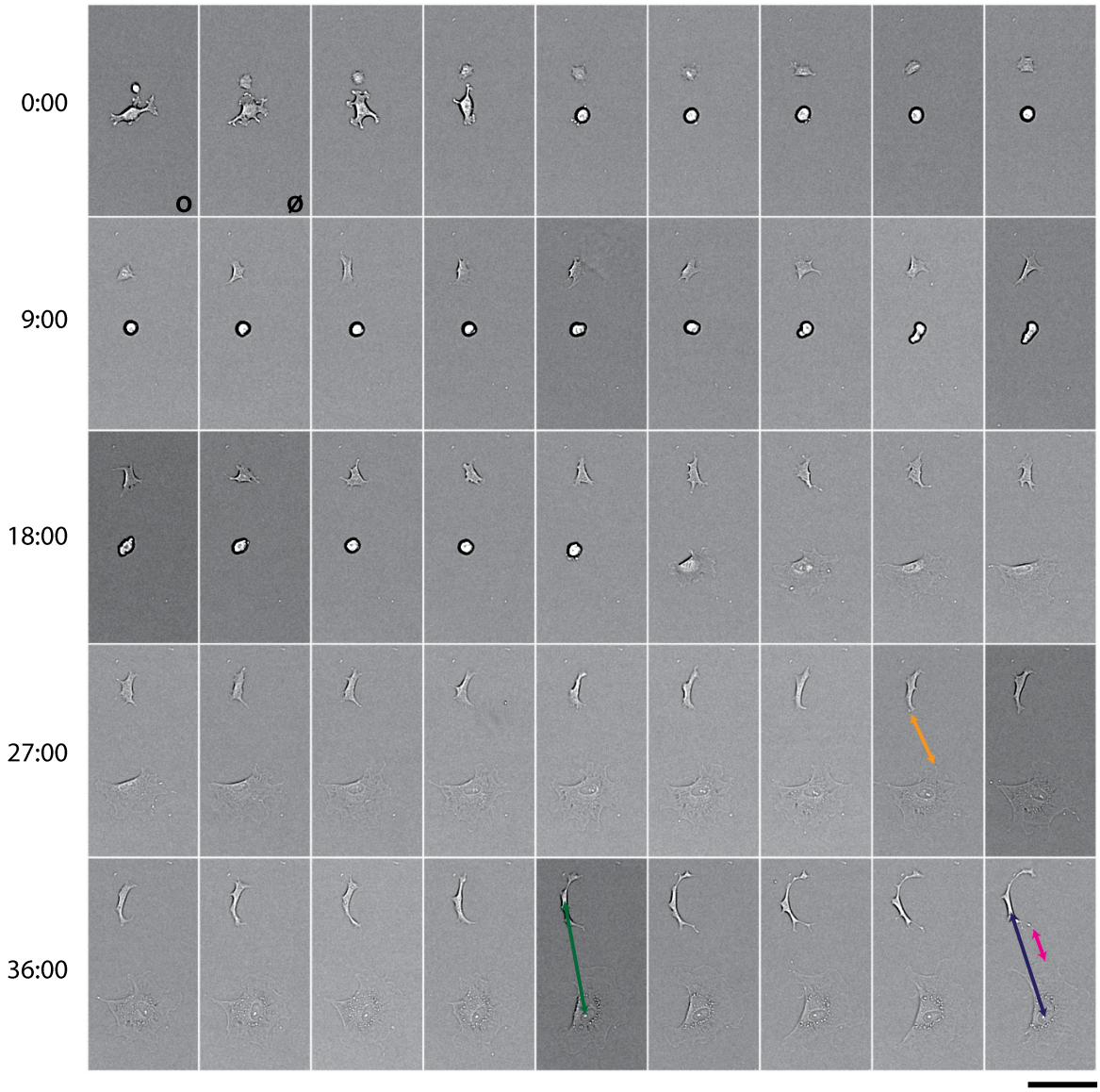

Supplementary Figure 2.5: Additional timelapse montages of cells patterned without polyHEMA boundaries. Notated using the same strategy as described in Supplementary Figure 4. The magenta arrow shows the final cell membrane distance.

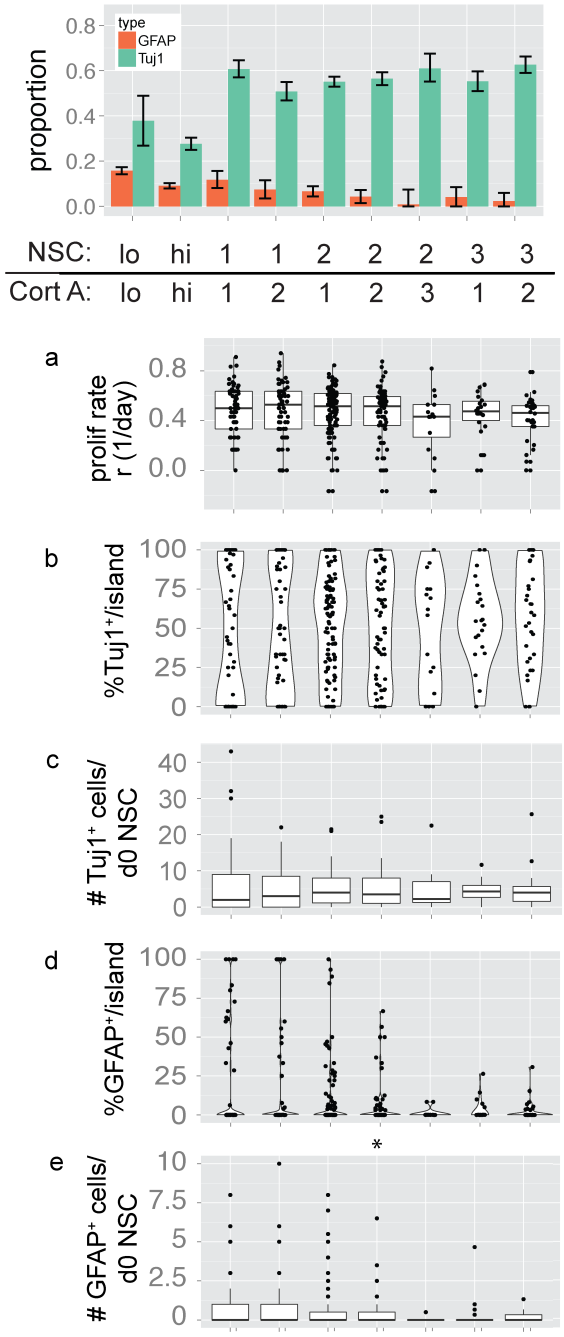

Supplementary Figure 2.6. Additional plots for NSCs patterned with naïve astrocytes. NSCs patterned with 1, 2, and 3 astrocytes exhibited higher differentiation rates than NSCs patterned in bulk, at either high (5000 cells cm^{-2}) or low density (500 cells cm^{-2}). (a) Proliferation rates. (b) Distribution of % $Tuj1^+$ $island^{-1}$ shows that increasing the number of initial NSC progenitors cause wider bellies in the distributions, reflecting the lower likelihood that all progeny adopt the same fate. (c) Boxplot of the number of $Tuj1^+$ cells generated from each initial NSC. (d) Violin plots of the distributions of % $GFAP^+$ $island^{-1}$. (e) Boxplot of the number of $GFAP^+$ cells (initial NSC) $^{-1}$. All error bars are 95% confidence intervals.

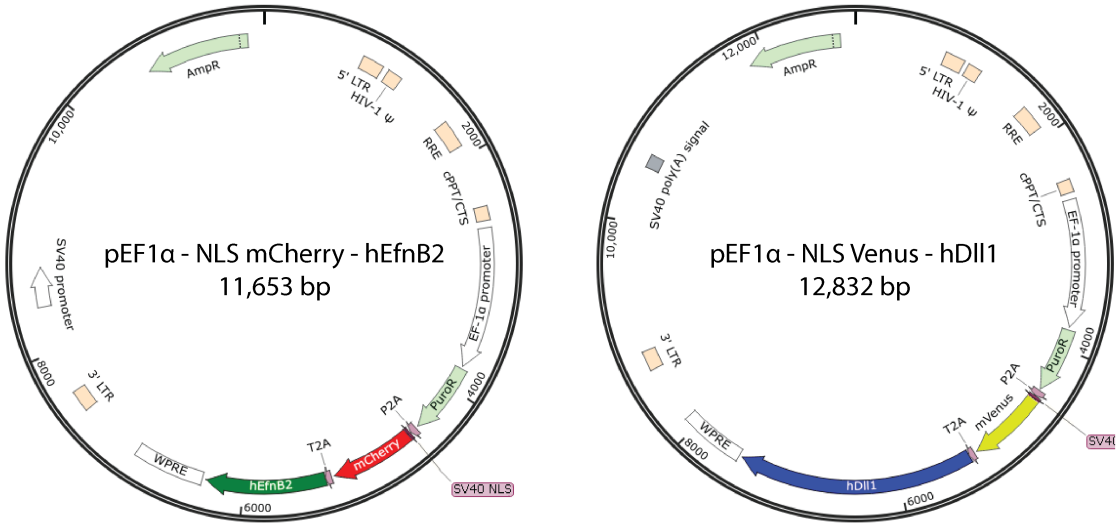

Supplementary Figure 2.7. Plasmid maps for expression vectors.

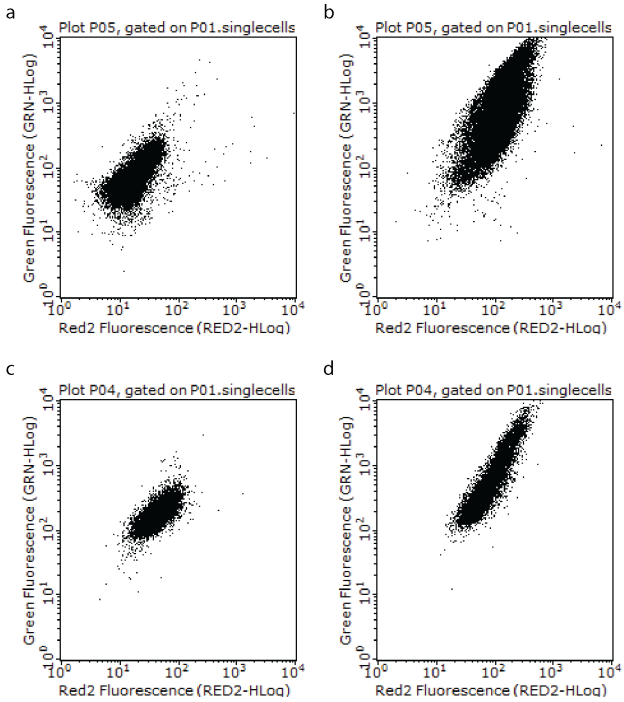

Supplementary Figure 2.8. Two-color immunoflow results show linear relationship between NLS-mCherry and Dll1 or EfnB2. (a) Naïve astrocytes stained with Dll1 antibody. (b) Dll1 lentivirus-infected astrocytes show linear relationship between mCherry fluorescence (Red2) and Dll1 488 antibody (Green). (c) and (d) show the same for naïve astrocytes and EfnB2-overexpressing astrocytes, each stained for EfnB2.

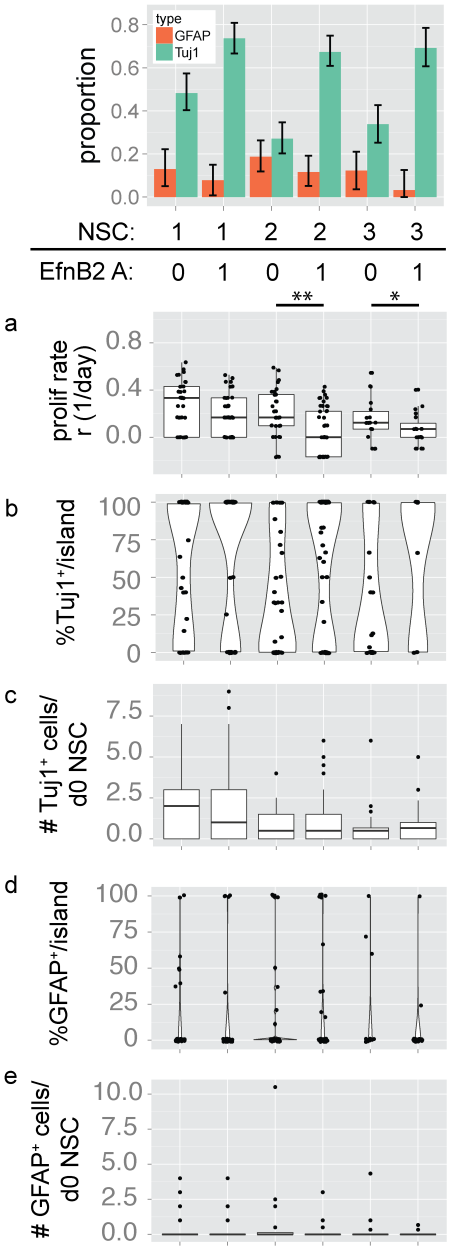

Supplementary Figure 2.9. Additional plots for NSCs patterned with EfnB2-expressing astrocytes. NSCs patterned with single hEfnB2-overexpressing cells exhibited enhanced Tuj1$^+$ differentiation. (a) In the presence of an EfnB2-astrocyte, the mean proliferation rate decreases, which is statistical in the case of 2 initial NSCs (**, p=0.0012, t-test) and 3 initial NSCs (*, p=0.06, t-test). (b) NSCs exhibited enhanced Tuj1$^+$ differentiation as evident in the wide distributions within the upper portion of the violin plots. (c) Boxplot of the number of Tuj1$^+$ cells generated (initial NSC)$^{-1}$. No differences in the mean number of Tuj1$^+$ cells were observed with the addition of one EfnB2 expressing astrocyte (for NSC = 1, 2, and 3). EfnB2 thus functions by increasing the fraction of NSCs islands^{-1} that give rise to a high proportion of Tuj1$^+$ cells rather than increasing the number of Tuj1$^+$ cells NSC^{-1} within a microisland. (d) Distribution of % GFAP$^+$ island^{-1}. (e) Boxplot of the number of GFAP$^+$ cells (initial NSC)$^{-1}$ reveal that very few GFAP$^+$ cells are produced overall. All error bars are 95% confidence intervals.

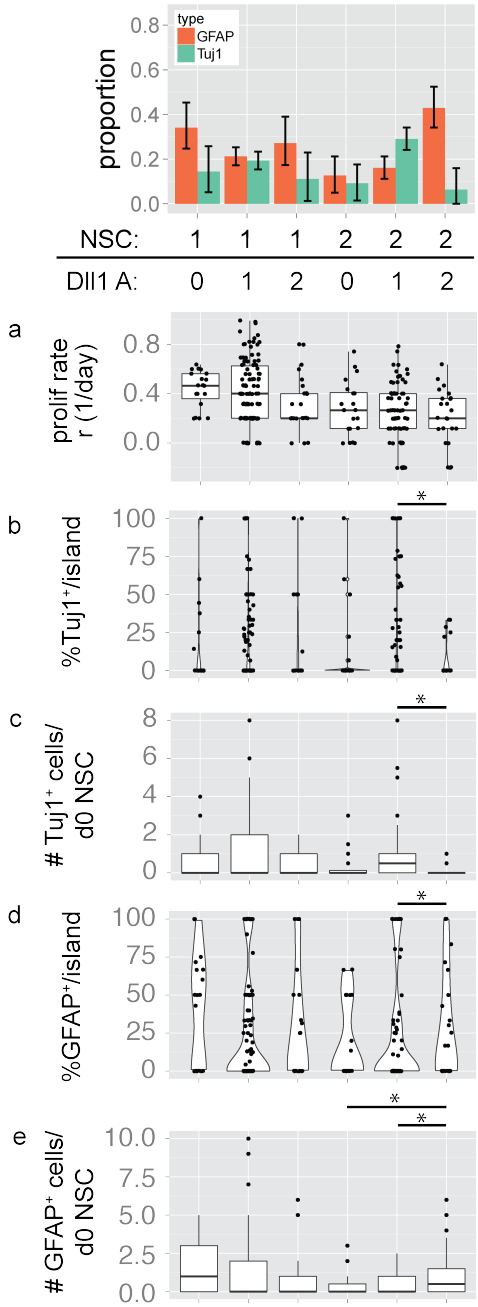

Supplementary Figure 2.10. Additional plots for NSCs patterned with Dll1-expressing astrocytes. NSCs patterned with single hDll1-overexpressing astrocyte exhibited reduced Tuj1. (a) Proliferation rates show no differences in the mean with the addition of Dll1-overexpressing astrocytes. (b) Narrow distributions for %Tuj1 island^{-1} reflect low Tuj1 differentiation rates. Asterisk indicates significant difference between samples. (c) Boxplot of the number of Tuj1^{+} cells generated (initial NSC)$^{-1}$. Asterisk indicates significant difference between samples. (d) Distribution of % GFAP island^{-1}. Asterisk indicates significant difference between samples. (e) Boxplot of the number of GFAP^{+} cells (initial NSC)$^{-1}$. Asterisk indicates significant difference between samples. All error bars are 95% confidence intervals; all p values obtained from ANOVA with Tukey HSD. *p<0.05.

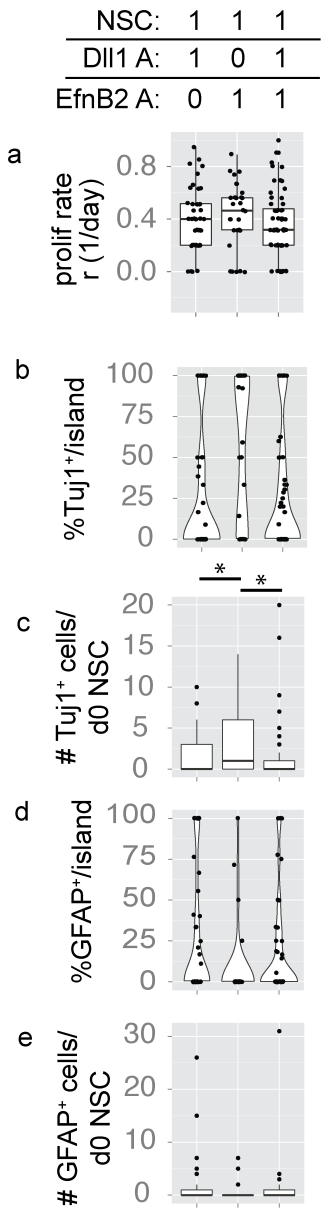

Supplementary Figure 2.11. Additional plots for NSCs patterned with EfnB2-expressing and Dll1-expressing astrocytes. (a) Proliferation rates show similar medians in patterns with only Dll1 and patterns with both signals. However, mean proliferation rates are not significantly different (p=0.6, ANOVA). (b) Violin plot showing similar distributions of %Tuj1 pattern^{-1} between patterns with only one Dll1-astrocyte and patterns with both types of astrocytes. By contrast, the %Tuj1 island^{-1} measurements with only one EfnB2 astrocyte were significantly elevated to higher levels ($p<0.0.5$, ANOVA with post-hoc Tukey Honest Significant Difference test). (c) Boxplot of the number of Tuj1^{+} cells with respect to initial NSC shows that islands with a Dll1-astrocyte and microislands with both a Dll1-astrocyte and a EfnB2-astrocyte produce significantly fewer Tuj1^{+} cells compared to microislands with only EfnB2 (p=0.022 and p=0.024 compared to the left and right columns, ANOVA with Tukey HSD). (d) Distribution of % GFAP island^{-1} does not reveal significant differences across samples (p=0.16, ANOVA). (e) Boxplot of the number of GFAP^{+} cells (initial NSC)$^{-1}$, with no significant differences across sample means (p=0.44, ANOVA). All error bars are 95% confidence intervals.

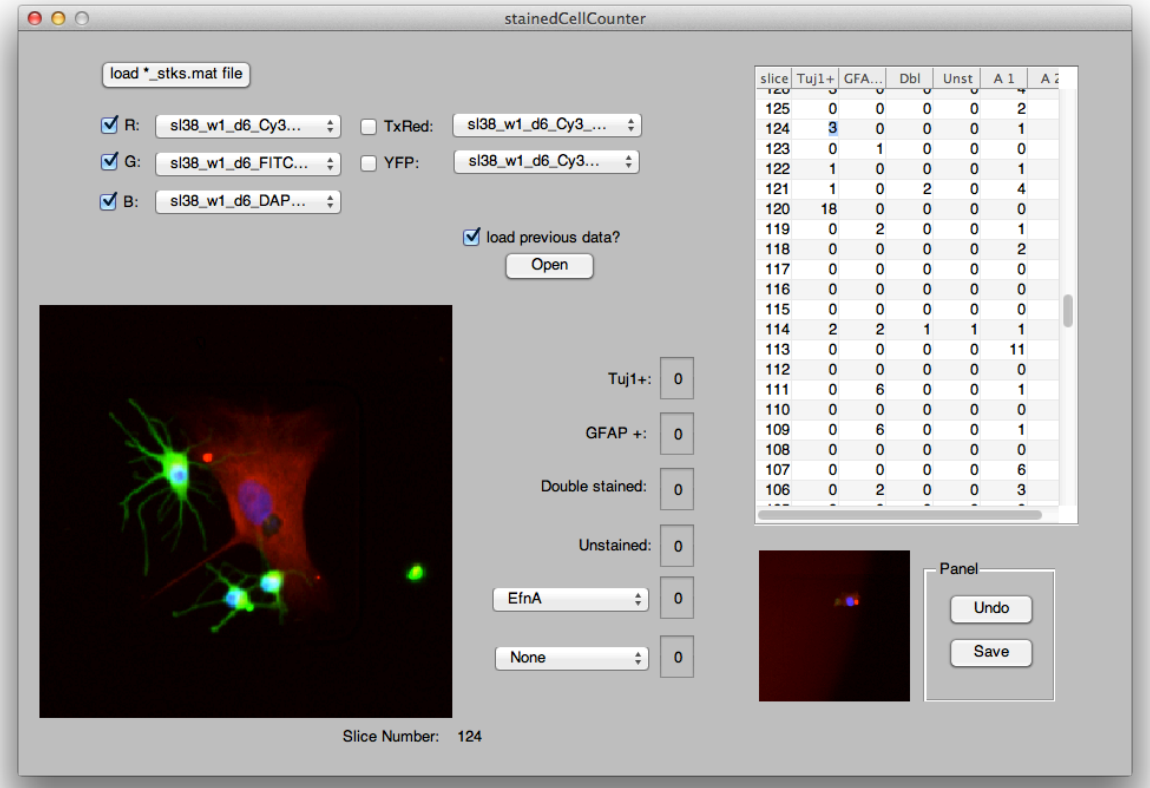

Supplementary Figure 2.12. Matlab GUI to facilitate the manual tabulation of cell counts. The software interface – described in greater detail in the Methods section – loads a series of images into red, green, and blue channels with optional extra channels for images of NLS-conjugated fluorescent proteins. Manually tabulated counts are entered into a table, which is stored in a data structure upon hitting 'save'. The editable table makes it easy to review and edit counts. To avoid bias, immunostaining counts are performed blinded to day 0 information on numbers and types of cells per island.

2.6.2 Supplementary Tables

#	community composition	n
1	1NSC + 1CortA	61
2	1NSC + 2CortA	59
3	2NSC + 1CortA	110
4	2NSC + 2CortA	67
5	2NSC + 3CortA	16
6	3NSC + 1CortA	22
7	3NSC + 2CortA	32
8	1NSC + 0EfnA	33
9	1NSC + 1EfnA	44
10	2NSC + 0EfnA	32
11	2NSC + 1EfnA	46
12	3NSC + 0EfnA	20
13	3NSC + 1EfnA	24
14	1NSC + 0DeltaA	19
15	1NSC + 1DeltaA	106
16	1NSC + 2DeltaA	21
17	2NSC + 0DeltaA	20
18	2NSC + 1DeltaA	65
19	2NSC + 2DeltaA	23
20	1NSC + 0EfnA + 1 DeltaA	45
21	1NSC + 1EfnA + 0 DeltaA	29
22	1NSC + 1EfnA + 1 DeltaA	57

Supplementary Table 2.1: Number of samples for each type of community composition.

Sequence Name	DNA Sequences (5' – 3')
A	GTA ACG ATC CAG CTG TCA CT TTTTTTTTTT TTTTTTTTTT TTTTTTTTTT TTTTTTTTTT TTTTTTTTTT TTTTTTTTTT ACTG ACTG ACTG ACTG ACTG
A'	GTA ACG ATC CAG CTG TCA CT TTTTTTTTTT TTTTTTTTTT TTTTTTTTTT TTTTTTTTTT TTTTTTTTTT TTTTTTTTTT CAGT CAGT CAGT CAGT CAGT
B	GTA ACG ATC CAG CTG TCA CT TTTTTTTTTT TTTTTTTTTT TTTTTTTTTT TTTTTTTTTT TTTTTTTTTT TTTTTTTTTT TCATACGACTCACTCTAGGG
B'	GTA ACG ATC CAG CTG TCA CT TTTTTTTTTT TTTTTTTTTT TTTTTTTTTT TTTTTTTTTT TTTTTTTTTT TTTTTTTTTT CCCTAGAGTGAGTCGTATGA
F	GTA ACG ATC CAG CTG TCA CT TTTTTTTTTT TTTTTTTTTT TTTTTTTTTT TTTTTTTTTT TTTTTTTTTT TTTTTTTTTT AGA AGA AGA ACG AAG AAG AA
F'	GTA ACG ATC CAG CTG TCA CT TTTTTTTTTT TTTTTTTTTT TTTTTTTTTT TTTTTTTTTT TTTTTTTTTT TTTTTTTTTT TTC TTC TTC GTT CTT CTT CT
G	GTA ACG ATC CAG CTG TCA CT TTTTTTTTTT TTTTTTTTTT TTTTTTTTTT TTTTTTTTTT TTTTTTTTTT TTTTTTTTTT AGC CAG AGA GAG AGA GAG AG
G'	GTA ACG ATC CAG CTG TCA CT TTTTTTTTTT TTTTTTTTTT TTTTTTTTTT TTTTTTTTTT TTTTTTTTTT TTTTTTTTTT CTC TCT CTC TCT CTC TGG CT
CoAnchor	AGT GAC AGC TGG ATC GTT AC

Supplementary Table 2.2: Complementary pairs of cell-labelling and surface-printed DNA sequences in addition to the CoAnchor sequence for stabilizing cell-labelling oligonucleotides.

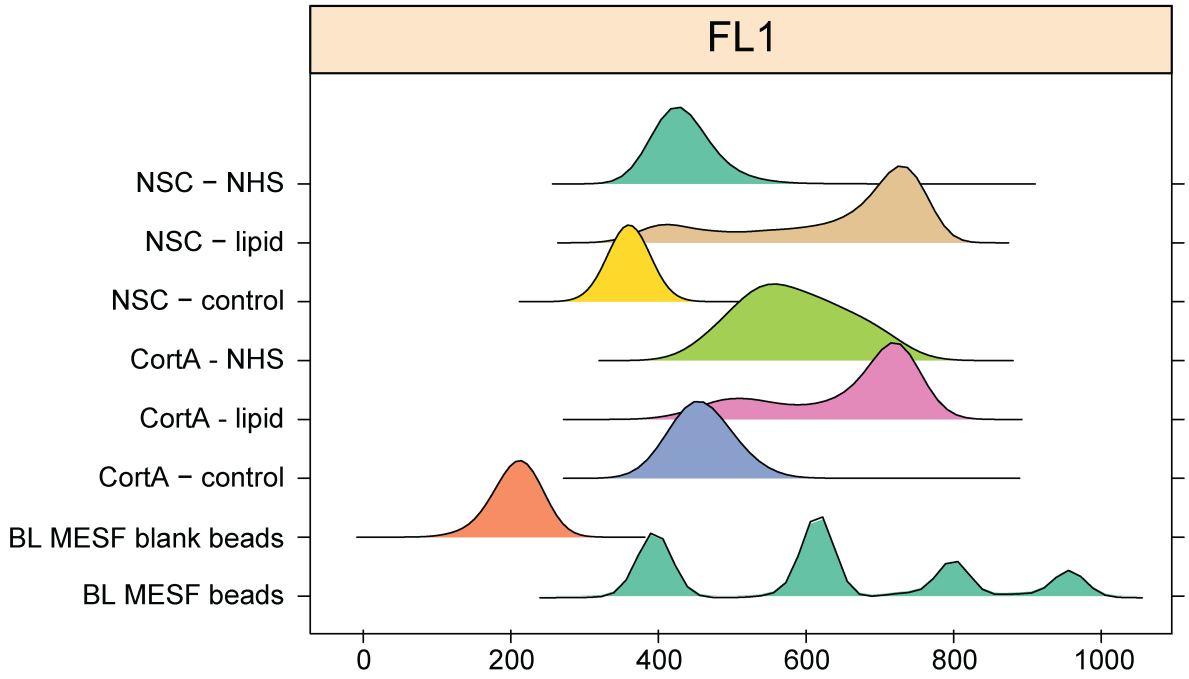

Type	Peak (strands cell^{-1})	5th percentile (strands cell^{-1})	95th percentile (strands cell^{-1})
NSC - NHS	4,606	3,125	10,727
NSC – lipid	107,809	3,701	139,626
NSC – control	2,437	1,808	3,556
CortA – NHS	18,355	7,498	84,914
CortA - lipid	90,136	7,498	135,521
CortA - control	5,732	3,666	13,619

Supplementary Table 2.3: Assessment of DNA incorporation into cells. After cell labeling by lipid DNA or NHS-DNA, cells were incubated with Alexa 488-conjugated complementary oligonucleotides and assessed by flow cytometry. Lipid DNA outperformed NHS-DNA for both NSCs (108k vs. 5k strands cell^{-1}) and astrocytes (90k vs. 18k strands cell^{-1}).

2.6.3 Supplementary Notes

Supplementary Note 2.1.

Our ability to measure many metrics from each patterned community yields data that can be displayed in a variety of ways. Here, we provide extensive descriptions of the supplementary plots from each experiment (below) with some guidelines for interpretation.

Proliferation rate: The proliferation rate is calculated as described in the Methods section. In these plots, a boxplot of the proliferation rate measurement is overlaid with jittered points, each representing a measurement from one island.

% Tuj1^{+} island^{-1}: For each island, the %Tuj1^{+} island^{-1} value is calculated by dividing the number of Tuj1^{+} cells over total number of NSC-progeny at day 6. For each type of community composition, a violin plot of the %Tuj1^{+} island^{-1} distribution is overlaid with jittered points, each representing a measurement from one island. For most plots there may be a large number of 0% Tuj1^{+} measurements, making it impossible

to infer an idea of the distribution from looking at the jittered points alone. Thus, the interpolated lines of the violin plot provide a better sense of the true distribution of values along the 0-100% y-axis.
 # Tuj1^{+} cells (d0 NSC)$^{-1}$: For each microisland, the # Tuj1^{+} cell at day 6 is divided by the total number of NSCs at day 0. This provides a measure of the average number of Tuj1^{+} cells produced from each NSC. In communities with only one initial NSC, this is a measure of the absolute number of Tuj1^{+} cells produced. These data are represented as a boxplot with the line designating the median, with upper and lower "hinges" corresponding to the first and third quartiles (the 25th and 75th percentiles).
% GFAP^{+} island^{-1}: Similar to % Tuj1^{+} island^{-1}. In general, since GFAP marker expression is less frequent than Tuj1 expression, we have less statistical power when analyzing GFAP data. Note that the GFAP^{+} NSC progeny can readily be distinguished from the cortical astrocytes (which are much larger and flatter) and, in many cases, by cortical astrocyte expression of a NLS fluorescent protein.
 # GFAP^{+} cells NSC^{-1}: Similar to # Tuj1^{+} (d0 NSC)$^{-1}$
For each of these plots, interesting and significant results are described in the figure legend. Plots without significant differences are presented without comment. For ANOVA, we subset the data based on the number of initial NSCs to assess the impact of additional astrocytes.

2.6.4 Supplementary Methods of Image Processing

It should be noted that longitudinal imaging of this patterning platform on the IXM—and possibly other imaging platforms—may require post-hoc image processing due to positional shifts and rotation of the imaged regions of interest. This is particularly the case for experiments that involve imaging at numerous timepoints (and therefore removing/inserting the patterned chamber slide onto a stage). Positional shifts and rotation will prevent proper stacking, montaging, cropping, and concatenation of individual regions of interest. To account for these changes, simple geometric corrections and transformation can be made to images, as outlined below with included ImageJ scripts. This process is appropriate for experiments with a reasonably low number to timepoints (e.g. $n < 15$).

The general pipeline for image corrections for simplification of downstream image analysis are as follows:

1. Angle correction of complete-well montaged image for individual timepoints.
2. Chronologically stack individual time points
3. Align stack of images using a landmark translation for each timepoint
4. Crop single microislands, followed by optional concatenation.

2.6.4.1 Angle correction of individual timepoints.

First, regions of interest (ROIs) are drawn over microislands using the top left-most microisland as reference, using the following ImageJ script:

```
//input the number of rows and columns of microislands in the well grid
r = 30
c = 20
//Input x and y, which represent the coordinate of the top left-most microisland
x1 = x
y1 = y
//generate ROIs. Note, numbers for y and x transformations are empirically derived from the //grid of microislands used to patter the polyHEMA
```

```
for (i=0; i<=(r-1); i++) {
        y = y1 + 461.4725*i;
        for (j=0; j<=(c-1); j++) {
                x = x1 + 461.436*j;
                //setTool("rectangle");
                makeRectangle(x, y, 300, 300);
                roiManager("Add");
        }
}
```

These ROIs make clear the rotational shift in the image, as displayed in Figure XA. Next, manually move the ROI of the right top-most microisland to properly overlay the ROI over the microisland. Make note of the value of this manual y displacement, and the value of the total x displacement between the first and last ROIs of this top row (Figure XB). Use these values to solve for theta using the inverse tangent (arctan) function. Apply theta as an angular transformation to the image (in ImageJ, Image>Transform>Rotate), and, after resetting x1 and y1 in the script above, verify that the ROIs now properly align over the microislands (Figure XC). Save this image for downstream stacking and repeat for all timepoints.

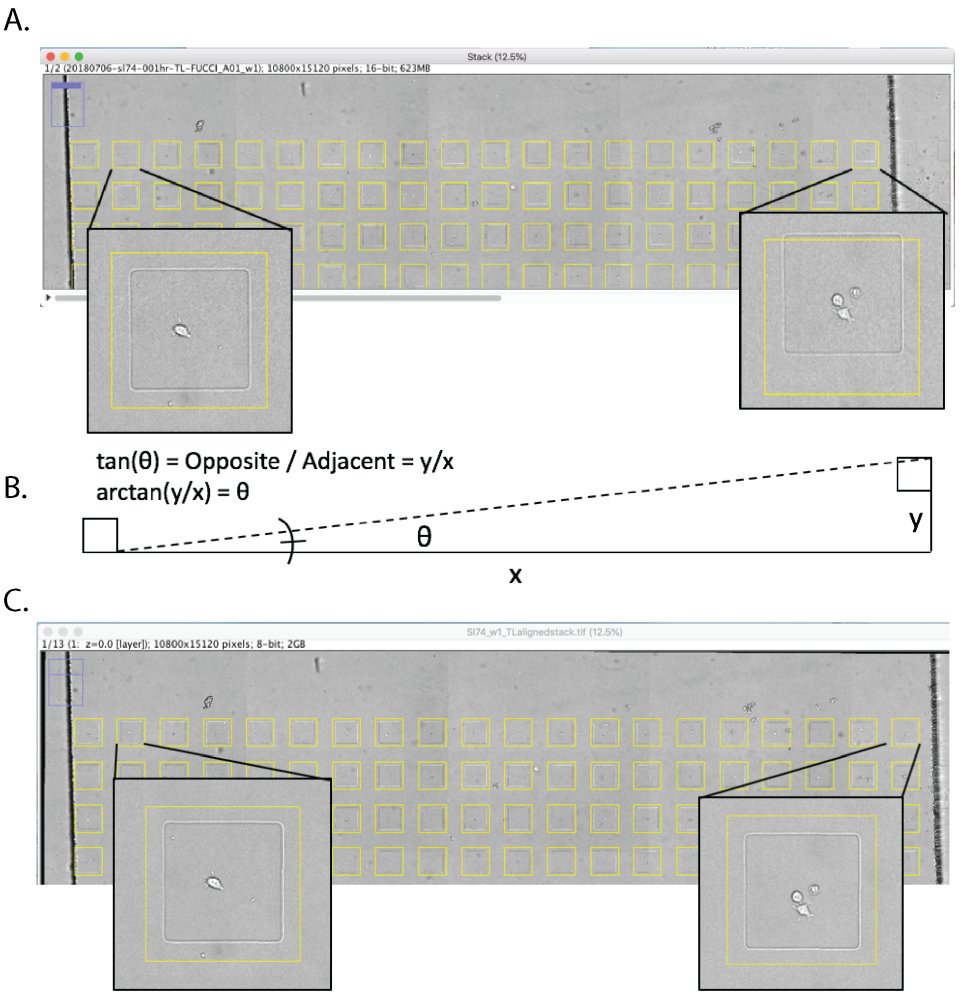

Supplementary Figure 2.13 Depiction of rotational tilt and tilt correction in image processing.

2.6.4.2 Stack angle-corrected individual timepoints

Open all relevant angle-corrected images of an experiment. Create a stack of the timepoints in chronological order using Image>Stacks>Images to Stack. While microisland grids of each image will be perpendicular to the x-y axes after angle correction, there is likely x and y displacement across images to prevent simple ROI microisland cropping. As such, save this stacked image for manual alignment of the time series in the following step.

2.6.4.3 Alignment of images across time using manual landmark registration.

To correct for x-y displacement across time, open the stacked image in File > New > TrakEM2 (blank), using default settings and slice thickness as 1. Then, right-click > Link > Unlink > "Yes" (in Execute? Window that pops up) to unlink stacked image to transform them separately. In the image, identify a microisland in your field of view that you can easily identify in every image. After ensuring this microisland is visible in all images of the stack without having to adjust the window, right-click > Align > Align layers manually with landmarks. This enables your cursor to generate a landmark on each image. Click a specific corner of the chosen microisland. You'll notice this generates a yellow "+1" landmark. Scroll to the next image in the stack, and click the same exact spot on the same microisland to generate a "+1" in the same location on the next image. Repeat for every image in the stack. Be sure to create only one landmark for each image. After creating one landmark on each image, scroll back to the first image in the stack and Right click > Apply transform. In the pop-up window, select Model: "Translation", and be sure the "Propagate to last layer" box is checked. Click OK. The images should now be aligned such that scrolling through the images shows the microislands remain stationary across the stack. Right click > Export > Make flat image. In the pop-up window, don't change any setting except the "End:" layer to the last layer. The "Start:" default should be at 1: z=0.0 [layer]. Click OK. This step may take a few moments, but it will open a new stacked image of the newly aligned images in the normal ImageJ window (outside of TrakEM2). Save this new, aligned image in the same location as the stacked image. I will typically name it exactly the same as the stacked image, but add "aligned" to the end. For example, the stacked "Sl69_well1_TLstack" will become "Sl69_well1_TLstackaligned". After saving the exported aligned image, close TrakEM2 (do not need to save the changes) and proceed to cropping and saving individual microisland stacks.

2.6.4.4 Crop, save, and concatenate individual microisland stacks.

If not already open, open the aligned stack from the previous section and the ImageJ script for creating ROIs above. Similar to the previous section, use the ROI Add Macro to create ROIs over each microisland. Double check that the ROIs are indeed aligned over microislands across the well over the time series by scrolling through the stack at various locations in the image. Then, apply the ImageJ script below to crop and save individual microislands. Importantly, change the appropriate text in the script that is specific for the slide, well, and wavelength of the stacked, aligned image, and the file location where you want to save the image.

```
for (i = 0; i<roiManager("count"); ++i) {
        roiManager("Select", i);
        run("Duplicate...", "title=Crop duplicate");
```

```
//Specify below the file path of where to save the cropped microisland image, and the specifics
//of the microisland crop to be saved.
        saveAs("Tiff","filepath/SlX_XXXhr_WellX_microisland"+(i+1)+".tif");
        close();
        selectWindow("Composite");
}
```

As the script runs, you should be able to watch as it selects each ROI, duplicates that region in a new window, saves it, closes it, and moves to the next microisland ROI. This script typically takes a few minutes for one well (typically 600 microislands). Undoubtedly there may be quicker ways to code this process, but I have generally found it preferable to visually check that the transformations and subsequently ROI cropping are correct. Lastly, depending on the needs of the experiment, it may be desirable to concatenate (Stacks>Tools>Concatenate) the stack of an individual microisland for downstream analysis. The end product of this protocol is shown in Figure XX below, where left-to-right concatenation shows one microisland over time.

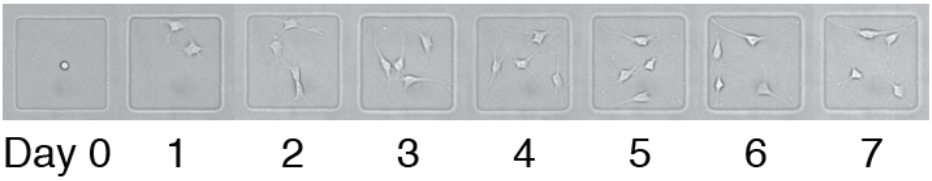

Supplementary Figure 2.14. Example concatenation of one microisland over time after image processing.

2.7 References

1. Klein, L., Kyewski, B., Allen, P. M. & Hogquist, K. A. Positive and negative selection of the T cell repertoire: what thymocytes see (and don't see). *Nature reviews. Immunology* **14**, 377-391, (2014).
2. Junttila, M. R. & de Sauvage, F. J. Influence of tumour micro-environment heterogeneity on therapeutic response. *Nature* **501**, 346-354, (2013).
3. Scadden, D. T. Nice neighborhood: emerging concepts of the stem cell niche. *Cell* **157**, 41-50, (2014).
4. Mirzadeh, Z., Merkle, F. T., Soriano-Navarro, M., Garcia-Verdugo, J. M. & Alvarez-Buylla, A. Neural stem cells confer unique pinwheel architecture to the ventricular surface in neurogenic regions of the adult brain. *Cell Stem Cell* **3**, 265-278, (2008).
5. Morrison, S. J. & Spradling, A. C. Stem cells and niches: mechanisms that promote stem cell maintenance throughout life. *Cell* **132**, 598-611, (2008).
6. Nusse, R. Wnts and Hedgehogs: lipid-modified proteins and similarities in signaling mechanisms at the cell surface. *Development* **130**, 5297-5305, (2003).
7. Fuchs, E., Tumbar, T. & Guasch, G. Socializing with the neighbors: stem cells and their niche. *Cell* **116**, 769-778, (2004).
8. Gage, F. H., Takahashi, J. & Palmer, T. D. The Adult Rat Hippocampus Contains Primordial Neural Stem Cells. *Molecular and Cellular Neuroscience* **8**, 389-404, (1997).
9. Palmer, T. D., Markakis, E. A., Willhoite, A. R., Safar, F. & Gage, F. H. Fibroblast growth factor-2 activates a latent neurogenic program in neural stem cells from diverse regions of the adult CNS. *The Journal of Neuroscience* **19**, 8487-8497, (1999).
10. Willhoite, A. R., Gage, F. H. & Palmer, T. D. Vascular niche for adult hippocampal neurogenesis. *The Journal of Comparative Neurology* **425**, 479-494, (2000).
11. Ashton, R. S. *et al.* Astrocytes regulate adult hippocampal neurogenesis through ephrin-B signaling. *Nat Neurosci* **15**, 1399-1406, (2012).
12. Gaiano, N. & Fishell, G. The role of notch in promoting glial and neural stem cell fates. *Annual Review of Neuroscience* **25**, 471-490, (2002).
13. Lie, D. C. *et al.* Wnt signalling regulates adult hippocampal neurogenesis. *Nature* **437**, 1370-1375, (2005).
14. Lai, K., Kaspar, B. K., Gage, F. H. & Schaffer, D. V. Sonic hedgehog regulates adult neural progenitor proliferation in vitro and in vivo. *Nat Neurosci* **6**, 21-27,(2003).
15. Ma, D. K., Ming, G. L. & Song, H. Glial influences on neural stem cell development: cellular niches for adult neurogenesis. *Current Opinion in Neurobiology* **15**, 514-520, (2005).
16. Kaji, H., Camci-Unal, G., Langer, R., Khademhoseeini, A. Engineering systems for the generation of patterned co-cultures for controlling cell-cell interactions. *Biochimica et Biophysica Acta* **1810**, 239-250, (2011).
17. Hui, E. E. & Bhatia, S. N. Micromechanical control of cell-cell interactions. *Proc Natl Acad Sci USA* **104**, 5722-5726, (2007).
18. Selden, N. S. *et al.* Chemically programmed cell adhesion with membrane-anchored oligonucleotides. *J Am Chem Soc* **134**, 765-768, (2012).
19. Weber R. J., Liang, S. I., Selden, N. S., Desai, T. A., Gartner, Z. J. Efficient targeting of fatty-acid modified oligonucleotides to live cell membranes through stepwise assembly. *Biomacromolecules* **15**, 4621-4626, (2014).

20. Todhunter, M. E. *et al*. Programmed synthesis of three-dimensional tissues. *Nat Methods* **12**, 975-981, (2015).
21. Gracz, A. D. *et al*. A high-throughput platform for stem cell niche co-cultures and downstream gene expression analysis. *Nature Cell Biology* **17**, 340-349, (2015).
22. Ables, J. L. *et al*. Notch1 is required for maintenance of the reservoir of adult hippocampal stem cells. *J Neurosci* **30**, 10484-92, (2010).
23. Kano, I., Darbouret, D., & Mabic, S. UV Technologies in Water Purification Systems. http://www.learnpharmascience.com/emd/docs/UV%20technologies%20in%20water%20purification%20systems.pdf, (2012).
24. Bonaguidi, M. A. *et al.* In vivo clonal analysis reveals self-renewing and multipotent adult neural stem cell characteristics. *Cell* **145**, 1142-1155, (2011).
25. Hsiao, S. C. *et al.* Direct cell surface modification with DNA for the capture of primary cells and the investigation of myotube formation on defined patterns. *Langmuir* **25**, 6985-6991, (2009).
26. Palmer, T. D., Ray, J. & Gage, F. H. FGF-2 responsive progenitors reside in proliferative and quiescent regions of the adult rodent brain. *Molecular and Cellular Neuroscience* **6**, 474-486, (1995).

Chapter 3: Activation strength of the canonical Wnt/β-catenin signaling pathway regulates the extent of adult neural stem cell proliferation during neuronal differentiation.

3.1 Introduction

Neural stem cells (NSCs) reside within at least two niches in the adult mammalian brain, including the subgranular zone of the hippocampal dentate gyrus[1]. Throughout adulthood, these cells retain the two hallmark properties of stem cells: the ability to self-renew and the capacity to differentiate down multiple lineages into more-specialized cell types. NSCs of the adult hippocampus differentiate into mature glutamatergic neurons of the granular layer, as well as cells of a glial identity[2].

Adult neurogenesis is the highly-ordered process through which adult NSCs differentiate into newborn neurons. During this process, radial glia-like cells (RGLs), the putative stem cell of the hippocampus, progress from a mostly quiescent state through a transit amplifying stage in which neuronal-committed progenitors lose stem cell markers and gain neuronal markers like Tuj1[3]. These transit amplifying progenitors may or may not undergo cell division before giving rise to post-mitotic immature neurons, which themselves undergo a weeks-long maturation phase before integrating into the existing hippocampal neural network[4]. *In vivo* clonal analysis suggests highly heterogeneous fate decisions arising from single RGLs, including wide heterogeneity in the final total number of cells that can arise from a single clone[4].

Fate decisions of NSCs are tightly regulated by various biomolecular and other cues that are presented within the stem cell niche, including those of the canonical Wnt/β-catenin signaling pathway ("Wnt")[5]. The Wnt pathway is highly conserved and plays a critical role in development and tissue homeostasis throughout adulthood[6]. In the absence of Wnt ligands, cytoplasmic β-catenin is constitutively phosphorylated by the multi-protein "destruction complex", including GSK3β, which targets it for degradation. When Wnt ligands are present, they bind their cognate co-receptors Frizzled and LRP5/6, whose intracellular domain then recruit proteins of the destruction complex to the cell membrane. This relieves the inhibition of β-catenin, which increases in concentration in the cytoplasm, enables it to translocate to the nucleus, where it acts as a transcriptional co-factor for downstream target Wnt genes[7].

The canonical Wnt/β-catenin signaling pathway is a master regulator of adult neurogenesis. Wnt activation has been shown to drive a neuronal fate specification in adult NSCs[5], and has also been linked to the proliferation of neuronal-committed cells *in vitro*[8] and *in vivo*[9]. Further, others have found Wnt to be necessary for NSC self-renewal[10], an effect likely mediated in part by the additional presence of growth factors, namely FGF2[11]. The ability of the Wnt pathway to regulate these two cell fates concurrently—proliferation and differentiation—is not exclusive to adult neural stem cells[12], suggesting that factors which "fine tune" the relationship between these two outcomes may have implications for other tissues.

The establishment and maintenance of morphogen gradients, including Wnts, is essential for proper development during embryogenesis including during anterior-posterior patterning and

gastrulation[13,14]. Further, differing strengths of activation of Wnt using the small molecule CHIR99021 was recently shown to direct the differentiation of human pluripotent stem cells into regional-specific neural progenitors[15] as well as specific subtypes of neurons[16]. How different strengths of activation of the canonical Wnt/β-catenin pathway influences adult neural stem cell behavior, however, has yet to be explored. As such, we sought to determine how different strengths of activation of the canonical Wnt/β-catenin signaling pathway may impact NSC fate decisions, and specifically explored the interplay between neuronal differentiation and proliferation.

3.2 Results

3.2.1 Probability of neuronal differentiation, but not total output of neuronal-committed cells, increases with stronger Wnt signaling.

To observe the effect of canonical Wnt/β-catenin pathway activation strength on NSC fate behavior, we assayed cells for Tuj1$^+$ neuronal-committed differentiation after 5 days *in vitro* at different concentrations of the GSK3β-inhibitor CHIR99021 (1.5μM, 10μM) and a negative DMSO control. In agreement with previous studies, we found activation of the canonical Wnt pathway via CHIR as a strong driver of neuronal differentiation, with the effect increasing in a dose-dependent manner (Figure 3.1). Stronger levels of pathway activation yielded increased total percentage of cells displaying the early and immature neuronal marker Tuj1 (Figure 3.1A, 3.1D). However, we unexpectedly observed a marked increase in the final total number of cells in mid-level Wnt pathway activation (1.5μM CHIR, Figure 3.1B, 3.1D). This also corresponded to increased final total numbers of Tuj1$^+$ neuronal-committed cells (Figure 3.1C, 3.1D).

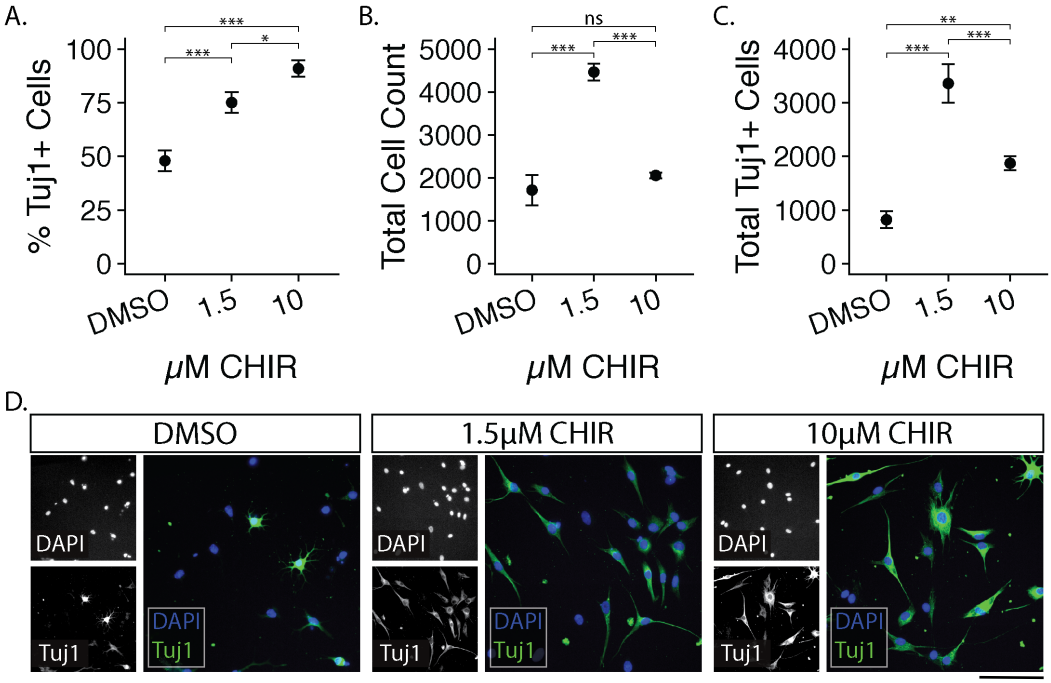

Figure 3.1 Strength of Wnt signal activation regulates probability of neuronal differentiation and final cell count. A. Percentage of Tuj1$^+$ neuronal-committed cells after 5 days in culture at different strengths of canonical Wnt pathway activation. B. Total number of cells after 5 days in culture at different strengths of canonical Wnt pathway activation. C. Total number of Tuj1$^+$ neuronal-committed cells after 5 days in culture at different strengths of canonical Wnt pathway activation. D. Representative immunostaining images of neuronal marker Tuj1 after 5 days in culture. *p<.05, **p<.01, ***p<.001 (ANOVA with TukeyHSD post-hoc test). Scale bar 100μm.

3.2.2 Wnt/β-catenin signaling is insufficient to induce long-term proliferation of NSCs, but mid-level Wnt activation displays extended mitogenic capacity.

Increased final numbers of Tuj1$^+$ neuronal-committed cells in mid-level Wnt conditions could be caused by increased cell death in higher Wnt conditions, or by increased proliferation of cells in mid-level Wnt. We observed no difference in the percentage of live cells in a wide range of CHIR concentrations (Supplementary Figure 3.1), so we turned to investigate the influence of Wnt signal strength in driving NSC proliferation. First, we verified this expanded range of CHIR concentrations increases the activation of the Wnt//β-catenin pathway in a dose-dependent manner (Supplementary Figure 3.2). Then, to observe proliferation in real time we used the two-color fluorescent ubiquitylation-based cell-cycle indicator (FUCCI)[17] system to observe the cell cycle state of a population of FUCCI-NSCs (Figure 3.2A). After 5 days in vitro, the vast majority of all cells in every Wnt condition displayed G1 phase FUCCI markers (Figure 3.2B). This included most cells that had not differentiated into Tuj1$^+$ neuronal-committed cells, suggesting that no level of Wnt is sufficient to induce NSC self-renewal (Figure 3.2C).

To observe how different strengths of Wnt signal activation influence NSC proliferation over time, we counted cells undergoing G1-S transition in a 4-hour period at Days 1-5 in culture. Cells undergoing G1-S transition display a brief period of double-positive FUCCI markers (Figure 3.2A). Interestingly, we observed an immediate dose-dependent increase in the number of cells undergoing G1-S transition on at Day 1 (Figure 3.2D, 3.2D′). However, strong Wnt conditions (3 and 10μM CHIR) experienced an immediate reduction in the number of G1-S transition cells by Day 2, a trend that continued for the duration of the experiment (Figure 3.2D, 3.2D″, 3.2D‴, 3.2E). In contrast, however, we observed the number of cells undergoing G1-S transition in mid-level Wnt conditions (1.5μM CHIR) increase on Day 2, and G1-S cell counts remained greater than weaker and stronger Wnt conditions for the remainder of the experiment (Figures 3.2D, 3.2D″, 3.2D‴, Figure 3.2E). These data suggest that mid-level Wnt conditions enable extended proliferation of cells as compared to different strengths of Wnt pathway activation.

3.2.3 Prolonged duration of cell proliferation in mid-level Wnt conditions occurs in neuronal-committed cells.

We sought to examine the neuronal differentiation states of proliferating cells over the timecourse of Wnt pathway activation. To do so, we made use of the thymidine analog 5-ethynyl-2'-deoxyuridine (EdU) which is selectively incorporated into cells during the DNA replication phase of the cell cycle (S-phase). Following a 4-hour EdU pulse prior to fixation at Day 1, 3, or 5 *in vitro*, we assayed cells for EdU incorporation and the neuronal commitment marker Tuj1. We observed an increasing percentage of Tuj1$^+$ cells in each bulk population over time for all conditions, with maximum differentiation percentage saturating after 3 days in culture at and above 3μM CHIR (Figure 3.3A). Similar to results observed in Figure 1, at 5 days in vitro we observed a dose-dependent relationship between percent Tuj1$^+$ differentiation and strength of Wnt pathway activation (Figure 3.3A′). All levels of Wnt activation except the 0μM CHIR negative control experienced an initial increase in total cell number from Day 1 to Day 3, prior to a reduced final cell count after 5 days in vitro (Figure 3.3B). As observed in Figure 3.1, total cell count after 5 days in vitro was markedly lower in high CHIR levels as compared to 1.5μM CHIR (Figure 3.3B′). These trends similarly translated to total Tuj1$^+$ cell counts (Figure 3.3C, 3.3C′). We observed EdU

incorporation that closely matched FUCCI results, with strong Wnt conditions experiencing immediate decreases in proliferation after Day 1, while we observed the capacity for low- and mid-level Wnt conditions to prolong cell cycle activation (Figure 3.3D, 3.3F). Further, EdU^{+} cells in all conditions displayed high neuronal differentiation, indicating that the proliferative response to any level of Wnt signaling is occurring primarily in neuronal-committed cells (Figure 3.3E).

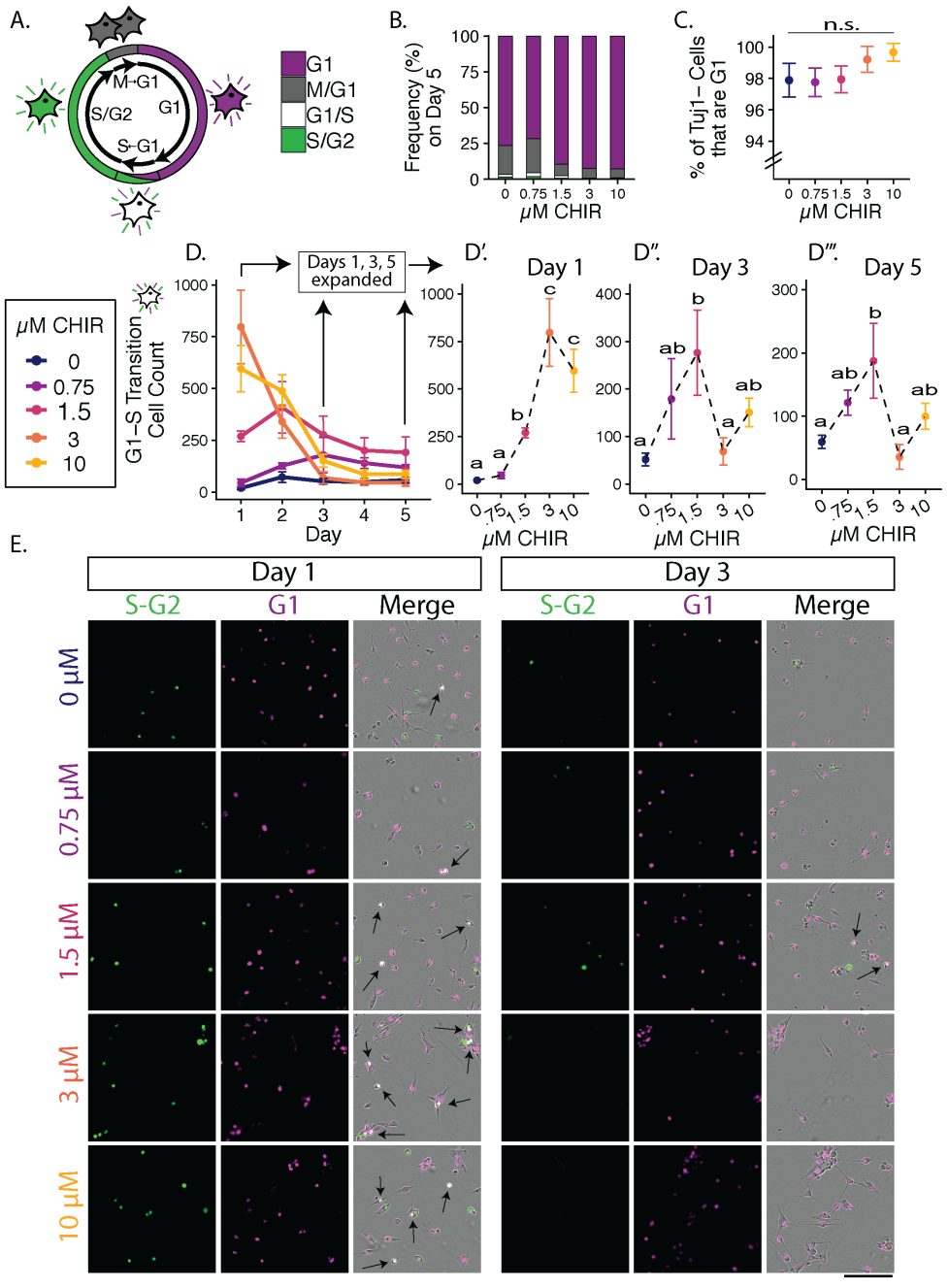

Figure 3.2 Strength of Wnt/β-catenin signaling regulates cell cycle activation in NSCs A. FUCCI2 system enables identification of cell cycle phase through fluorescent markers. B. Frequency of cells in each FUCCI cell cycle phase after 5 days in vitro. C. Percent of Tuj1^{-} cells that display G1 phase FUCCI markers. D. Mean G1-S transition cell count during 4-hour window over 5 days in culture. D′, D″, and D‴ respectively display data from Days 1, 3, and 5 across an axis of different strengths of Wnt pathway activation. Lowercase letters display statistical groups (ANOVA

with post-hoc TukeyHSD test, $p < .05$ between all groups). E. Representative images from Days 1 and 3. Black arrows indicate cells in G1-S transition phase of cell cycle. Scale bar 100 µm.

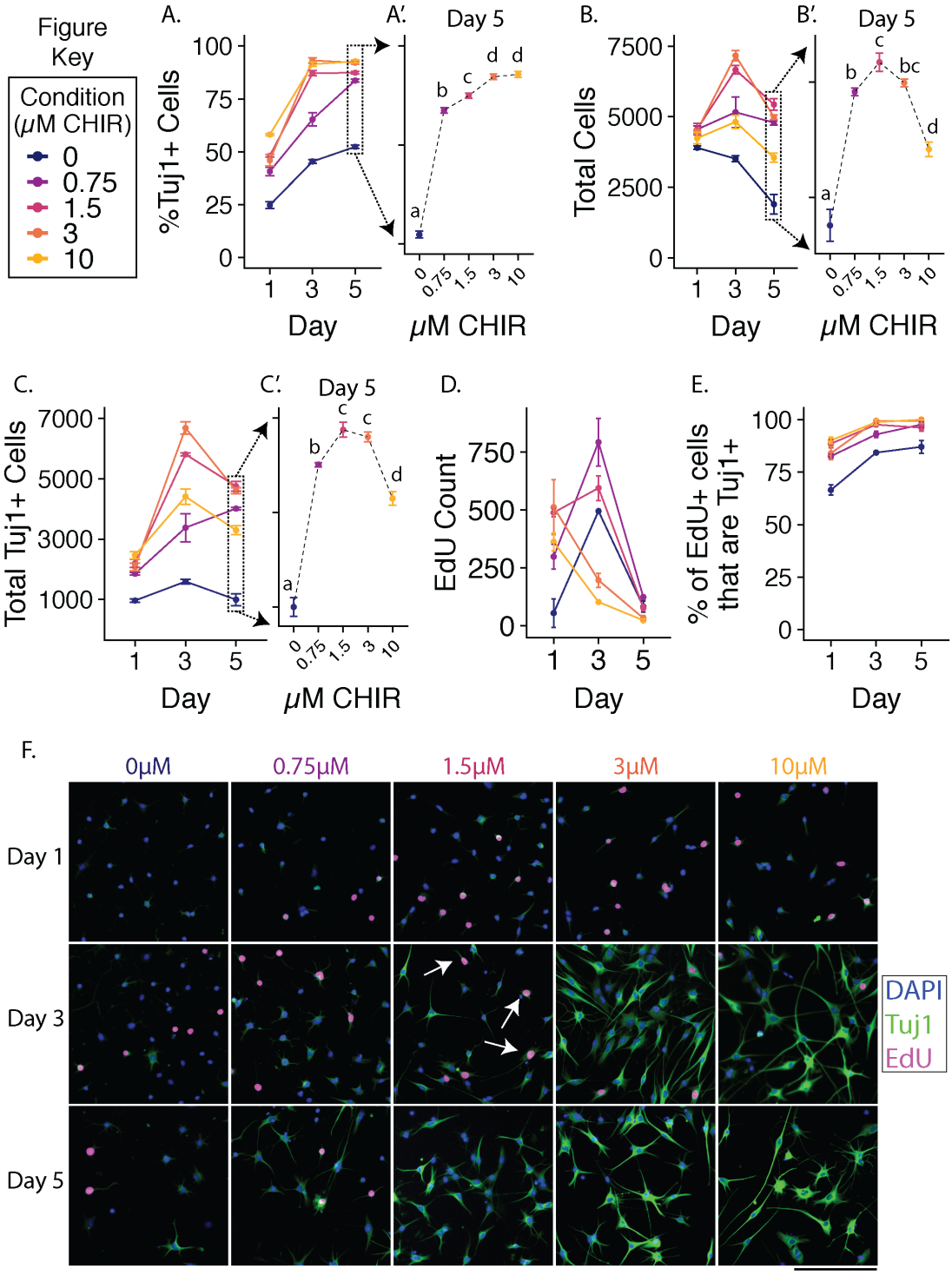

Figure 3.3 Strength of Wnt/β-catenin signaling regulates timecourse of differentiation and proliferation of neuronal-committed cells. A. Percentage of Tuj1$^+$ neuronal-committed cells over time. (A′, after 5 days in culture). B. Total number of cells over time. (B′, 5 days in culture). C. Total number of Tuj1$^+$ neuronal-committed cells over time. (C′, 5 days in culture). D. Count of EdU$^+$ cells over time. E. Percentage of EdU$^+$ cells that display the neuronal-

committed marker Tuj1 over time. F. Representative images of NSC timecourse of differentiation ($Tuj1^+$) and proliferation (EdU^+). Lower case letters represent statistical groups (ANOVA with post-hoc TukeyHSD test, $p < .05$ between all groups). Scale bar 100μm.

3.2.4 Proliferative potential of single neural stem cells is expanded in mid-level strength of Wnt activation.

While our previous observations showed cell-cycle activation in mid-level Wnt conditions for an extended time period, they did not address whether cells undergoing proliferation at later times were cells that had previously divided, or cells in the bulk population that were undergoing their first mitotic event. To address this question, we sought to track the behavior of single NSCs in our tested range of Wnt signal activation strengths. To do so, we turned to a single-cell patterning platform that we recently developed which enables long-term tracking of single cells and their progeny in physically isolated "microislands"[18]. On a modified 4-well chamber slide, a non-cell adherent polyHEMA surface surrounding each microisland prevents cells and their progeny from migrating out of their initial patterned area, enabling us to track cell division of single NSCs and the proliferation of their respective progeny over time. We coupled this observation with a traditional end-point immunostaining assay to probe for neuronal differentiation (Figure 3.4A).

Generally, we observed broad heterogeneity in proliferative outcomes of single NSCs (Figure 3.4B) and again observed strong neural differentiation of NSCs in response to CHIR (Figure 3.4C). In agreement with our previous findings, the timecourse of cell proliferation was extended in mid-level Wnt conditions (1.5μM CHIR) compared to weaker or stronger levels of Wnt activation (data not shown). Interestingly, by tracking the cumulative number of cell divisions per microisland, we observed single cells in mid-level Wnt conditions capable of undergoing an increased number of cell divisions as compared to higher and lower levels of CHIR (Figure 3.4D). As such, the distribution of cumulative cell divisions per microisland in 1.5μM CHIR was wider than, and statistically distinct from, other conditions. Further, this increased proliferative capacity also corresponded to a wider distribution of final $Tuj1^+$ cell count, indicating that mid-level Wnt activation was capable of enabling some single cells to produce increased numbers of clonal $Tuj1^+$ neuronal-committed cells (Figure 3.4E).

3.3 Discussion

The canonical Wnt/β-catenin signaling pathway regulates multiple stages of adult neurogenesis, including the proliferation and neuronal differentiation of adult NSCs. While previous work has elucidated this duel role, questions still abound as to how these two concurrent fate commitments interplay with one another, and how Wnt signaling acts to modulate the balance between them. Our work here identifies the strength of Wnt pathway activation as a conditional factor in regulating NSC behavior by modulating the extent of proliferation during neuronal differentiation.

Our results show that while strong Wnt pathway activation yields the greatest probability of neuronal differentiation, it counterintuitively yields fewer overall immature neurons as compared to mid-level pathway activation as a result of diminished proliferative capacity. This may be driven through a differential balance of intracellular signal propagation that is linked to downstream neurogenic processes. NSCs undergoing neuronal differentiation become post-mitotic and are incapable of undergoing cell cycle activation, thus our results heavily imply that stronger Wnt

conditions drive cells to this post-mitotic stage at a faster timescale than lower pathway activation strengths. Further, low levels of pathway activation may not be sufficient to induce the Wnt-driven cell cycle activation in cells, thus also yielding lower levels of total immature neurons. Additional

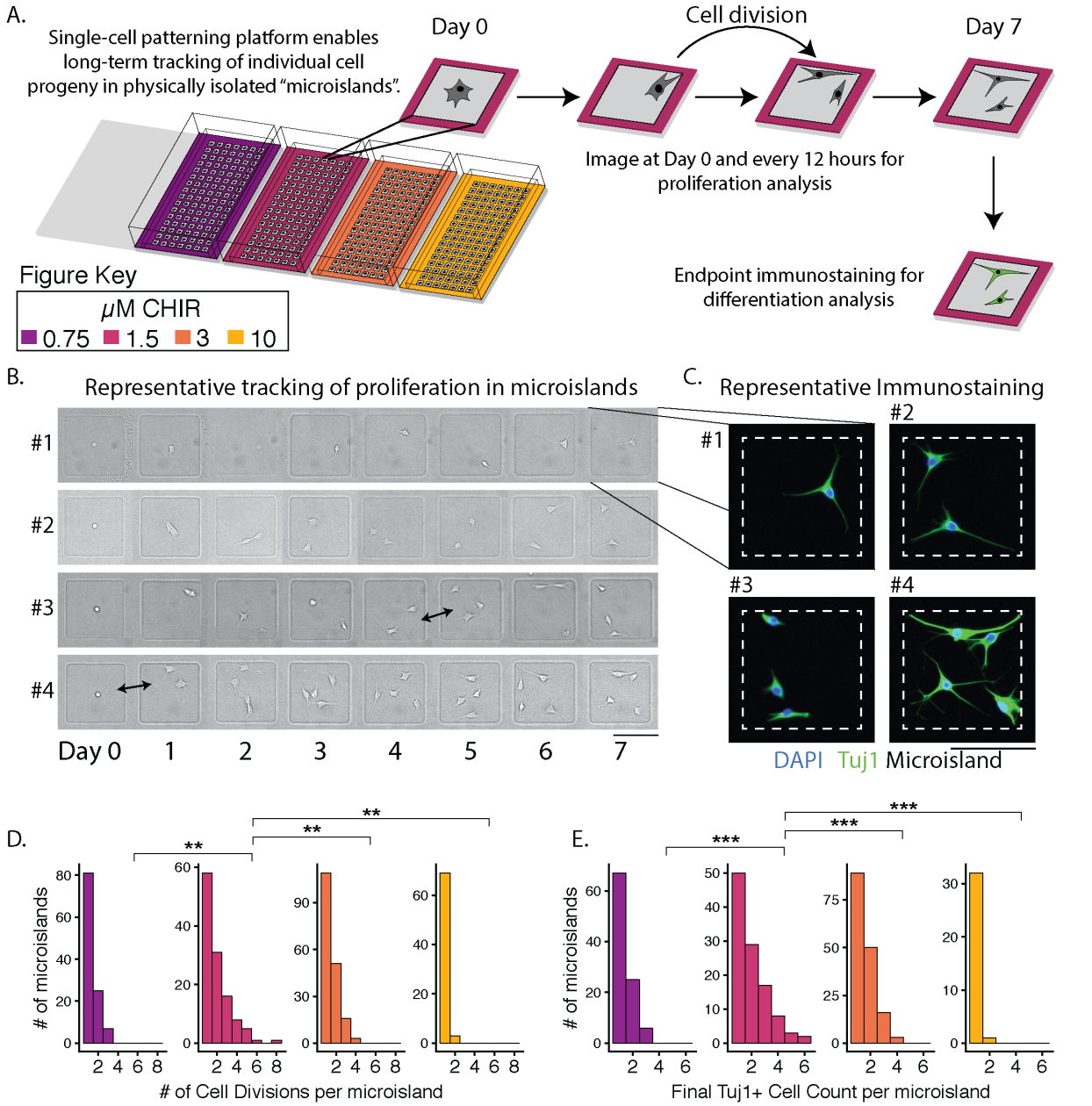

Figure 3.4 Single-cell tracking of NSCs in response to different strengths of Wnt activation. A. Schematic of single-cell patterning platform and downstream proliferation and differentiation analysis. B. Concatenated timecourse of four representative microislands displaying proliferation outcomes from single cells. C. Representative immunostaining of four representative microislands. D. Distribution of the cumulative number of cell divisions per microisland over duration of experiment. **p < .01, ANOVA with TukeyHSD post-hoc test. E. Distribution of final Tuj1^{+} neuronal-committed cell count per microisland. **p < .001, ANOVA with TukeyHSD post-hoc test. Scale bars = 100μm.

studies exploring the precise mechanisms through which this behavior is regulated would provide deeper answers to the balance of proliferation and differentiation, and could further assist emerging technologies like optogenetics[19] to gain even finer precision over controlling cell behavior.

In vivo clonal analysis has revealed broad heterogeneity with relation to the number of newborn neurons that can arise from single NSCs[2]. Given the *in vivo* role Wnt plays in driving NSC proliferation and differentiation, our results may further allude to a process through which this heterogeneity arises. Other factors including cell-cell contacts or the specific stage of the cell cycle at which a cell receives a Wnt or other biomolecular cue may also further contribute to this heterogeneity.

More broadly, our work here displays an important consideration for studies using small molecules to activate or inactive biomolecular signaling networks *in vitro*. Specifically, our work highlights how small changes to concentrations used or differences in stock potency may result in drastically different cell behavior. Altogether, our results reveal an intricate interplay between Wnt-driven proliferation and differentiation of NSCs in response to different levels of pathway activation, which has implications for regenerative medicine.

3.4 Methods

3.4.1 Cell Culture

Adult hippocampal neural stem cells (NSCs) isolated from Fischer 344 rats were cultured as previously described on poly-L-ornithine/laminin-coated plates[20]. Prior to experiments, cells were cultured in DMEM/F-12 medium with added N2 supplement and 20ng/mL FGF-2, receiving fresh media every other day and passaged onto fresh plates with Accutase upon reaching 80% confluency. During experiments, cells were cultured in DMEM/F-12/N2 medium supplemented with stated concentrations of CHIR99021 (Stemgent, dissolved in DMSO to manufacturer recommendations) and a within-experiment DMSO volume control. During experiments, cells received one-half fresh media changes daily.

3.4.2 FUCCI-NSCs

To generate FUCCI-NSCs, NSCs were double-transduced with retroviruses encoding the mCherry-hCdt1(30/120) and mVenus-hGem(1/110) FUCCI2 constructs. NSCs were subsequently puromycin selected for transduction followed by mCherry/mVenus double-positive FACSorting to identify cells with successful double transduction. These double-positive cells were expanded several passages until the loss of cell cycle synchronization (assayed by fluorescence) and then utilized for FUCCI experiments.

3.4.3 EdU Labeling

For EdU experiments, cells were given a 4-hour 10μM EdU pulse delivered in one-half fresh media immediately prior to fixation at listed experimental times. EdU incorporation was detected using Invitrogen's Click-it Plus EdU Alexa Fluor 555 kit (C10638) using manufacture's recommendations, and performed immediately prior to immunostaining.

3.4.4 Immunostaining

Cells were fixed after stated times in culture using 3% paraformaldehyde for 15 minutes at room temperature. Cells were then washed 3x with PBS and placed in a permeabilization/blocking PBS buffer containing 5% donkey serum and 0.3% Triton X-100 (PBS-DT) for a minimum one hour. Mouse anti-β Tubulin III (Tuj1) primary antibody (Sigma T8578, 1:1000) was added to samples in PBS-DT and incubated overnight. After overnight incubation, primary antibodies were removed using 3x PBS washes, followed by a one-hour incubation with secondary antibody (Donkey anti-Mouse IgG Alexa fluor 488, Invitrogen A21202, 1:250) and DAPI (1:1000). After secondary antibody incubation, samples were washed with PBS three times and stored in PBS until imaging.

3.4.5 Imaging and Image Analysis

Live-cell experiments (except those with live FUCCI-NSCs) and all fixed/immunostained samples were imaged using an ImageXpress Micro (IXM) high-throughput automated imager with either a 10x or 20x objective. FUCCI-NSCs were imaged using an IncuCyte Live Cell Analysis System (Essen Bioscience). Image analysis for IXM images was performed using a custom multiple wavelength cell scoring program designed in the IXM's accompanying MetaXpress software. For quantification, DAPI-stained nuclei were used to generate a mask applied to the remaining fluorescence channels of interest, with negative controls used to set thresholds for signal intensity.

3.4.6 Single cell patterning experiments

Single cell patterning experiments were performed as previously described[18]. Briefly, aldehyde-functionalized glass slides (Schott) were coated with a non-cell adhesive layer of polyHEMA (Sigma). A 30x30 grid of 141μm x 141μm microisland squares were "etched" into the polyHEMA using a custom quartz mask with the corresponding grid pattern (Photosciences Inc.). Single-cell sized spots of amine-modified DNA was "printed" in the microislands using a Nano eNabler (Bioforce Nano), then covalently bonded using a brief sodium borohydride reductive amination reaction (Sigma, 0.25% in PBS). Lipid-modified DNA complementary to that of the printed DNA was transiently incorporated into cell membranes, and used to "tether" cells in DNA-spotted areas. Excess cells were washed, and culture media was introduced for the duration of the experiment.

3.4.7 Western Blotting

Western blotting was performed with standard protocols using ThermoFisher Scientific NuPAGE precast gels with MOPS buffer. Antibodies used include Rabbit anti-Non-phospho (active) β-catenin D13A1 (Cell Signaling #8814, 1:1000); Mouse anti-β-catenin Clone 14 (BD Biosciences 610153, 1:1000); and Mouse anti-β-actin Clone AC-15 (Sigma A1978, 1:1000). Secondary antibodies used include Goat anti-Rabbit IgG HRP (ThermoFisher A16110 1:10,000) and Goat anti-Mouse IgG HRP (ThermoFisher 31430, 1:10,000). Blots were developed with SuperSignal West Dura extend duration substrate kit (ThermoFisher 34076) and imaged on a BioRad ChemiDox imager.

3.5 Appendices

3.5.1 Supplementary Figures

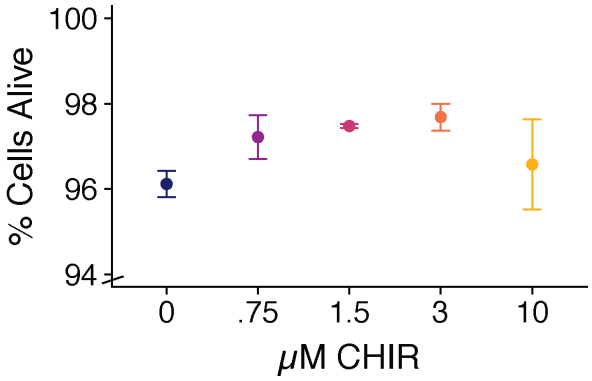

Supplementary Figure 3.1 NSC viability in varying levels of Wnt signal activation. Increasing levels of Wnt pathway activation via higher CHIR concentrations does not cause changes in cell viability. (ANOVA p = .0329; only 0μM:3μM shows significant TukeyHSD comparison, p = .04, all other comparisons p > .05).

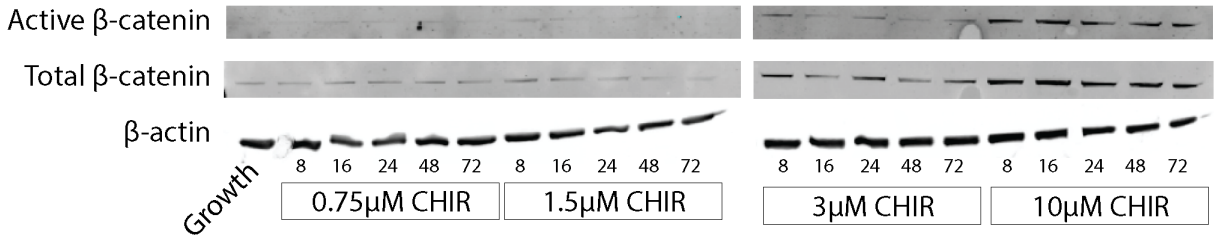

Supplementary Figure 3.2 Activation of the canonical Wnt/β-catenin signaling pathway across increasing levels of CHIR. Total and active (non-phosphorylated) β-catenin increases with increasing concentrations of CHIR. Dose-dependent pathway activation is stable over time (numbers represent hours).

3.6 References

1. Eriksson, P. S. *et al.* Neurogenesis in the adult human hippocampus. *Nature medicine* **4**, 1313 (1998).
2. Bonaguidi, M. A. *et al.* In Vivo Clonal Analysis Reveals Self-Renewing and Multipotent Adult Neural Stem Cell Characteristics. *Cell* **145**, 1142–1155 (2011).
3. Zhang, J. & Jiao, J. Molecular Biomarkers for Embryonic and Adult Neural Stem Cell and Neurogenesis. *BioMed Research International* **2015**, 1–14 (2015).
4. Kempermann, G. *et al.* Human Adult Neurogenesis: Evidence and Remaining Questions. *Cell Stem Cell* **23**, 25–30 (2018).
5. Kuwabara, T. *et al.* Wnt-mediated activation of NeuroD1 and retro-elements during adult neurogenesis. *Nature Neuroscience* **12**, 1097–1105 (2009).
6. Steinhart, Z. & Angers, S. Wnt signaling in development and tissue homeostasis. *Development* **145**, dev146589 (2018).
7. Holstein, T. W. The Evolution of the Wnt Pathway. *Cold Spring Harbor Perspectives in Biology* **4**, a007922–a007922 (2012).
8. Lie, D.-C. *et al.* Wnt signalling regulates adult hippocampal neurogenesis. *Nature* **437**, 1370–1375 (2005).
9. Kotterman, M. A., Vazin, T. & Schaffer, D. V. Enhanced selective gene delivery to neural stem cells in vivo by an adeno-associated viral variant. *Development* **142**, 1885–1892 (2015).
10. Qu, Q. *et al.* Orphan nuclear receptor TLX activates Wnt/β-catenin signalling to stimulate neural stem cell proliferation and self-renewal. *Nature Cell Biology* **12**, 31–40 (2010).
11. Israsena, N., Hu, M., Fu, W., Kan, L. & Kessler, J. A. The presence of FGF2 signaling determines whether β-catenin exerts effects on proliferation or neuronal differentiation of neural stem cells. *Developmental Biology* **268**, 220–231 (2004).
12. Bohnenpoll, T. *et al.* Canonical Wnt signaling regulates the proliferative expansion and differentiation of fibrocytes in the murine inner ear. *Developmental Biology* **391**, 54–65 (2014).
13. Pera, E. M., Acosta, H., Gouignard, N., Climent, M. & Arregi, I. Active signals, gradient formation and regional specificity in neural induction. *Experimental Cell Research* **321**, 25–31 (2014).
14. Christian, J. L. Morphogen gradients in development: from form to function: Morphogen gradients in development: from form to function. *Wiley Interdisciplinary Reviews: Developmental Biology* **1**, 3–15 (2012).
15. Kirkeby, A. *et al.* Generation of Regionally Specified Neural Progenitors and Functional Neurons from Human Embryonic Stem Cells under Defined Conditions. *Cell Reports* **1**, 703–714 (2012).
16. Lu, J. *et al.* Generation of serotonin neurons from human pluripotent stem cells. *Nature Biotechnology* **34**, 89–94 (2016).
17. Sakaue-Sawano, A., Kobayashi, T., Ohtawa, K. & Miyawaki, A. Drug-induced cell cycle modulation leading to cell-cycle arrest, nuclear mis-segregation, or endoreplication. *BMC Cell Biology* **12**, 2 (2011).
18. Chen, S. *et al.* Interrogating cellular fate decisions with high-throughput arrays of multiplexed cellular communities. *Nature Communications* **7**, 10309 (2016).

19. Bugaj, L. J., Choksi, A. T., Mesuda, C. K., Kane, R. S. & Schaffer, D. V. Optogenetic protein clustering and signaling activation in mammalian cells. *Nature Methods* **10**, 249–252 (2013).
20. Peltier, J., Ormerod, B. K. & Schaffer, D. V. Isolation of Adult Hippocampal Neural Progenitors. in *Protocols for Adult Stem Cells* (eds. Conboy, I. M., Schaffer, D. V., Barcellos-Hoff, M. H. & Li, S.) **621**, 57–63 (Humana Press, 2010).

Chapter 4: Expanding the parameter space of complex biomolecular signaling logic with the cell cycle and cell density

4.1 Introduction

In Chapters 2 and 3, I explore two factors—the presence of competing cues and the strength of pathway activation—that serve as additional logical arguments in determining neural stem cell fate decisions in response to biomolecular signals. What other factors might play a role in determining how a cell responds to particular cues from its microenvironment? The framework of complex biomolecular logic opens extensive new questions as to the precise mechanisms and contexts through which cellular decisions are made. In this chapter, I present two additional factors—differential cell cycle phases upon reception of a signal, and cell density—that may contribute to adult neural stem cell behavior in response to biomolecular signaling.

4.2 Results

4.2.1 The Cell Cycle

The cell cycle is a tightly regulated process through which a cell replicates its DNA, segregates two sets of chromosomes, and undergoes cytokinesis to divide into two daughter cells. The cell cycle is divided into 4 main phases, sometimes referred to as stages: the gap 1 or growth 1 "G1" phase, the synthesis or "S" phase, the gap 2 or growth 2 "G2" phase, and the mitosis or "M" phase[1,2]. An additional phase of "G0" is often used to describe a quiescent or post-mitotic cell that is not actively progressing through the cell cycle or can no longer divide. It is well understood that a variety of nodes of many signaling networks fluctuate during different periods of the cell cycle. This fluctuation provides the mechanistic underpinnings of FUCCI systems, as FUCCI consists of fluorescent proteins that are genetically tethered to peptides that are selectively targeted for degradation during different periods of the cell cycle[3]. Further, these fluctuations and cell cycle stage differences enable the cell to precisely control its progression through the cell cycle by using cell cycle "checkpoints" to ensure proper DNA replication and correction, and eventual cytokinesis[1,2].

Extensive studies have explored the connections between various signaling pathways, cell fate decisions, and the cell cycle[4,5]. This includes the topic of Chapter 3, the canonical Wnt/β-catenin pathway, through two lenses: first as having proteins that are functional players in proper cell division[6] in addition to signal propagation, and second by exhibiting differential activation across cell cycle stages[7]. Connections to the cell cycle and neural stem cell fate decisions have also been explored[4]. Interestingly, previous work in *Drosophila* has shown that some NSCs are quiescent in the G2 phase—as opposed to a G0 phase—and that this difference of cell cycle regulates a cell's response to insulin signaling[8].

We explored preliminary avenues through which the cell cycle might regulate adult hippocampal neural stem cell fate decisions in response to Wnt signaling (Figure 4.1). Previous work has shown that the Wnt receptor LRP6, critical for canonical Wnt signal activation, contains five PPPSP dual

phosphorylation sites that are necessary for Wnt signal propagation. It was further found that the most N-terminal PPPSP site, containing the S1490 residue, is regulated by the G2/M cyclin protein Cyclin Y and its associated cyclin-dependent kinase Cdk14. As such, S1490 is selectively phosphorylated during the G2/M phases of the cell cycle in HEK293 cells, thereby "priming" cells to be responsive to Wnt during that phase[7].

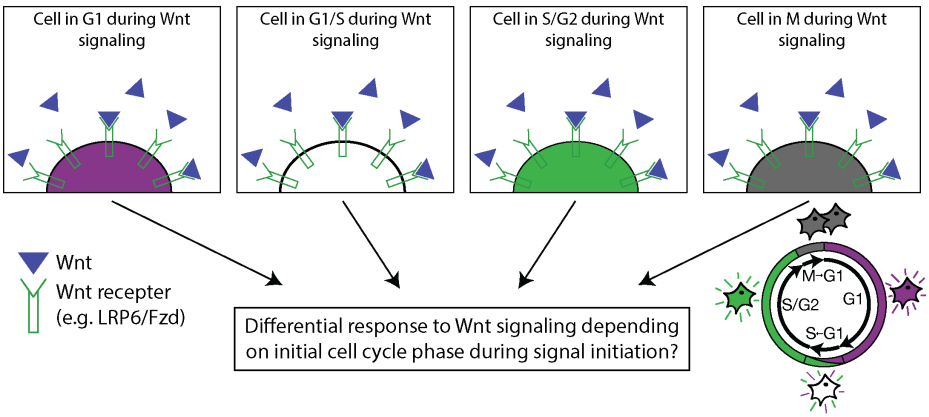

Figure 4.1 Investigation of cell cycle differences in Wnt signal response. Conceptual overview of how a cell may respond differently to Wnt signaling depending on what phase of the cell cycle it is in.

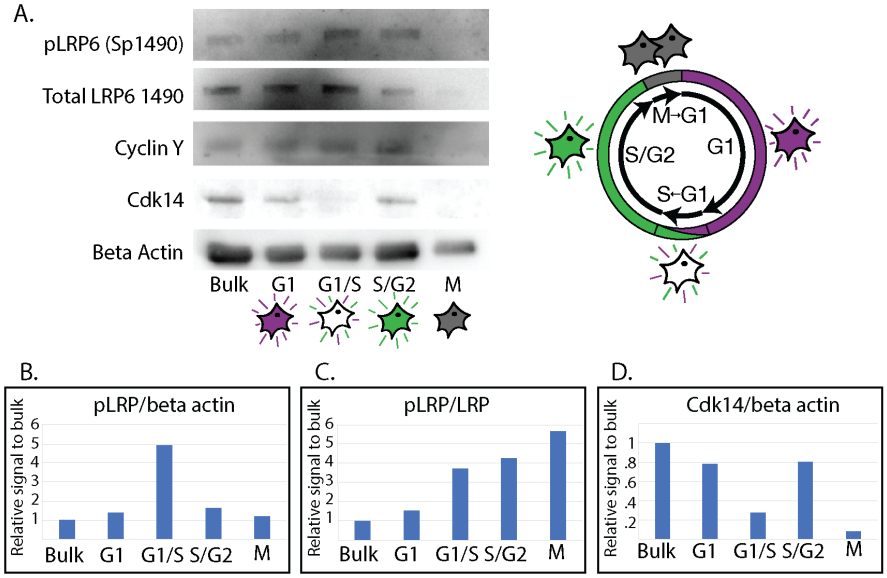

Figure 4.2 Cell cycle regulation of Wnt signaling in adult NSCs. A. Western blot image probing for proteins that are known to regulate Wnt signaling during different periods of the cell cycle. B. Relative pLRP signal to total protein control during different cell cycle phases. C. Ratio of pLRP6 to total LRP6 during different cell cycle phases. D. Relative Cdk14 signal to total protein loading control during different periods of the cell cycle.

We sought to explore if this selective phosphorylation event is also present in adult neural stem cells. To do so, we performed FACSorting on unsynchronized FUCCI-NSCs, collecting populations of cells in the G1, S-G1 transition, S/G2, and M phases (data not shown, see Methods). We then performed western blotting to analyze the presence of Cyclin Y, Cdk14, and phosphorylated LRP6 at S1490 (pLRP6 Sp1490) (Figure 4.2A). We observed the highest pLRP6

signal during the G1/S transition phase relative to others (Figure 4.2B). Further, we found the ratio of pRLP6 to total LRP6 to steadily increase from the G1 to the M phase (Figure 4.2C). Interestingly, this occurred despite the minimal presence of Cdk14 during the G1/S transition phase (Figure 4.2D). Of note, our results show different expression patterns for these target proteins than reported for HEK293 cells[7]. This may suggest that the mechanisms through which Wnt is cell-cycle regulated are context-specific and vary between cell type.

4.2.2 Cell Density

Adult hippocampal neural stem cells of the subgranular zone, as well as immature neurons migrating into the granular zone of the dentate gyrus, are located in a cell- and specifically neuron-dense environment[9]. The cellular density of this region has been estimated, including in the context of aging where decreases in cellular density were observed[10]. Neural stem cells are known to secrete important factors like Cystatin C and VEGF that self-regulate their behavior through an autocrine and paracrine signaling mechanism[11–13]. Because of these cues, density may play a role in heterogeneous clonal outcomes of single NSCs[14]. Therefore, changes in cellular density to the neural stem cell microenvironment represents an additional factor that warrants investigation (Figure 4.3).

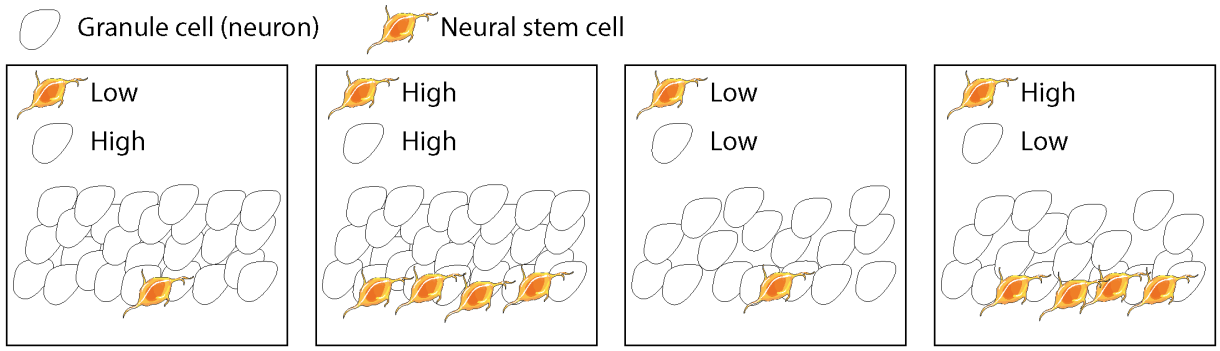

Figure 4.3 Investigation of adult neural stem cell density. Graphical representation of differences in cell density that may play a role in driving cell behavior.

We investigated the role of density in driving neuronal (Tuj1$^+$) and astrocytic (GFAP$^+$) differentiation in three different media conditions: mixed conditions that drive both neuronal and astrocytic differentiation (Figure 4.4A); pro-neuronal conditions (Figure 4.4B); and low growth factor conditions (Figure 4.4C). We found the proportion of cells that display a neuronal fate decision (Tuj1$^+$) increase with increasing density. However, subsequent experiments failed to replicate this observation with consistency or statistical significance (data not shown). This suggests that additional factors that are not controlled for in these initial experiments may be influencing the results. Further, other factors like cell death in low density conditions may play a role in density-driven differentiation and our observations. In total, our initial results suggest some possibility that density plays a role in adult neural stem cell differentiation, but that additional layers of control exist in dictating cell behavior.

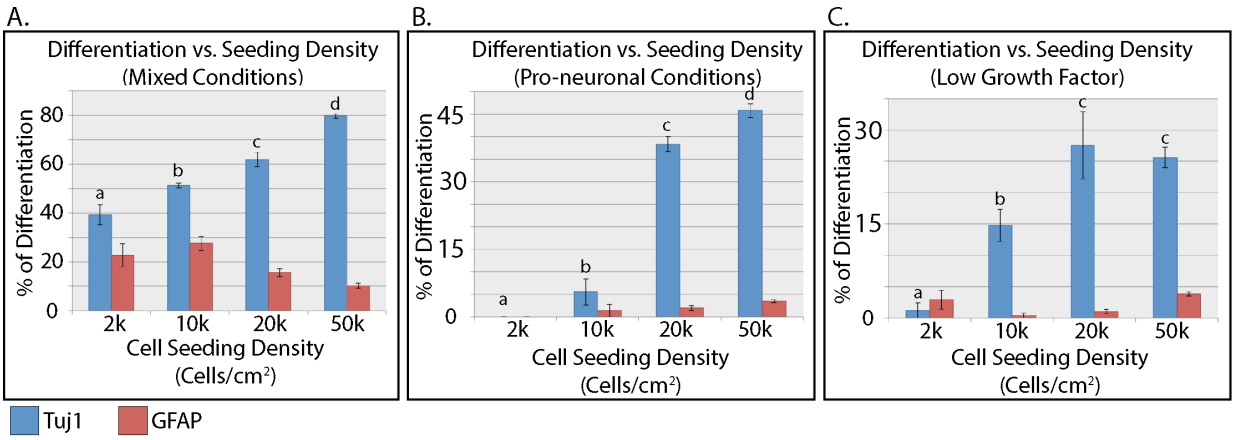

Figure 4.4 Effect of cell density on neural stem cell differentiation. A. Differentiation versus cell density in mixed media conditions. B. Differentiation versus cell density in pro-neuronal media conditions. C. Differentiation versus cell density in low growth factor media conditions.

4.3 Discussion

Our results identifying differential expression of key players in Wnt receptor phosphorylation during the cell cycle suggest that Wnt receptor activation is cell-cycle regulated in NSCs, which is consistent with the literature. However, our results as to specific cell cycle phases in which this activation occurs was not consistent with what others have shown, suggesting that "priming" of Wnt signaling via LRP6 phosphorylation by cell-cycle regulation is context-specific. The coordination between the cell cycle and Wnt signaling in driving adult neural stem cell fate behavior could be further explored through selective knock-downs or knock-outs of critical players in regulating LRP6 intracellular phosphorylation sites, particularly those that are cell cycle regulated: for example, Cdk14 and Cyclin Y. Alternatively, LRP6 S1490 loss-of-function phospho-null and gain-of-function phospho-mimetic mutants could be generated and tested in NSCs. Lastly, cell-cycle synchronized NSCs could be briefly exposed to Wnt ligands during a specific phase of the cell cycle, then relieved from those ligands after a short duration of time to explore the activation of Wnt signaling in NSCs during specific cell cycle phases and its impact on downstream fate decisions. The results of that experiment could be tied to our results of Chapter 3, wherein we display differential NSC fate decisions in response to different strengths of Wnt signal activation.

While our initial results exploring cell density looked promising, additional follow-up experiments suggested that our first observations were not unadulterated, and that additional factors were influencing our results. A possible path could be to perform RNA sequencing on bulk populations of NSCs at different densities over time, and to observe changes in transcription of various signaling pathways. This may narrow the focus of questions on how density plays a role in driving various adult neural stem cell fate decisions.

4.4 Methods

4.4.1 Cell Culture and FUCCI-NSCs

Adult hippocampal neural stem cells, including FUCCI-NSCS, were cultured as previously described (Chapter 3, Section 4). Mixed conditions included 0.5% FBS and 1μM retinoic acid; pro-neuronal conditions included 1μM retinoic acid and 10μM forskolin; low growth factor conditions included 0.1 ng/mL FGF2.

4.4.2 Fluorescence-activated cell sorter (FACS)

Unsynchronized FUCCI-NSCs were lifted with Accutase and filtered through 40μM cell filters in DMEM/F12 media prior to cell sorting into fresh media using a BD Biosciences influx v7 Sorter. Four populations were gathered, as measured by FUCCI marker fluorescence/cell cycle phase: mCherry-only (G1); mVenus-only (S/G2); double-positive (G1-S transition); or double-negative (M). A minimum of 67,000 cells were sorted of each population. After sorting, cells were centrifuged prior to lysing and downstream western blotting.

4.4.3 Western Blotting

FUCCI-sorted NSC lysates were prepared and assayed with standard western blotting procedures. Antibodies used were as follows: Mouse anti-beta actin (A1978 Sigma, 1:1000); Rabbit anti-LRP6 (total) (ab134146, Abcam, 1:1000); Rabbit anti-phospho-LRP6 (Ser1490) (2568T, Cell Signaling 1:1000); Rabbit anti-Cyclin Y (ab114086, Abcam 1:1000); Rabbit anti-PFTK1 (Cdk14) (NBP1-98270 Novus Biologicals, 1:1000). Anti-mouse HRP or anti-rabbit HRP, both 1:10,000 were used as secondary probes for imaging using a SuperSignal West Dura extend duration substrate kit (ThermoFisher 34076) and BioRad ChemiDoc imager.

4.4.4 Immunostaining

Immunostaining was performed as previously described (Chapter 3, Section 4). Primary antibodies used includes Mouse anti-Tuj1 (T8578 Sigma, 1:1000) and Rabbit anti-GFAP (ab7260 Abcam, 1:1000). Secondary antibodies were used at a 1:250 dilution and include Donkey anti-mouse 488 (Invitrogen A21202) and Donkey anti-rabbit 647 (Invitrogen A31573).

4.4.5 Imaging and Image Analysis

Immunostained samples were imaged and analyzed as previously described (Chapter 3, Section 4). Briefly, samples were imaged on an ImageXpress Micro (IXM) high-throughput automated imager using a 10x objective. Analysis and quantification of fluorescence was performed using a custom multiple wavelength cell scoring program designed in the MetaXpress software system.

4.5 References

1. Raven, P., Johnson, G., Mason, K., Loso, J. & Singer, S. *Biology*. (McGraw-Hill, 2011).
2. Mader, S. *et al. Biology*. (McGraw-Hill, 2013).
3. Sakaue-Sawano, A., Kobayashi, T., Ohtawa, K. & Miyawaki, A. Drug-induced cell cycle modulation leading to cell-cycle arrest, nuclear mis-segregation, or endoreplication. *BMC Cell Biology* **12**, 2 (2011).
4. Roccio, M. *et al.* Predicting stem cell fate changes by differential cell cycle progression patterns. *Development* **140**, 459–470 (2013).
5. Dalton, S. Linking the Cell Cycle to Cell Fate Decisions. *Trends in Cell Biology* **25**, 592–600 (2015).
6. Bryja, V., Červenka, I. & Čajánek, L. The connections of Wnt pathway components with cell cycle and centrosome: side effects or a hidden logic? *Critical Reviews in Biochemistry and Molecular Biology* **52**, 614–637 (2017).
7. Davidson, G. *et al.* Cell Cycle Control of Wnt Receptor Activation. *Developmental Cell* **17**, 788–799 (2009).
8. Otsuki, L. & Brand, A. H. Cell cycle heterogeneity directs the timing of neural stem cell activation from quiescence. *Science* **360**, 99–102 (2018).
9. Gonçalves, J. T., Schafer, S. T. & Gage, F. H. Adult Neurogenesis in the Hippocampus: From Stem Cells to Behavior. *Cell* **167**, 897–914 (2016).
10. Driscoll, I. *et al.* The aging hippocampus: A multi-level analysis in the rat. *Neuroscience* **139**, 1173–1185 (2006).
11. Taupin, P. *et al.* FGF-2-responsive neural stem cell proliferation requires CCg, a novel autocrine/paracrine cofactor. *Neuron* **28**, 385–397 (2000).
12. Hu, Y. *et al.* Role of Cystatin C in Amyloid Precursor Protein-induced Proliferation of Neural Stem/Progenitor Cells. *Journal of Biological Chemistry* **288**, 18853–18862 (2013).
13. Kirby, E. D., Kuwahara, A. A., Messer, R. L. & Wyss-Coray, T. Adult hippocampal neural stem and progenitor cells regulate the neurogenic niche by secreting VEGF. *Proceedings of the National Academy of Sciences* **112**, 4128–4133 (2015).
14. Bonaguidi, M. A. *et al.* In Vivo Clonal Analysis Reveals Self-Renewing and Multipotent Adult Neural Stem Cell Characteristics. *Cell* **145**, 1142–1155 (2011).

Chapter 5: Conclusions and Future directions

Adult hippocampal neural stem cells offer a promising avenue into the future of regenerative therapies for a host of neurological disorders and disease. To reach this potential, and to fully dissect their fascinating biology, a more complete picture of the highly complex signaling mechanisms that guide their behavior is necessary. Over the last two decades since the first evidence of their presence in the adult human brain was published, much work has revealed the influence of many biomolecular signaling factors in controlling their behavior. In parallel, work has shed light on the specialized *in vivo* "niche" these cells reside in, and the immensely multiplexed signaling milieu it harbors. As the field of adult neural stem cell biology and adult neurogenesis continues to mature, our efforts to understand how biomolecular signaling mechanisms influence their self-renewal, differentiation, quiescence, migration, and other fate behaviors must continue to move toward a model that includes the complexity of their native location.

In this dissertation, I first discuss "complex biomolecular signaling logic" as a framework to explore how conditional arguments beyond the simple presence or absence of a single isolated factor control adult NSC behavior. This concept demands the expansion of traditional (but, not to be remiss, useful and scientifically-sound) methods of investigating single isolated factors in prescribing cellular responses. Instead, the concept of complex logic aims to introduce the natural intricacies of biomolecular signaling factors that neural stem cells—and all cells—are constantly exposed to, and through which they make decisions.

We have applied this framework to investigate potential hierarchies in biomolecular signaling logic. Specifically, we aimed to investigate how Notch signaling and Eph/ephrin signaling may "compete" with one another to ultimate drive their respective cell behavior. To answer this question, I present our work in establishing a novel, DNA-based, single-cell patterning platform that relies on Franklin-Watson-Crick base pairing and enables long-term tracking of single-cell behavior. By culturing and confining single neural stem cells in the presence of two cells that each display either Notch or Eph/ephrin pathway ligands, we uncover how neural stem cells appear to "listen" more closely to the Notch signaling cue to self-renew and remain undifferentiated.

Next, I explore the canonical Wnt signaling pathway and how the strength of activation of this pathway regulates downstream cell behavior. In particular, I show that strong activation of signaling yields the highest proportion of cells selecting a neuronal fate. However, this coincides with a lower proliferative potential during differentiation; in other words, mid-level strength of activation produced the highest total number of neuronal-committed cells. I show this effect occurs at the population and single-cell level.

Lastly, I briefly explore two additional factors—the cell cycle and cell density—that may contribute to the complex logic through which adult NSC fate decisions are made. While these results are preliminary, they provide hints to yet-uncovered mechanisms that are important for neural stem cell biology.

Altogether, our results validate the framework of complex logic when investigating adult neural stem cell fate decisions in response to biomolecular signaling. Our results have implications for

regenerative medicine and may help inform cell-based strategies for therapeutic interventions of a host of neurological diseases and disorders. They also further uncover the fascinating and deeply exquisite regulation of stem cell behavior. This framework could be further extended to other cell types and tissues to provide an even deeper appreciation for the intricacies of the biological world.